2003

The transport phase of pyrolytic oil exiting a fast fluidized bed reactor

Daren Einar Daugaard
Iowa State University

The transport phase of pyrolytic oil exiting a fast fluidized bed reactor

by

Daren Einar Daugaard

A dissertation submitted to the graduate faculty
in partial fulfillment of the requirements for the degree of
DOCTOR OF PHILOSOPHY

Major: Mechanical Engineering

Program of Study Committee:
Robert C. Brown (Major Professor)
Kenneth M. Bryden
Srinivas Garimella
Steven J. Hoff
Brent H. Shanks

Iowa State University
Ames, Iowa
2003

ProQuest Information and Learning Company
300 North Zeeb Road
P.O. Box 1346
Ann Arbor, MI 48106-1346

Graduate College

Iowa State University

This is to certify that the doctoral dissertation of

Daren Einar Daugaard

has met the dissertation requirements of Iowa State University

Signature was redacted for privacy.

Major Professor

Signature was redacted for privacy.

For the Major Program

DEDICATION

This research is dedicated to my daughter, Mable Jean, and my wife, Tara Jean.

TABLE OF CONTENTS

LIST OF TABLES

LIST OF FIGURES

ACKNOWLEDGEMENTS

Dr. Robert C. Brown served as my major professor and provided exceptional guidance through my research. My committee members include Professors Srinivas Garimella, Kenneth M. Bryden, Brent H. Shanks, and Steven J. Hoff. The Iowa Energy Center (IEC) provided financial assistance for this research. Jerod Smeenk, Andy Suby, Joe Ritzert, and David Starks assisted in many capacities on technical issues related to this work. My wife, Tara, patiently supported me and provided editorial reviews.

ABSTRACT

An unresolved and debated aspect in the fast pyrolysis of biomass is whether the bio-oil exits as a vapor or as an aerosol from the pyrolytic reactor. The determination of the bio-oil transport phase will have direct and significant impact on the design of fast pyrolysis systems. Optimization of both the removal of particulate matter and collection of bio-oil will require this information. In addition, the success of catalytic reforming of bio-oil to high-value chemicals will depend upon this transport phase.

A variety of experimental techniques were used to identify the transport phase. Some tests were as simple as examining the catch of an inline filter while others attempted to deduce whether vapor or aerosol predominated by examining the pressure drop across a flow restriction. In supplementary testing, the effect of char on aerosol formation and the potential impact of cracking during direct contact filtering are evaluated.

The study indicates that for pyrolysis of red oak approximately 90 wt-% of the collected bio-oil existed as a liquid aerosol. Conversely, the pyrolysis of corn starch produced bio-oil predominately in the vapor phase at the exit of the reactor. Furthermore, it was determined that the addition of char promotes the production of aerosols during pyrolysis of corn starch. Direct contact filtering of the product stream did not collect any liquids and the bio-oil yield was not significantly reduced indicating measurable cracking or coking did not occur.

1. INTRODUCTION

The objective of this study is to determine whether bio-oil generated during the fast pyrolysis of biomass exits the pyrolytic reactor as a vapor or an aerosol. Secondary processing of the product stream, such as filtering or catalytic reforming, is directly influenced by this determination and therefore impacts the design of ancillary systems of fast pyrolysis located downstream from the fast pyrolysis reactor.

1.1. Fast Pyrolysis of Biomass

Pyrolysis of biomass is a process in which biomass is subjected to heat in an oxygen-free environment resulting in its conversion to char, liquid, and noncondensable gases. This process is illustrated in Figure 1. The liquid product is commonly referred to as bio-oil, bio-crude, or pyrolytic oil [1]. In fast pyrolysis, the biomass is quickly heated to 400 to 600 °C with the primary goal being maximization of bio-oil yields. The bio-oil can be used both as a fuel for power generation and refined for specific chemical production.

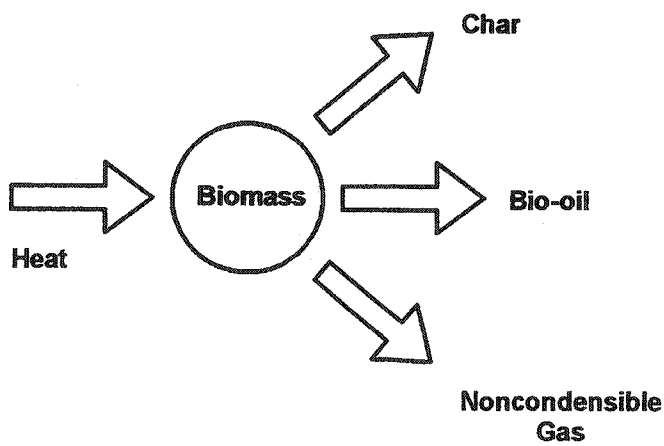

Figure 1. Pyrolysis of biomass particle

1.2. Dissertation Organization

This dissertation begins with an overview of fast pyrolysis in Chapter 2. The main aspects and challenges associated with the field are discussed. These include:

- methods of biomass thermal chemical conversion
- mechanics of fast pyrolysis
- products of fast pyrolysis
- discussion of aerosol versus vapor transport phase of bio-oil
- current fast pyrolysis technology

Chapter 3 details the system constructed for this research and describes typical operating conditions. Chapter 4 presents the methodology used for a systematic study to determine whether condensable organic compounds exit the reactor as aerosols or vapors. The results of these evaluations are presented in Chapter 5. The impact of these results on bio-oil processing and study conclusions are summarized in Chapter 6.

2. CURRENT STATE OF FAST PYROLYSIS OF BIOMASS

The thermal chemical conversion of biomass will play an important role in future energy markets. The utilization of biomass and other renewable sources for energy production will directly reduce the consumption of crude oil and other fossil fuels. Environmentally, the use of fossil fuels results in a net increase of carbon dioxide released into the atmosphere and is linked to global warming. Both the transportation and electricity production industries will directly benefit from the development of technologies to process biomass and other waste material into usable fuels. Additionally, chemical product extraction from the thermal conversion of biomass is being researched to increase the value of biomass.

The review of the current state of fast pyrolysis will include a brief discussion of alternative forms of the thermal chemical conversion of biomass. The theory and principles of fast pyrolysis will be explained. The mechanisms by which liquids, solids, and gases are formed from biomass are detailed. The properties and chemical content of the liquid, solid, and gas products will be included. The fast pyrolysis reactor and ancillary systems including solid removal and liquid collection components of common fast pyrolysis systems will be detailed.

2.1. Methods of Thermal Chemical Conversion of Biomass.

There are four main methods of converting biomass to usable sources of energy: combustion, gasification, liquefaction, and pyrolysis.

Combustion. Combustion is an exothermic reaction of biomass in the presence of sufficient oxygen to completely convert the fuel to the end of products of H_2O and CO_2. Combustion is a multiple step process [2,3] that begins with conduction of heat into the biomass particle. Water contained in the biomass is

vaporized and released. After this drying process, the temperature of the biomass continues to rise and devolatilization of the biomass begins. With water vapor and volatiles flowing from the biomass, oxygen is not permitted to flow to the surface. Therefore, at elevated temperatures, the surface material reacts in the absence of oxygen, in a process known as pyrolysis.

Once the outer portion of a biomass particle has devolatilized, a porous char matrix is left in through which water vapor and volatiles must flow. When the volatiles from the pyrolysis step reach the oxygen-rich environment outside the char layer, they react to form H_2O and CO_2. Char combustion is the last stage of the combustion process. Once the original biomass has completely devolatilized the flow of water and volatiles cease. This allows the oxygen to diffuse into the char matrix. The char, which is primarily carbon, oxidizes to produce CO and CO_2.

Gasification. Gasification is an endothermic process in which the biomass is exposed to a reducing environment to produce a low to medium value gas consisting of carbon monoxide, carbon dioxide, hydrogen, methane, nitrogen, and small quantities of additional hydrocarbons. Gasification is a multiple step process [2,4,5] similar to combustion. First, heat is introduced and transferred to the biomass. This is accomplished by an external heat supply or by combusting a limited amount of the biomass. The heat initiates drying by evaporating trapped moisture. The second stage, called pyrolysis, involves the devolatilization of the biomass in the absence of oxygen. The products of pyrolysis must travel through the porous char matrix to enter the surrounding environment. Instead of oxidizing, the volatiles react with the char layer and a set of reactions ensue. These reactions are termed gas-solid reactions consisting of endothermic and exothermic processes. Brown [2] and Reed [4] describe these reactions in detail. The final step of gasification is gas-phase reactions. The gas-phase reactions result in the final composition of the producer

gas. Components contained in the gas consist of CO, CO_2, H_2, and various hydrocarbons.

The producer gas can be combusted to supply energy for electrical generation or be used as a cooking gas. Typical operating temperatures of gasification are 1000 to 1500 °C with an operating pressure from atmospheric to 20 bar. Yields of gas range from 100 and 250 wt-% of dry biomass [6].

Liquefaction. The process of liquefaction involves converting biomass under modest temperatures of 250 to 325 °C with large operating pressures of 5 to 20 MPa [7]. To begin, the biomass is mixed with water to form an aqueous solution. A catalyst is typically added to promote the conversion of the biomass mixture to bio-oil. Minowa et al utilized a 10:1 mixture on a mass basis of water to biomass [8]. Sodium carbonate is added to the mixture and acts as a catalyst for the hydrolysis of cellulose, hemicellulose, and other large molecules into smaller fragments [9]. This solution is pressurized and heated to the operating conditions. The solution is maintained at these conditions for several minutes to several hours. Minowa et al reported a hold time of 30 minutes to complete the process [8]. The system is then cooled and the products are withdrawn.

The primary product of liquefaction is a bio-oil with yields of up to 50 wt-%. The secondary products of this process consist of a low heating value gas with yields up to 20 wt-% and char with yields up to 30 wt-%. The bio-oil from liquefaction has a heating value of 30 MJ/kg, which is a higher energy content than bio-oil produced in the other thermal chemical conversion processes such as pyrolysis [6].

Pyrolysis. Pyrolysis is the thermal decomposition of a substance in the absence of oxygen to produce liquid, char, and gas products.

Pyrolysis is not a recent technology, forms of it having existed since early civilizations. Early pyrolysis targeted solid char products in a process called carbonization, which converts biomass to carbon. In the past century, pyrolysis technology has expanded from targeting the production of char to other products. Near the turn of the 20th century, Henry Ford used a related process known as wood distillation to process scrap lumber from his automobile factories [10:255-257]. From this process, liquids were used to develop a variety of chemicals including methanol. In addition, the char and noncondensable gas were used as a heat source for his automotive manufacturing plant. In this application, the solid char, liquid extract, and producer gas were utilized in manufacturing processes. Recently, pyrolysis technology has become more sophisticated with the development of various types of reactors and the use of advanced controls for system monitoring.

Pyrolysis can occur in two distinct modes: slow pyrolysis and fast pyrolysis. For slow pyrolysis systems, the primary yield is char whereas fast pyrolysis systems target high liquid yields.

In slow pyrolysis, the biomass is converted in an oxygen-free environment at temperatures of 400 to 600 °C. This process converts the biomass to char with yields up to 30 wt-% [6]. The principal remaining product is noncondensable gases with a higher heating value of 5 to 10 MJ/m^3 [6].

In the late 20th century, the focus of pyrolysis shifted to production of organic liquids, known as bio-oil, which can be used as either a liquid fuel or source of chemicals. In fast pyrolysis, the thermal decomposition occurs at very high heating rates of several thousand degrees Celsius per minute [11]. Additional criteria for fast pyrolysis of biomass include stable reaction temperatures near 500 °C with a reactor residence time of two seconds or less. Rapid cooling of the exit stream is also important to maximize the bio-oil yield [12]. The process of fast pyrolysis is slightly endothermic when the reactor temperature is near 500 °C [13]. The bio-oil is a dark brown liquid with a density of approximately 1.2 kg/liter [14]. The bio-oil yield can be

as high as 70 wt-% with a heating value of 23 MJ/kg [6]. The remaining mass balance is secondary products consisting of char and noncondensable gases.

2.2. Mechanisms of Fast Pyrolysis

Fast pyrolysis involves many unknown and complex chemical reactions. Cellulose will be converted to levoglucosan under fast pyrolysis conditions. Also, alkali content in biomass will act as a catalyst and dehydrate the cellulose into hydroxyacetaldehydes. However, under slow pyrolysis conditions, cellulose will convert to char and water through dehydration. Fast pyrolysis reactions also convert hemicellulose to furanoses and furans and lignin to aromatic compounds [2].

The process of pyrolysis of biomass has been modeled by several researchers [15,16,17,18,19,20,21] and utilized by di Blasi [22], Bryden [23,24,25], and Molaaen et al [26] relies on a global approach to represent the actual reactions. These reactions characterize the overall degradation of biomass, which consists of cellulose, lignin, and hemicellulose. Three competing primary reactions convert the biomass to condensable bio-oil, solid char, and noncondensable gases. The secondary reactions convert the bio-oil fraction to char and noncondensable gases. Figure 2 provides a summary of the global primary reactions (1, 2, and 3) and the secondary reactions (4 and 5). The reactions follow an Arrhenius type expression.

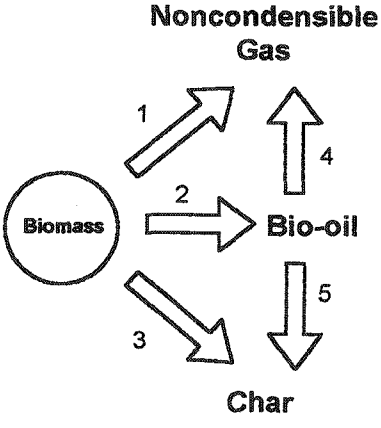

Figure 2. Reaction scheme for thermal decomposition of biomass

In fast pyrolysis, the primary reactions are targeted mainly for the production of bio-oil. The secondary reactions are avoided because the bio-oil is transformed into noncondensable gas and char. Therefore, the residence time from the reaction zone to the condensation apparatus should be minimized.

The biomass introduced into a fast pyrolysis reactor is finely ground to a sieved dimension of 1 mm or less for typical fast pyrolysis. This size ensures rapid heating of the particle in order to maximize bio-oil yield. Small particle size also prevents large spatial thermal gradients within the particle, which adversely affect the bio-oil yield. If the particle is thermally large, the surface material of the particle will be at the appropriate temperature and heating rate for fast pyrolysis, but inner material will be at reduced temperatures and heating rates, which are more consistent with slow pyrolysis. The fast pyrolysis reactor system selected must be capable of generating high heat transfer rates in which the particle temperature increases rapidly. As mentioned previously, fast pyrolysis thermal decomposition often occurs at very high heating rates of several thousand degrees Celsius per minute [11]. "As particle size increases, liquid yields reduce as secondary reactions within the particle become increasingly significant [12]."

In addition to sufficiently small biomass particles, the biomass should have moisture content of 10 wt-% or less. The evaporation of water is energy intensive causing a higher energy requirement to pyrolyze the biomass. In addition, if the moisture content of the bio-oil is sufficiently high (30 wt-% or greater), the bio-oil may separate into two phases resulting in low quality fuel [27].

Liquid Product. The bio-oil yield from biomass can be as high as 70 wt-%. The bio-oil has a density of approximately 1.2 kg/liter and ranges in color from dark green to dark red to black. The color is dependent on the biomass feedstock and the amount of char that is contained in the bio-oil. The properties of the bio-oil pyrolyzed from wood are detailed in Table 1. The lower heating value suggests that

its energy content is less than half of the energy content of light fuel oils. The fraction of water ideally should be near 15 wt-% to avoid separation of the bio-oil. The acidic nature of the bio-oil, as indicated by the pH level, gives the bio-oil a distinct, acidic odor.

Table 1. General properties of bio-oil [28]	
Property (wet basis)	**Range**
Density, kg/liter	1.11 – 1.30
Lower heating value, MJ/kg	13 – 18
Viscosity, cSt	13 – 80 (at 50 °C)
Thermal conductivity, W/m-K	0.35 – 0.43
Specific heat capacity, kJ/kg-K	2.6 – 3.8 (at 25 – 60 °C)
Pour point, °C	-9 – -36
Coke residue, wt-%	14 – 23
Flash point, °C	50 – 110
Ignition point, °C	110 – 120
Water, wt-%	15 – 30
pH	2.0 – 3.7
Char, wt-%	0.01 – 1
Vapor pressure, kPa	5.2 at 33.5 °C 62.5 at 75.4 °C
Surface tension, mN/m	29.2

The elemental analysis of the bio-oil derived from woody biomass is described in Table 2. Note that this bio-crude oil contains a high fraction of oxygen; thus, the mixture is often known as an oxygenated organic fuel. The molecular weight of the bio-oil is typically several hundred Daltons [11].

Table 2. Elemental analysis of bio-oil [28]	
Element (wet, mass basis)	**Range**
Carbon, wt-%	32 – 49
Hydrogen, wt-%	6.9 – 8.6
Nitrogen, wt-%	0 – 0.1
Oxygen, wt-%	44 – 60
Sulfur, ppm	60 – 500
Chlorine, ppm	3 – 75
Potassium and Sodium, ppm	5 – 500
Ash, wt-%	0.01 – 0.20

Bio-oil is comprised of many chemicals of which the main chemical classes are listed in Table 3 as reported by Radlein [29]. Pyrolytic lignin represents a large fraction of the oil.

Table 3. Compound classes in bio-oil [29]	
Chemicals by class	wt-% of bio-oil
C1 compounds (formic acid, methanol and formaldehyde, carbon dioxide)	5 – 10
C2 – C4 compounds (linear hydroxyl and oxo substituted aldehydes and ketones)	15 – 35
C5 – C6 compounds (hydorxyl, hydroxymethyl and/or oxo substituted furans, furanones, and pyranones)	10 – 20
C6 compounds (Anhydrosugars)	6 – 10
Pyrolytic Lignin	15 – 30
Other	11 – 25

Also reported by Radlein [29] are specific chemicals in bio-oil from tests with Eastern Spruce biomass at 500 °C. Table 4 summarizes these values. On a moisture free basis, pyrolytic lignin represents 32 wt-% of the bio-oil.

Table 4. Components bio-oil from fast pyrolysis of Eastern Spruce [29]

Component	Wt -% of bio-oil for Eastern Spruce
Formic Acid/ Formaldehyde	8.9
Hydroxyacetaldehyde	9.6
Acetic Acid	4.8
Diacetyl	1.1
Glyoxal	3.1
Acetol	1.5
Levoglucosan	4.9
Cellobiosan	3.1
Water	22.4
Pyrolytic Lignin	24.2

If the biomass is pretreated, the amount of levoglucosan can increase significantly. Radlein reports that with a prehydrolyis pretreatment of a Poplar-Aspen hardwood mixture, the levoglucosan ($C_6H_{10}O_5$) increased from 3.0 to 30.4 wt-% of the biomass [30]. In the same test, cellobiosan increased from 1.3 to 5.7 wt-%. Levoglucosan and cellobiosan represent major components of the bio-oil.

Solid Product. The char yield can range from 5 to 20 wt-% depending on the type of biomass and the fast pyrolysis conditions. The volatile matter in the char can range from 15 to 45 wt-% with a lower heating value of 32 MJ/kg [11]. The char also

contains essentially all of the ash content and alkali metals of the original biomass feedstock. Pyrolytic char can be very reactive when exposed to an oxidizing environment. It is not unusual for this char to auto-ignite when exposed to air even after being cooled to room temperature. The size of char particles is largely dependent on the size of the original biomass particles and range in size from submicron particles to larger than 0.5 mm.

Gas Product. The noncondensable gases created during fast pyrolysis account for 10 to 25 wt-% of the yield. Table 5 provides data from a specific test of fir and spruce bark in a vacuum pyrolysis reactor [1]. The various fractions of each gas can vary greatly depending on biomass type, pyrolysis reactor type, and residence time. It should be noted that nitrogen is often used as a carrier gas and the components of producer gas are given on a nitrogen-free basis.

Table 5. Composition of noncondensable gases from a vacuum pyrolysis reactor* [1]

Gas component	% Volume
H_2	6.6
CH_4	10.0
CO	32.0
CO_2	41.5
C_2H_6	1.5
C_2H_4	1.5
C_3H_6	1.4
C_3H_8	0.4
CH_3OH	0.4
C_4H_{10}	0.4
C_4H_8	0.6
C_5H_{12}	0.6
Other species	3.1

*Fir and Spruce Bark

2.3. Current Challenges in Fast Pyrolysis

Current industry challenges include both economic and technical issues. The economic challenges will likely determine the success of this technology publicly and politically.

Similar to the crude-oil industry, the economics of the operation will likely be based on the ability to produce high-value chemicals. Technology development in this area will be a key to the economic viability of fast pyrolysis. Current work focuses on a bio-refinery concept [31], which could produce various value-added products. For example, anhydrosugars could undergo hydrolysis and fermentation to produce alcohol. Fertilizers, adhesives, and fuel enhancers can be derived from bio-oil. The liquid could also undergo catalytic reforming to produce hydrogen [32].

Additional challenges revolve around removing char from the product stream with various types of solid separators. The use of a bio-oil as a suitable fuel in gas turbines is plausible when a pyrolysis system is developed which produces essentially char free bio-oil, has a minimal pressure drop, and is low maintenance. However, the economics to compete with current coal technologies will not be enough to justify its use. Other advantages include reduced NO_X and SO_X emissions as well as a CO_2 net production of zero [33]. This combination of being char-free as well as having good emission characteristics will allow bio-oil to be a successful fuel in gas turbines.

2.4. Aerosol Versus Vapor Formation

In the fast pyrolysis community, there has been much debate on the transport phase of bio-oil exiting a pyrolysis reactor. At pyrolysis temperatures, the condensable bio-oil may form as liquid droplets in the reactor or it may circumvent the liquid phase and vaporize.

Knowledge of the condensable transport phase is important in making fast pyrolysis economically viable as it allows for greater optimization of fast pyrolysis systems. For instance, if the condensables are present in vapor form in the reactor, catalytic reforming potentially can be used to target the production of specific high-value chemicals. Maximization and quality of the bio-oil yield have direct impact on the economics of the fast pyrolysis process. Bio-oil collection and solid removal systems can be designed more efficiently based on the state of the bio-oil as it leaves the reactor. For example, if the bio-oil exits the reactor in the form of liquid aerosols, there are possible issues of cracking if a direct contact solid separator is used before condensation. Also, identifying the transport state of the condensable fraction will directly impact mathematical modeling given that the vast majority of modelers assume that the bio-oil is a vapor in the reactor [34,35,36,37].

The high heat and mass transfer rates imposed by most fast pyrolysis reactors suggest that liquids produced from the particle evaporate and are removed from the surface of the biomass particle. Suuberg [38,39] suggests that despite the low measured vapor pressures for cellulose and levoglucosan, any possible liquids will quickly leave as a vapor under fast pyrolysis conditions. Additionally, current literature does not propose a mechanism for aerosol generation during pyrolysis.

Colbeck defines aerosol as "a dispersion of fine solid particles or liquid droplets in a gas" [40]. Similarly, Reist defines aerosol as "a suspension of solid or liquid particles in a gas" [41]. Although the precise definition of aerosol suggests the particle is a solid or a liquid, in the case of pyrolysis, aerosol refers to small liquid droplets. Typical sizes of liquid aerosols range from 0.01 μm for smoke up to 20 or 30 μm for fog [40]. Most often, aerosol science is applied water droplet formation in the atmosphere, but the general principles apply to any liquid aerosol.

Many visual observations of the product stream exiting a fast pyrolysis reactor suggest that the bio-oil is a liquid aerosol because of its smoky appearance. Smoke is considered a collection of micron and sub-micron sized liquid droplets. Many

experimentalists believe the collected fraction is all or mostly liquid aerosols at the exit of the freeboard [11].

Oja and Suuberg [38] have measured the saturation vapor pressure of levoglucosan and cellobiose ($C_{12}H_{22}O_{11}$), which is closely related to cellobiosan. At 404.98 K, the vapor pressure of levoglucosan was measured at 4.15 Pa. At 488.02 K, the vapor pressure of cellobiose was measured at 0.0186 Pa. Also, Radlein suggests that pyrolytic lignin has a negligible vapor pressure at pyrolysis temperatures [29]. The low vapor pressures for these compounds suggest that they exist as liquid, not vapors, at pyrolysis temperatures.

There is also experimental evidence for bio-oil production as aerosol. Diebold [42] performed a hot wire experiment in which electric current was passed through a wire and used to cut into a piece of biomass. While cutting through the biomass, the current is discontinued and the reaction products are frozen to the wire. Upon visual inspection of the biomass cut, a "brownish varnish" is evident on either side of the cut. In a related experiment by Lédé, biomass was forced into a heated spinning disk [43]. The high contact pressure promotes heat flow to the piece of biomass, which initiates devolatilization. During the experiment, a liquid trail could be observed behind the biomass on the spinning disk. This visual evidence of a liquid suggests that it is feasible that the bio-oil is formed as a liquid and exits as liquid aerosols.

Lédé et al [44] suggests that internal pressures created during the fast pyrolysis process may cause the liquid droplets to be ejected from the particle and into the product stream. Another possibility is that shear forces between the gas flow and particle causes droplets to become entrained in the gas flow.

A model for cellulose pyrolysis suggests that biomass enters an "active" intermediate state before the primary reactions begin. Experimental evidence suggests that the biomass in the "active" intermediate state is in liquid form [45]. Before any primary reactions have occurred, the liquid in this intermediate state

potentially exits from the reactor providing a source of liquid aerosols. Piskorz et al [46] suggest that based on the high molecular weight of the compounds present in bio-oil, these compounds are entrained in the gas flow during the "active" intermediate state.

As with formation of water droplets in the atmosphere, liquid aerosols usually require a nucleation site to begin the formation of the droplet. Typically, the surrounding gas is saturated with respect to the condensing species. Heterogeneous nucleation is defined as the condition where the droplet nuclei are not of the same composition as the condensing liquid. Nuclei can range in size from a small cluster of molecules called ions to particles of 2 μm in diameter. If char acts as a nucleation site in fast pyrolysis, these nuclei would be classified as "large" with diameter ranging from 0.4 to 2 μm [41].

2.5. Current Technology

Many different system configurations for fast pyrolysis have been developed. There has been extensive research on many different types of reactors [47]. These reactors are discussed in the following section. A variety of solid collectors have been studied to remove the char from the product stream. The condenser train often consists of several components to efficiently gather bio-oil from the product stream. In addition, various methods for pre-processing the biomass have been utilized in order to bring the smallest dimension of the biomass to 1 mm or less.

2.5.1. Fast Pyrolysis Reactors

The following reactor descriptions are intended to give a brief overview of the technology that exists to thermally process biomass under the fast pyrolysis regime. The main reactors that have recently been explored and their relative advantages and disadvantages are discussed.

Vacuum pyrolysis. Although heating rates are much lower than traditional fast pyrolysis methods, vacuum pyrolysis has the advantage of quickly removing the product stream. Often this process is performed in a hearth type reactor and has the advantage of using larger particles than are typically required in fast pyrolysis. The main disadvantages are larger equipment and higher costs [47]. Another type of vacuum pyrolysis reactor consists of a complicated system where molten salt provides the heat to quickly pyrolyze the incoming biomass. The product stream is rapidly withdrawn from the reactor. The main disadvantage is the complexity of the system compared to the hearth design.

Ablative reactor. Heating of the biomass particle occurs by forcing the biomass against a heated surface as shown in Figure 3. Through this action, the biomass devolatilizes and exits the reactor [48]. The main advantages of this type of reactor include no use of carrier gas. The biomass particles can also be larger than in other fast pyrolysis processes. Scale-up issues limit this process through the amount of heat which can be supplied to the relatively small reactor.

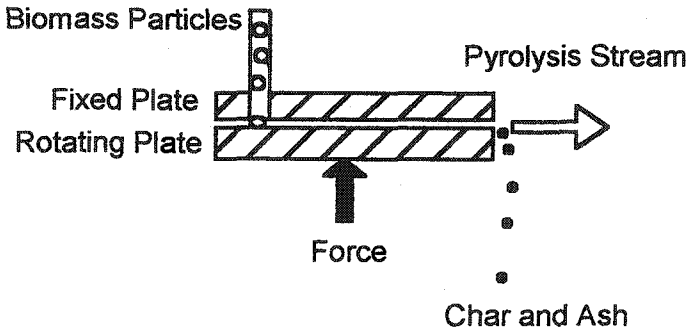

Figure 3. Ablative pyrolysis

Fluid bed. The fluid bed reactor consists of a sand bed in which an inert gas bubbles through the sand causing it to behave similar to a liquid as shown in Figure

4. When heated to pyrolysis temperatures, heat is transferred by convection and conduction to the incoming biomass particles. This type of reactor is easily controlled resulting in consistent temperatures in the sand bed. Preprocessing of biomass is required to achieve small particles with the smallest dimension of 1 mm or less. Many types of biomass including woods and agricultural residues have successfully been fast pyrolyzed with bio-oil yields ranging from 40 to 70 wt-% [49].

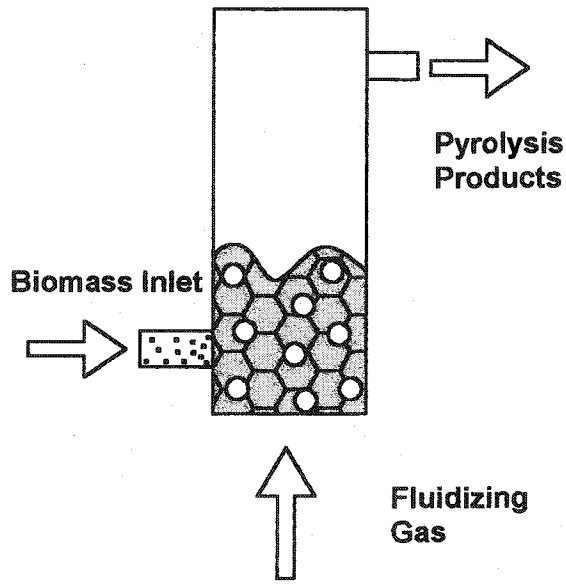

Figure 4. Fluid bed pyrolysis

Circulating fluid bed. Similar to the fluid bed, the circulating fluid bed reactor allows for the sand to be ejected from the reactor and separated by a cyclone as shown in Figure 5. The collected sand is then circulated back into the reactor. This type of fluid bed has the advantage of higher inert gas flow which results in a lower residence time in the reactor. This theoretically limits the secondary reactions which can reduce the bio-oil yield. This system is more expensive to construct compared to the standard fluid bed. This technology is developed and a unit capable of processing 650 kg/hr has been constructed [48].

Vortex reactor. The vortex reactor concept, illustrated in Figure 6, operates by flowing gas at high velocities and forcing biomass particles into the cylindrical reactor. The particles are entrained in the flowing gas and are heated by rotating around the hot inner surface of the cylindrical reactor [48,50]. This type of reactor has lower bio-oil yields than typically achieved by other reactor types.

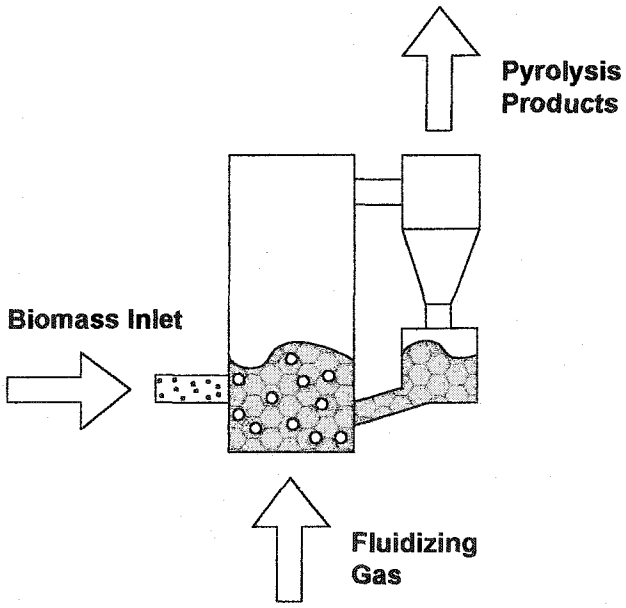

Figure 5. Circulating fluid bed pyrolysis

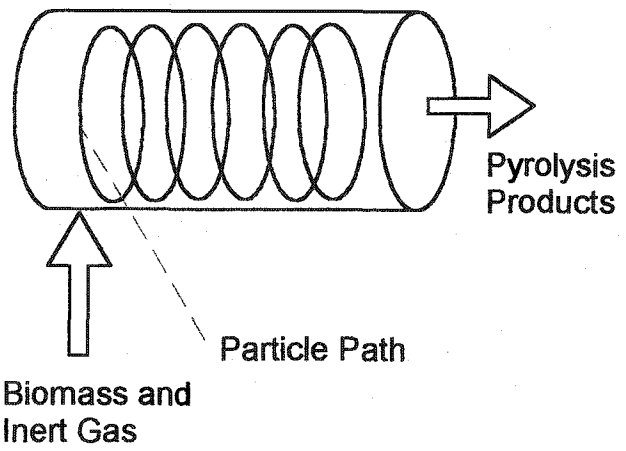

Figure 6. Vortex pyrolysis

2.5.2. Solid Removal Systems

After the exit of the fast pyrolysis reactor, the product flow often is passed through a solid removal system. This system is required primarily to remove char produced by the fast pyrolysis process. For reactors that include a sand or catalytic media, the cyclones also remove this granular material that escapes the reactor. Normally, the purpose is to remove all solids from the flow in an effort to collect bio-oil that is free of char and other particles. As the char is removed, much of the alkali from the original biomass feedstock is also removed since the char contains the vast majority of this fuel contaminant.

Cyclones. The most common component of solid removal systems is the cyclone separator as shown in Figure 7. The product stream that exits the reactor enters a cylindrical body in which solid particles are forced out of the flow and are collected in catch containers below the cyclones. Advantages are low cost and minimal pressure drop; however, this technology is typically not efficient for particles smaller than 5 μm. Many current and accepted design methods related to cyclones are organized by Hoffman and Stein [51].

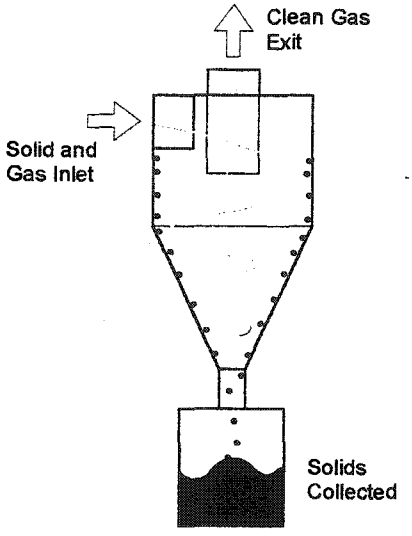

Figure 7. Cyclone separator

Sintered filters. In this method, the exiting hot product stream enters a sintered metal filter, as shown in Figure 8, which captures the solid particles as the product flow pass through the filter. Czernik et al [52] have successfully utilized this filter type in reducing the ash content in the collected bio-oil to less than 0.01 wt-%. The pressure drop across the filter increases with time as the solids are collected. While the pyrolysis system is operating, regeneration of the filter is difficult due to the adhesive nature of the char.

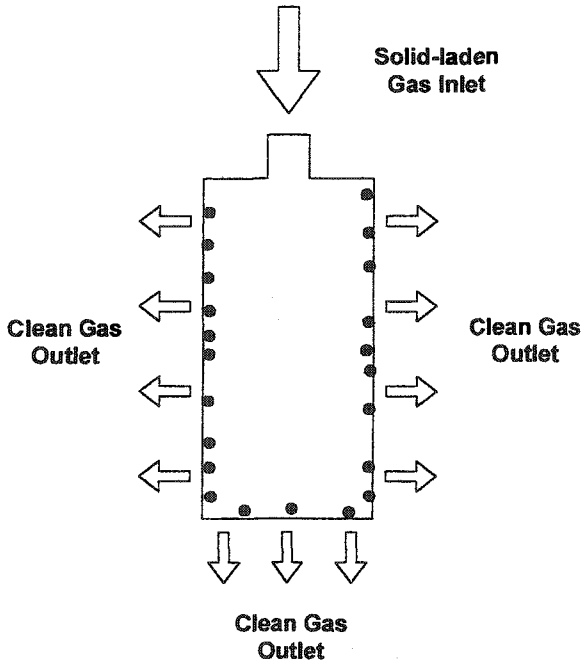

Figure 8. Sintered filter

Liquid filtration. Liquid filtration involves filtering the bio-oil after it is collected to remove the solids. The main issue involves the loss of liquid due the formation of sludge around collected char particles. This sludge clogs the filter reducing the usefulness of the process [52].

Moving bed granular filter. The moving bed granular filter shown in Figure 9 represents the most recent developments in the separation of solids from the

product stream in fast pyrolysis. This filter operates by collecting the solids on a collection gradient established in slow flowing aggregate. If the filter was a packed bed design, the pressure drop would continue to rise and periodic cleaning of the filter would be required. After an initial startup period, the pressure drop remains constant in the moving bed. The effectiveness [53] of the filter at room temperature conditions indicates that this filter is capable of removing nearly all of the char, ash, and sand from the product stream. The filter, however, is still under development.

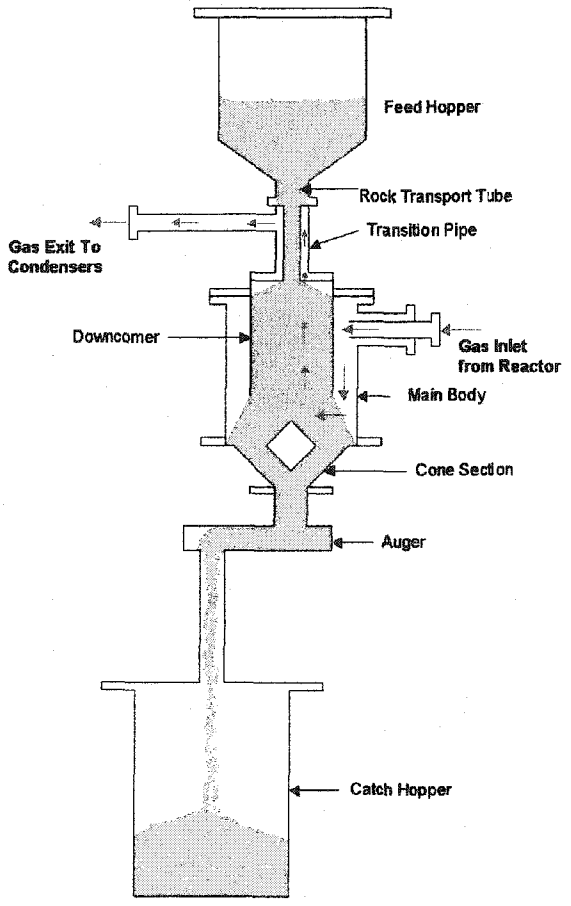

Figure 9. Moving bed granular filter

2.5.3. Liquid Collection

To collect the bio-oil after particulate removal, many systems have been developed that utilize multiple stages in an attempt to maximize the collection efficiency of the bio-oil. Usually the first step is to pass the product stream through a device that cools the mixture. One method uses direct contact between the cooling substance and the product stream. By wet scrubbing the product stream, a fine spray or mist is injected into the product stream and the bio-oil collects at the base of the device. Wet scrubbing requires the use of a pump and nozzles to circulate the cooling fluid. Another method relies on a shell and tube heat exchanger in which the cooling fluid is held separate from the product stream. Issues with this device include potential clogging of the product gas flow tubes.

After initial removal of bio-oil from the product stream, a secondary device(s) is often used. This may include the use of an electrostatic precipitator (ESP) that relies on charging already formed aerosols in the cooled stream and collecting them on a surface. A second method utilizes a packed bed filter, which has the advantage of simplicity. However, as bio-oil is collected, the pressure drop across the filter increases and can be a limiting factor during a fast pyrolysis test. A combination of the two devices may also be used to reduce the collection requirements of the packed bed.

2.6. Fast Pyrolysis Product Markets

Bio-oil primarily can be used as a stationary fuel for producing electricity in gas turbines as well as converted diesel engines. The fuel could also be burned in a boiler for heating purposes if a lower quality bio-oil is produced. Possible chemical conversions and refining may allow for the bio-oil to occupy current gasoline or diesel markets. A promising option as a fuel would be to couple the pyrolysis plant with a combined cycle plant to produce electricity [33].

Another important area for the bio-oil lies in the chemical production of targeted high value products. Levoglucosan is one chemical that is actively targeted in research as a likely compound for extraction from the bio-oil [30]. In addition, the bio-oil has been processed to produce food flavoring, resins, and fertilizers.

The secondary products also have significant potential markets. The char yield collected is currently being marketed as a food grilling fuel replacing traditional charcoal products. The char is currently being investigated as an activated carbon [54] and may prove useful in collecting mercury emissions or as a catalyst.

3. EXPERIMENTAL APPARATUS

3.1. Fast Pyrolysis System Components

The pyrolysis system utilized in this study is shown in Figure 10 and details of each subsystem are provided. The system consists of the following components:

- Fast pyrolysis reactor: fluid bed reactor and plenum
- Biomass feed system: feed hopper, feed auger, and injection auger
- Burner system (not shown)
- Cyclone solid separators
- Bio-oil collection system: condenser train and packed bed
- Data acquisition system (not shown)

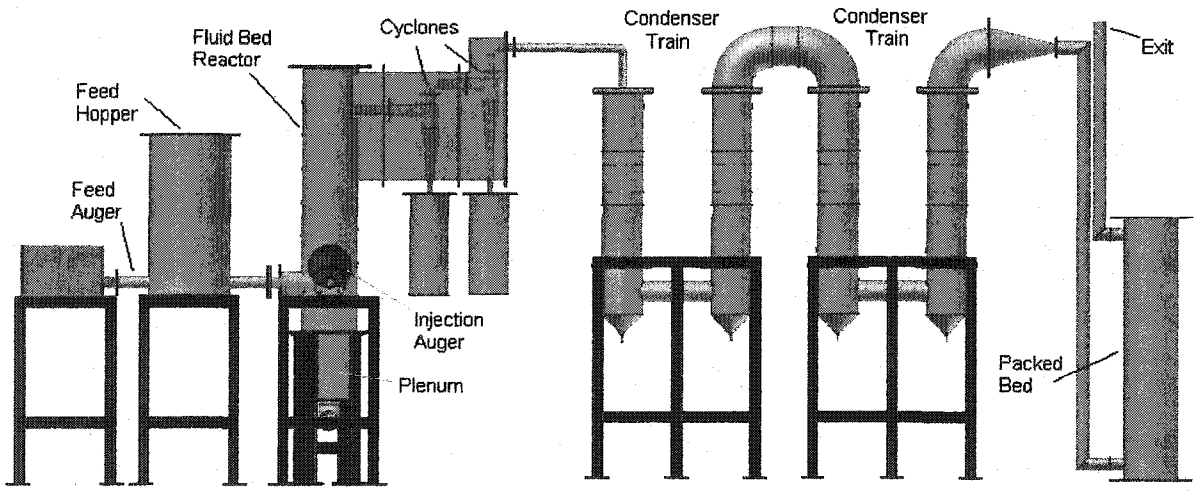

Figure 10. Illustration of pyrolysis system

Fast pyrolysis reactor. The pyrolysis reactor used in this study is dimensioned in Figure 11. The height of the reactor is 1 meter with a diameter of 16.2 cm. The reactor is constructed of stainless steel for corrosion resistance. The plenum located at the base of the unit allows for the inflow of gaseous nitrogen. In

addition, there is an inlet auger into the reactor for feeding biomass. The annulus allows for the flow of hot combustion gas around the bed, supplying the reactor with the heat required for fast pyrolysis. The unit has several thermocouples extending from the top of the unit to various depths ranging from 5 cm to 29 cm in the sand bed. In addition, pressure taps are located at the top of the reactor to monitor reactor pressure.

The sand bed located in the inner cylinder has a depth of 32 cm with a sieved diameter of the sand of 735 μm as shown in Figure 12. The sand originates from near Eau Claire, Wisconsin (Red Flint Sand and Gravel) and is approximately 95 wt-% Silica, 2 wt-% iron oxide, 0.9 wt-% aluminum oxide with the balance being trace amounts of other oxides.

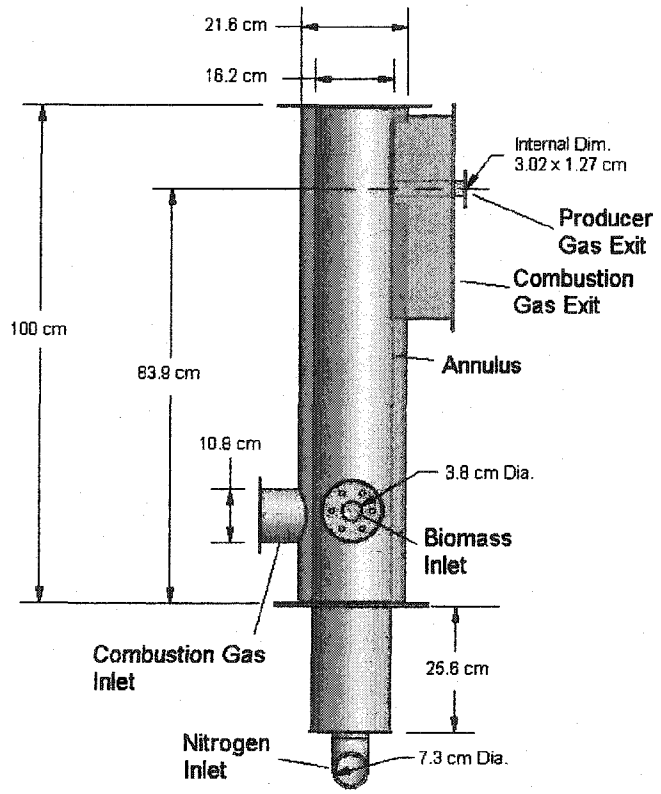

Figure 11. Fast pyrolysis reactor

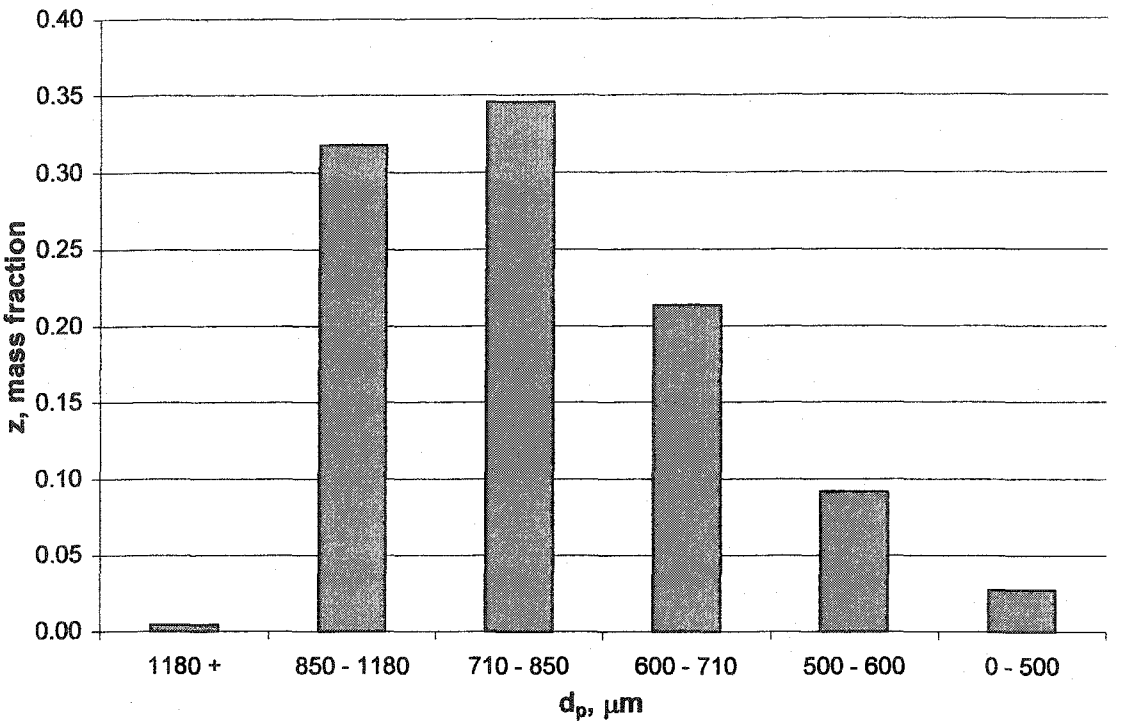

Figure 12. Particle size distribution of sand

Biomass feed system. The biomass feed system consists of a hopper, a metering auger, and an injection auger. The hopper stores the biomass and has a capacity of 45 liters. A metering auger screw regulates the amount of biomass being fed into the reactor. An injection auger quickly injects the biomass from the metering auger directly into the sand bed. This auger is water-cooled at the bed connection point to prevent premature devolatilization of the biomass. A purge flow of nitrogen flows through the injection auger tube into the bed, which prevents the back flow of producer gas and sand. An agitation arm is located inside the hopper and its function is to prevent bridging of the biomass during metering. The system is constructed of stainless steel with the exception of the carbon steel augers.

Burner system. The burner system provides heat required for endothermic pyrolysis. This system consists of a natural gas burner and a ceramic tube with a stainless steel shell. The diameter of the ceramic tube is 16.5 cm with a wall thickness of 3.8 cm. The tube length is 1.6 m. This burner is supplied house compressed air and utility-supplied natural gas. Upon combustion, the hot gas stream flows down the tube and exits into the annulus around the internal tube of the reactor which contains the sand bed. The hot gas stream then exits into a cavity surrounding the cyclone separators described in the next section. After the cyclones, the combustion product stream exits to the outside environment. The burner is capable of 44 kW_{th}.

Solid separator. This system consists of two 6 cm diameter cyclone separators in series. The cyclones are located at the exit of the reactor and remove the ash, sand, and char that are contained in the product stream. Attached to the base of the cyclones are two suspended catch cylinders with an approximate volume of 7 liters each. The cyclones and catches are constructed of stainless steel. The cyclones are designed with a 50% cut diameter of 3 μm at the typical flow rates of the system as described in Appendix C. However, the efficiency of particulate removal drops off below 10 μm, allowing some char to pass the cyclones and escape into the bio-oil collection system. The detailed dimensions of the cyclones are included in Figure 13.

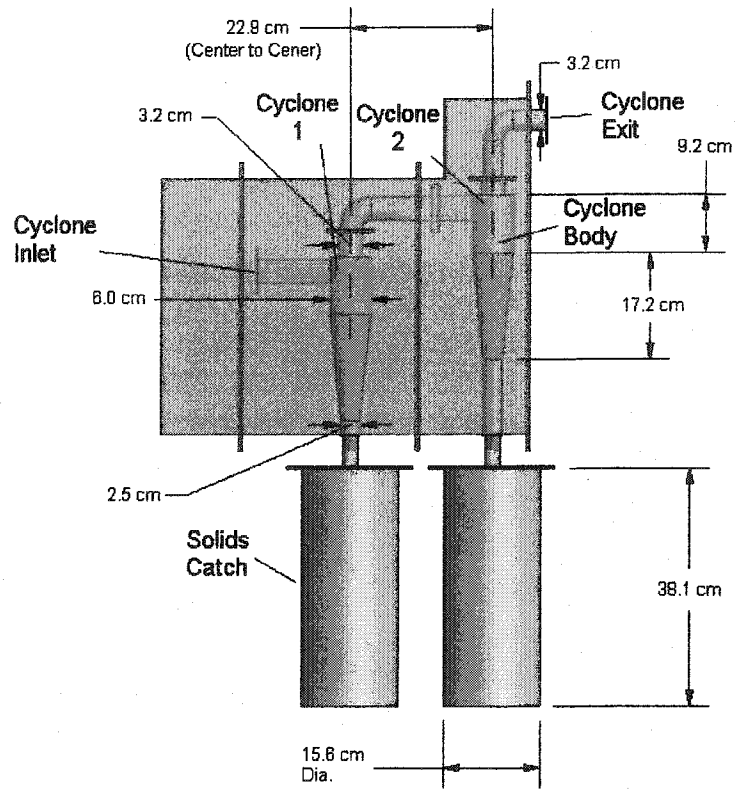

Figure 13. Cyclone system

Bio-oil collection system. The bio-oil collection system is comprised two main components. The first component is a condenser train designed to remove the bio-oil in fractions. The second component is a packed bed filter.

The condenser train is a shell and tube design as illustrated in Figure 14. The product stream flows on the inside of the tubes and cooling water flows on the outside. There are four stages included in this design with collection of liquids occurring at the base of each stage. The first stage contains a 3.2 cm pipe surrounded by a water jacket. Vapors flowing through the central pipe are cooled by the tap water flowing through the water jacket. A single pipe of relatively large diameter is used in this first stage of condensation to avoid plugging by viscous, high molecular weight organic compounds that condense at this stage. The second, third, and fourth stages contain seven 1.6 cm diameter tubes.

The flow enters condenser train at 450 °C and 5 wt-% of the total bio-oil is collected at the first stage. This fraction is typically the most viscous and has solidified upon cooling to room temperature. The flow enters the second stage at 145 °C and 45 wt-% of the total bio-oil is collected at this stage. The flow enters the third stage and collects 10 wt-% of the total bio-oil catch. This fraction of bio-oil contains the highest concentration of water at 50 to 65 wt-%. The flow enters the fourth condenser at 38 °C and collects 15 wt-% of the total bio-oil. The flow exits the condenser train at 15 °C. The remaining 25 wt-% of the total bio-oil collected is captured by a packed bed filter.

Upon exit from the condenser train, the flow enters a packed bed filled with glass fiber strands of 8 μm diameter. The height of the packed bed is 1 meter with a diameter of 20.3 cm. The filter is designed to remove remaining aerosols through interception and impaction on the glass fibers. After exiting the fixed bed the gas enters a volumetric gas meter and then exits to the atmosphere.

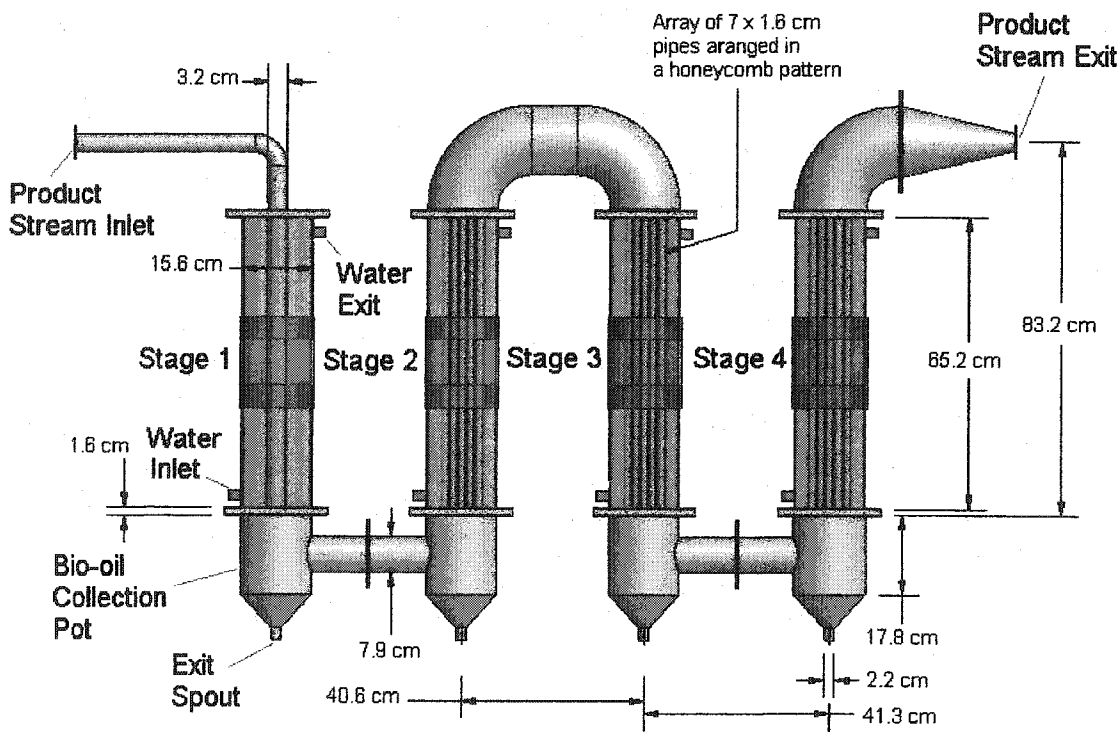

Figure 14. Condenser system

Data Acquisition System. The data acquisition system consists of LabVIEW 5.1 software on a Dell Dimension L500r personal computer to which a National Instruments SCXI-1000 chassis is connected. Through this platform, the signals from several thermocouples and pressure transducers are recorded. The software records raw data at a prescribed rate of 1 Hz and is analyzed in spreadsheet format. The pressure transducers and thermocouples can be relocated in the system as testing requires.

For some tests, a Varian CP-2003 micro-gas chromatograph was available to analyze the gas composition of the noncondensable gases. In this case, a sample stream was drawn at the exit of the packed bed filter. Additional details related to the data collection components is located in Appendix D.

3.2. Fast Pyrolysis Operating Conditions and Procedures

The fast pyrolysis system is typically operated at the conditions shown in Table 6. The pressure drop across an orifice in the gas burner measures the natural gas flow and is adjusted to maintain a sand bed temperature, T_{bed}, of approximately 500 °C. The combustion air to the burner remains constant. The mass flow on nitrogen, m_{N2}, remains constant through all tests.

Table 6. Typical fast pyrolysis operating parameters

T_{bed}	m_{N2}	m_b	d_s	d_b	t_{res}	p_{fb}	h_{bed}
°C	kg/hr	kg/hr	μm	mm	s	kPa	Cm
500	15.11	6 – 10	735	< 1	1.1	106 - 115	32

The biomass feed rate, m_b, ranges up to 10 kg/hr and is controlled by the metering auger. The sand has an average diameter, d_s, of 735 μm. The biomass has a sieved diameter, d_b, of 1 mm or less. The residence time in the reactor, t_{res}, is based

on a nitrogen flow of 15.11 kg/hr and a biomass flow of 8 kg/hr. The yield of noncondensable gas was assumed to be 25 wt-%. The bio-oil yield was assumed to be 65 wt-% with a water fraction of 27 wt-%. Only the water vapor component of the bio-oil is considered in the volumetric flow in the residence time calculation. The absolute pressure of the freeboard, p_{fb}, is usually slightly above atmospheric pressure. The sand bed height, h_{bed}, is constant for all tests.

To begin operation, an initial check determines if all pressure transducers and thermocouples are properly installed and are interfacing with the data acquisition system. After this point, ball valves are checked to insure flow is routed as required for the particular test being performed. In most tests, the flow is routed through the condensers, packed bed, and volumetric gas meter. Water valves are turned on to admit cooling water to the condensers as well as the cooling coil around the injection auger. Compressed air and natural gas valves are opened and the burner is ignited. The controller adjusts the natural gas flow rate. Natural gas and compressed air flows are set at prescribed flow rates to heat up the reactor.

With the fluid bed at desired temperature and with steady condenser temperatures, nitrogen flow is started. The fluid bed and condenser temperatures are allowed to stabilize. To prepare for the injection of biomass, the natural gas flow rate is slightly increased to compensate for the endothermic pyrolysis reactions. The agitator in the hopper is turned on to prevent bridging of the biomass. The injection auger is started followed by the metering auger, which is set to attain a prescribed biomass rate.

The system is monitored with respect to bed temperature and freeboard pressure to ensure acceptable running conditions. Typically, the natural gas must be fine-tuned to achieve the desired bed temperature. The system receives biomass flow for 30 minutes to 2 hours. Once the flow of biomass is stopped, the burner is turned off. The nitrogen flows for an additional 10 minutes to pyrolyze any

residual biomass in the bed. At the end of this period, the nitrogen and cooling water are stopped.

The pyrolysis unit is allowed to cool to room temperature, which takes approximately 10 hours. This step is required to achieve mass balance on the system. If oxygen was introduced while the bed or char collectors were at elevated temperatures, the char would oxidize, making it impossible to account for it in mass balance. Even with this precaution, the reactive char gathered from the cyclones has undergone occasional spontaneous combustion at room temperature. The remaining biomass, the produced char, and bio-oil are directly measured. A sample of bed material is collected and heated in an oven to 600 °C or higher to burn off reactive material from the sand. This is used to determine the amount of residual biomass or combustible byproduct that did not leave the bed. The noncondensable gases are measured by an American Meter AC-630 volumetric gas meter located at the exit of the system.

In Figure 15, a plot of temperature as a function of height in the sand bed is illustrated for a typical test. Note that the time zero point is when biomass is introduced into the bed. The time previous to biomass injection shows that the temperature of the sand bed is heated to approximately 540 °C and then cools to the steady pyrolysis temperature. The temperature of the stream in the freeboard stays warmer than the bed temperature due to influence of hot gases in the annulus.

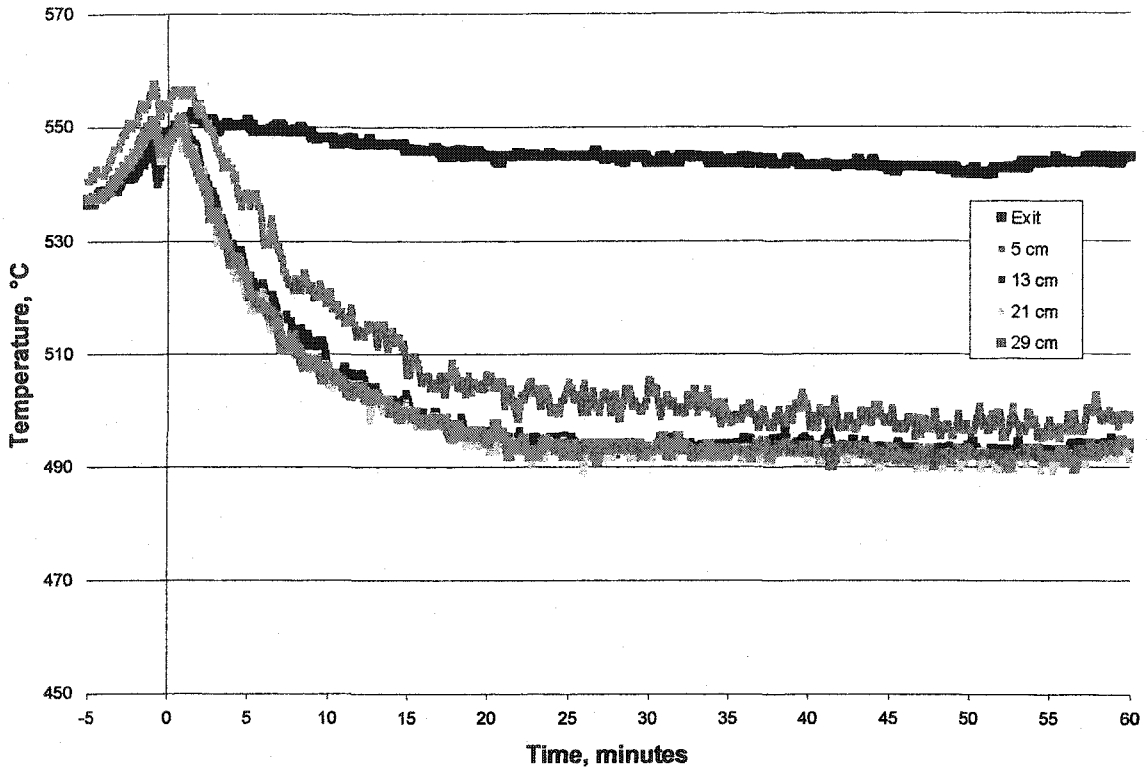

Figure 15. Typical fast pyrolysis temperature profiles

In Figure 16, the freeboard pressure as well as the pressure drop from the freeboard to the exit passage is monitored during tests. A pressure change is evident upon introduction of biomass at time zero. This change is attributed to the gas produced from the pyrolysis of biomass. In addition, the gradual rise of the freeboard pressure is due to bio-oil capture in the packed bed before the exit of the system.

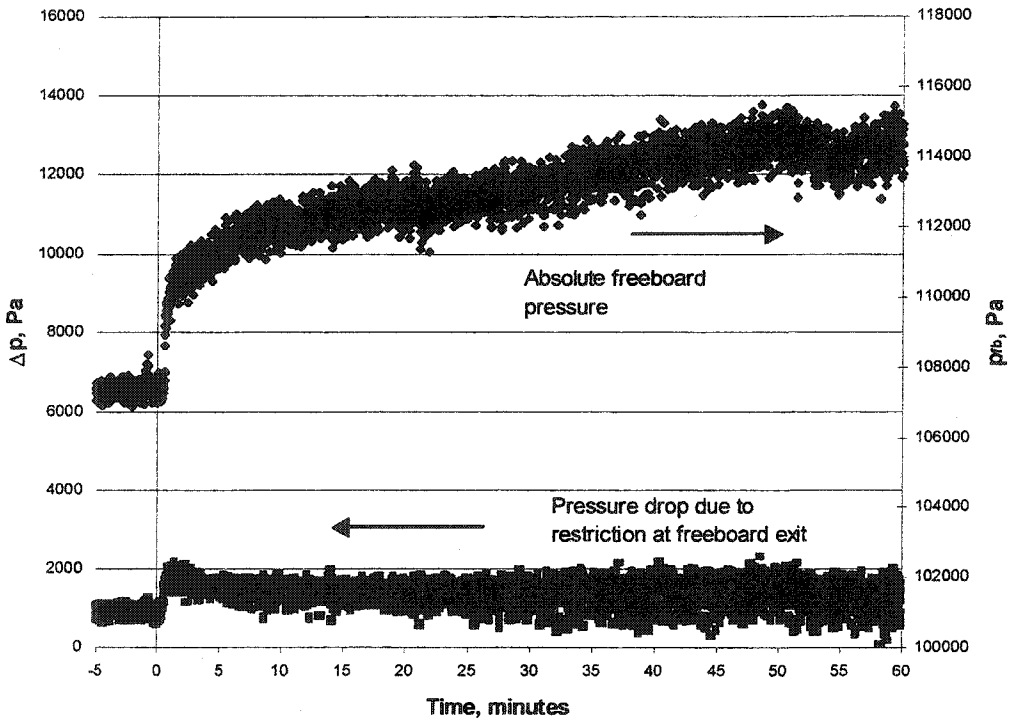

Figure 16. Typical fast pyrolysis pressure profiles

The composition of the gas exiting the packed bed filter, as determined by gas chromatography, is presented in Table 7 for red oak to give some idea of the apparent molecular weight, M_{NC}, of the gas mixture. The molecular weight, M_i, and the mole fraction, x_i, is given for each gas. Since the gas chromatograph does not measure all of the species present, the apparent molecular weight of the unknown gas was assigned a value of 70 kg/kmol. This value corresponds to 5 carbon molecules and is likely an overestimate of the actual unknown species present. The corresponding apparent molecular weight of the noncondensable gases would be 31.69 kg/kmol.

Table 7. Noncondensable gas analysis

Chemical	Chemical Formula	M_i $kg_i/kmol_i$	% Vol	x_i [a] $kmol_i/kmol$	$x_i M_i$ $kg_i/kmol$
nitrogen	N_2	28.01	92.7	-	-
carbon monoxide	CO	28.01	3.88	0.54	15.0
carbon dioxide	CO_2	44.01	1.58	0.22	9.61
methane	CH_4	16.04	0.85	0.12	1.89
hydrogen	H_2	2.02	0.24	0.03	0.07
acetylene/ethylene	C_2H_2/C_2H_4	27.05	0.20	0.03	0.73
ethane	C_2H_6	30.07	0.06	0.01	0.23
oxygen	O_2	32.00	0.01	0.00	0.05
propane	C_3H_8	44.09	0.01	0.00	0.05
unknown		70	0.42	0.06	4.06
				M_{NC} =	31.69 kg/kmol

[a] nitrogen free basis

In Table 8, the apparent molecular weight of the unknown gas was assigned the value of 16 kg/kmol, the molecular weight of CH_4. This value is likely an underestimate of the actual value for the unknown species. This corresponds to a noncondensable gas apparent molecular weight of 28.55 kg/kmol. Based on these results, the molecular weight of the noncondensable gas is quantified to be 30 ± 2 kg/kmol and this value is used in the analysis of fast pyrolysis tests.

Table 8. Noncondensable gas analysis

Chemical	Chemical Formula	M_i $kg_i/kmol_i$	% Vol	x_i [a] $kmol_i/kmol$	$x_i M_i$ $kg_i/kmol$
nitrogen	N_2	28.01	92.7	-	-
carbon monoxide	CO	28.01	3.88	0.54	15.0
carbon dioxide	CO_2	44.01	1.58	0.22	9.61
methane	CH_4	16.04	0.85	0.12	1.89
hydrogen	H_2	2.02	0.24	0.03	0.07
acetylene/ethylene	C_2H_2/C_2H_4	27.05	0.20	0.03	0.73
ethane	C_2H_6	30.07	0.06	0.01	0.23
oxygen	O_2	32.00	0.01	0.00	0.05
propane	C_3H_8	44.09	0.01	0.00	0.05
unknown		16	0.42	0.06	0.93

M_{NC} = 28.55 kg/kmol

[a] nitrogen free basis

4. EXPERIMENTAL METHODS

The purpose of this research is to provide experimental evidence as to whether bio-oil leaves a fast pyrolysis reactor as vapor or liquid aerosols. As stated previously, there is disagreement among researchers in the fast pyrolysis community on the bio-oil transport phase. If the bio-oil exists as vapor, catalytic reforming of the bio-oil would be convenient. As many catalytic processes require gaseous species in order to promote specific reactions, vaporization of the bio-oil droplets would be necessary if the bio-oil exits as liquid aerosols.

This study employs the scientific method of formulating hypotheses and performing tests of exclusion to elucidate the mechanism by which bio-oil leaves the fast pyrolysis reactor. An initial hypothesis was formulated based on anecdotal evidence. After testing of the initial hypothesis, additional hypotheses were formulated and tested to refine a theory on bio-oil formation. In this section, all of the hypotheses formulated in the course of this study and their corresponding tests of exclusions are described. Experimental results and their interpretation are not presented until Chapter 5.

In all tests, the biomass consisted of red oak or corn starch. Red oak is a representative lignocellulosic feedstock that produces approximately 10 wt-% char, 65 wt-% oil, and 25 wt-% noncondensable gases. Corn starch is an effective biomass for testing the effect of char on fast pyrolysis as typical char yields are 1 wt-% or less. A sieve analysis describing the red oak particle size is provided in Figure 17 and the corn starch sieve analysis is contained in Figure 18. The average sieve diameter, d_p, was 339 μm for red oak and 20 μm for corn starch.

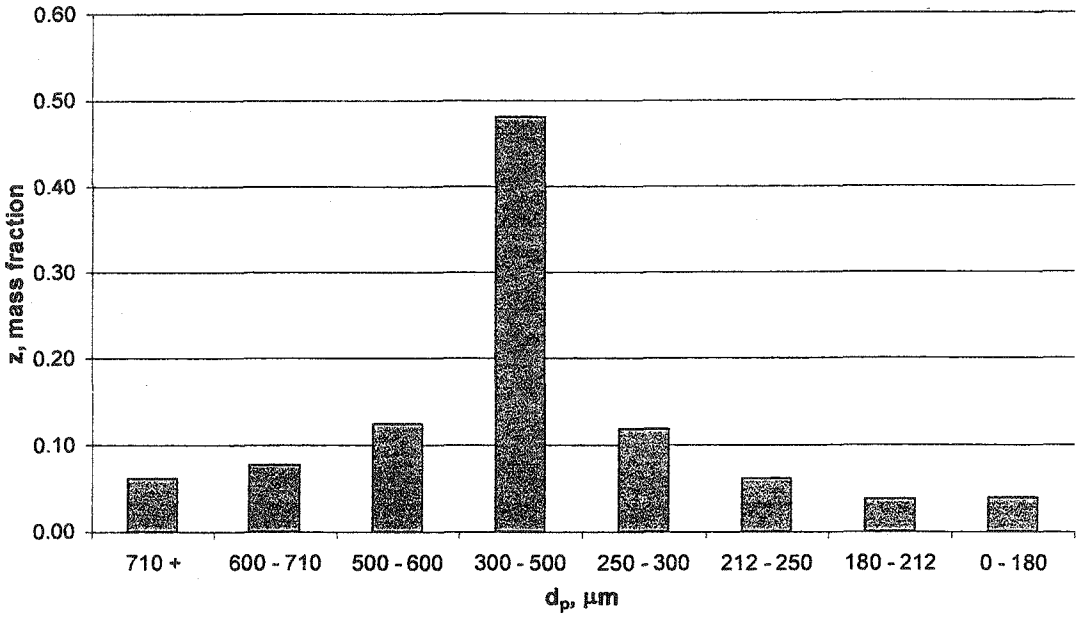

Figure 17. Particle distribution of red oak

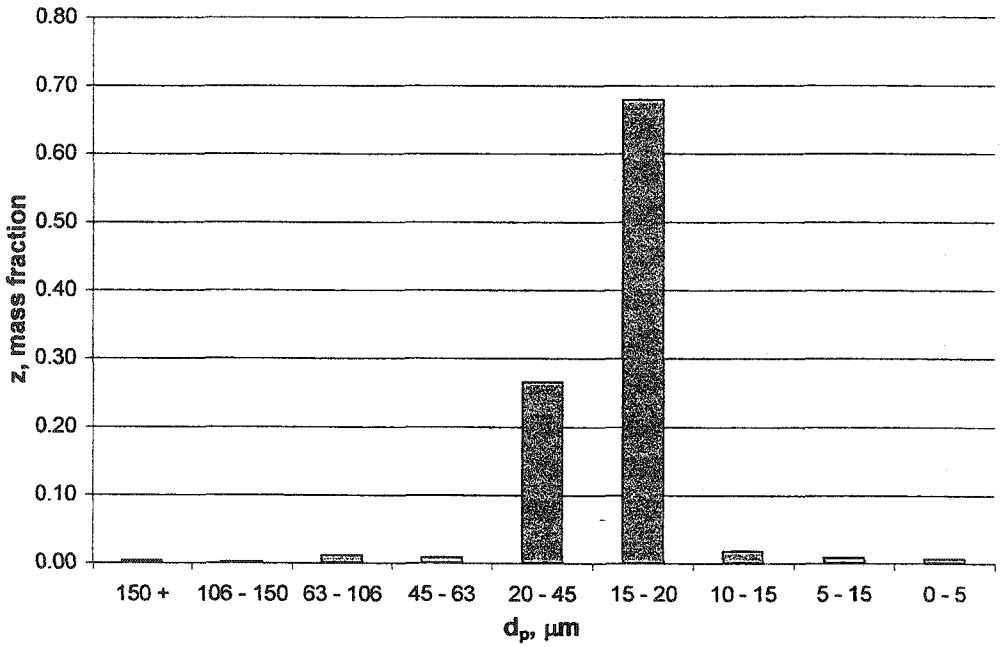

Figure 18. Particle distribution of corn starch

4.1. High Temperature Filtration Test

During typical fast pyrolysis tests, visual observations of the product slip stream venting from the freeboard suggest that the flow had the appearance of smoke. It is well-known that smoke is basically a cloud of liquid aerosols [41]. However, this visual observation does not answer whether all of the bio-oil exists as an aerosol. This observation is the basis of the first hypothesis test in that it was conceivable for the collected bio-oil to exist as liquid aerosols in the pyrolysis reactor. The molecular weight of the bio-oil has been measured to be greater than 500 Daltons [11] suggesting that the bio-oil is produced as a liquid aerosol.

Statement of the First Hypothesis. The organic hydrocarbons that are eventually collected as bio-oil are produced as liquid aerosols in the fast pyrolysis reactor.

Test of Exclusion. To test the first hypothesis, a slip stream from the reactor was passed through a packed fibrous filter. The stream was reinserted into the flow at the entrance of the condenser train as shown in Figure 19.

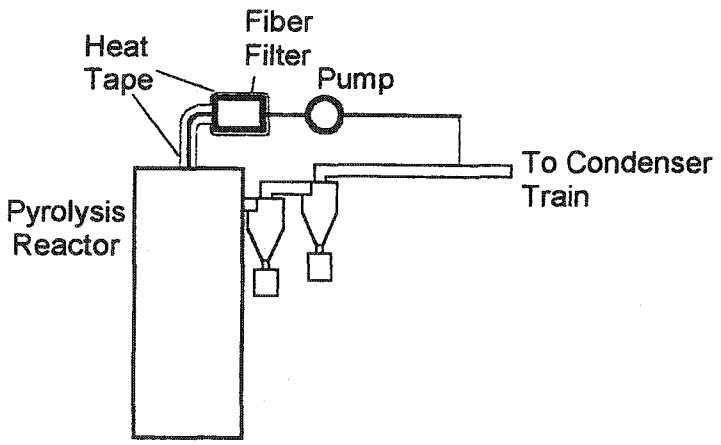

Figure 19. Fiber filter sample line

The fiber contained in the filter has a diameter of 8 μm and has been established as a suitable liquid aerosol interceptor as indicated by the packed bed filter located at the exit of the system. Also, the calculations in Appendix E indicate the theoretical capture efficiency of the filter is effectively 100% for 1 μm aerosols.

To begin testing, the system follows the typical warm-up procedure as described in Chapter 3. Once at pyrolysis temperatures, heated nitrogen flows from the bed through the filter to pre-heat the assembly in order to prevent premature condensation of the producer gas. As an extra precaution, heat tape is added around the filter and is powered before and during the test. At the end of the test, all flow of biomass and nitrogen is promptly discontinued. Once air cooled to atmospheric temperature, the filter is inspected and massed to determine the quantity of liquid captured.

If the filter does not contain visual or measurable evidence of liquid bio-oil, this excludes the existence of bio-oil aerosols.

4.2. Volumetric Flow Rate Test

Fast pyrolysis releases gas, vapor, and liquid droplets into the flow of nitrogen through the reactor. This will increase the volumetric flow rate at the exit compared to the inlet. Because the density of the liquid droplets is vastly greater than the density of vapor, the resulting difference offers a way to distinguish whether bio-oil exits the reactor as a vapor or aerosol.

Statement of the Second Hypothesis. The organic hydrocarbons that are eventually collected as bio-oil are produced as condensable vapors in the fast pyrolysis reactor.

Test of Exclusion. This test is based upon the monitoring of the product flow through a restriction. Figure 20 illustrates the location of pressure taps (p, p_1, and p_2) and the thermocouple (T) used to monitor the flow. The restriction occurs when the product stream is reduced from the large freeboard diameter of 16.2 cm to a hydraulic diameter of 1.8 cm at the exit of the reactor.

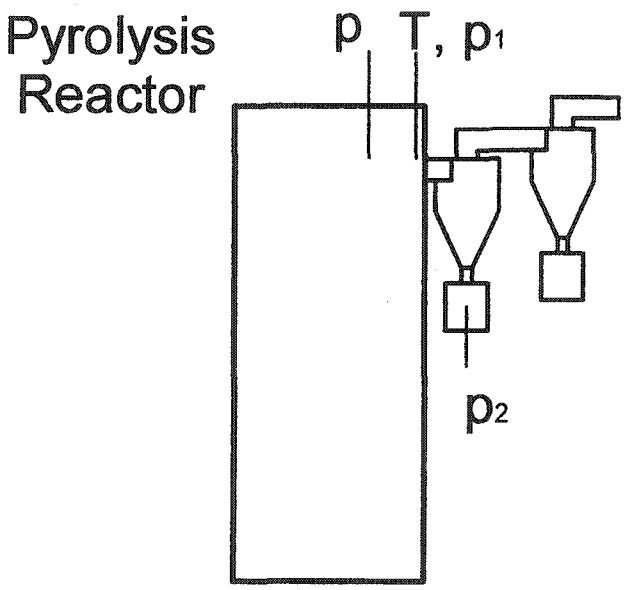

Figure 20. Transducer locations

By measuring the pressure drop through a restriction, it is possible to relate this pressure drop to the volumetric flow rate. The pressure drop can be derived from the Bernoulli equation as follows:

For cases where viscous effects are negligible, density is assumed constant, and the flow is steady the Bernoulli's equation often takes the form shown in Equation 1.

$$p_1 + \frac{1}{2}\rho V_1^2 + \gamma z_1 = p_2 + \frac{1}{2}\rho V_2^2 + \gamma z_2 \qquad (1)$$

The static pressure terms are represented by p_1 and p_2 and velocity terms by V_1 and V_2. The difference of the elevation terms, z_1 and z_2, can be assumed negligible in this application and therefore do not factor in the analysis. The density of the gas is represented by ρ. Rewriting, Bernoulli's equation may be simplified as illustrated in Equation 2.

$$p_1 - p_2 = \frac{1}{2}\rho\left(V_2^2 - V_1^2\right) \tag{2}$$

If the flow is assumed steady and the density is assumed constant in this process, the conservation of mass may be written as indicated by Equation 3 where A_1 and A_2 are cross-sectional areas.

$$\rho\ A_1\ V_1 = \rho\ A_2\ V_2 \tag{3}$$

Recognizing that the cross-sectional area of a flow multiplied by the velocity flow yields the volumetric flow at that location; Equation 4 gives the volumetric flow rate Q_{ideal}.

$$Q_{ideal} = A_1\ V_1 = A_2\ V_2 \tag{4}$$

Solving the ideal flow equation in terms of velocity results in Equation 5.

$$V_i = \frac{Q_{ideal}}{A_i} \quad \text{with index i for 1 and 2} \tag{5}$$

Substituting the velocity terms in Equation 2 with Equation 5, Bernoulli's equation can be written as shown in Equation 6.

$$p_1 - p_2 = \frac{1}{2}\rho\, Q_{ideal}^2 \left(\frac{1}{A_2^2} - \frac{1}{A_1^2} \right) \tag{6}$$

Solving Equation 6 for Q_{ideal} yields Equation 7:

$$Q_{ideal} = \left[\frac{2\,(p_1 - p_2)\,A_2^2}{\rho} \; \frac{1}{1 - \frac{A_2^2}{A_1^2}} \right]^{\frac{1}{2}} \tag{7}$$

If the pipe cross-section can be characterized by a hydraulic diameter, then the diameter ratio β can be applied as shown in Equation 8. This equation is often utilized in pipe flow rate meters such as orifice meters, nozzle meters, and venturi meters [55].

$$Q_{ideal} = A_2 \left[\frac{2(p_1 - p_2)}{\rho\left(1 - \beta^4\right)} \right]^{\frac{1}{2}} \qquad \text{with} \qquad \beta = \frac{d_2}{d_1} \tag{8}$$

Typically, Equation 8 is adjusted to match actual flow rate phenomena. The non-ideality of the actual flow is associated with the vena contracta region near the entrance into the small area pipe. Also, head loss occurs due to the abrupt

transition from the large diameter freeboard to the small hydraulic diameter exit. The actual flow rate Q is corrected through use of a discharge coefficient, C [55]. Equation 9 and 10 reflect this adjustment to the ideal flow formula.

$$Q = C\, Q_{ideal} \tag{9}$$

$$Q = C\, A_2 \left[\frac{2(p_1 - p_2)}{\rho\left(1 - \beta^4\right)} \right]^{\frac{1}{2}} \tag{10}$$

Equation 10 can be solved for the pressure difference as shown by Equation 11.

$$\frac{\Delta p}{\rho} = \frac{Q^2}{C^2 A_2^{\,2}} \frac{1 - \beta^4}{2} \qquad \text{with} \qquad \Delta p = p_1 - p_2 \tag{11}$$

If the flow has fixed geometry meaning the diameters of the large duct and restriction are constant, then β and A_2 are constant. Equation 11 can be rewritten as shown in Equation 12. The symbol k encompasses b, A_2, and C and represents an overall constant for the relationship.

$$\frac{\Delta p}{\rho} = k\, Q^2 \tag{12}$$

with:

$$k = \frac{1 - \beta^4}{2\left(C\, A_2\right)^2} \tag{13}$$

With ρ being the density of the flow gas in the system, a mathematical definition of ρ may be assigned as indicated by Equation 14 where m is the mass flow rate of the gas and Q is the volumetric flow rate of the gas.

$$\rho = \frac{m}{Q} \tag{14}$$

Rewriting Equation 14 by substituting the definition of density, Equation 15 shows a relationship in which the flow rate, Q, appears on both the left and right side of the equality.

$$\frac{\Delta p\ Q}{m} = kQ^2 \tag{15}$$

Solving for Q yields a relationship that given the mass flow rate and the pressure drop, the volumetric flow rate can be calculated without measuring the temperature or absolute pressure of the flow. This relationship is defined by Equation 16:

$$Q = \frac{\Delta p}{k\ m} \tag{16}$$

Equation 17 represents the flow form of the ideal gas law solved for the volumetric flow rate Q. R_u is the universal gas constant and M represents the molecular weight.

$$Q = \frac{m\ R_u\ T}{p\ M} \tag{17}$$

By applying the flow form of the ideal gas law to Equation 16, the generated result is represented by Equation 18.

$$\frac{m R_u T}{p M} = \frac{\Delta p}{k m} \tag{18}$$

Simplifying Equation 18 and solving for the molecular weight of the gas, M, results in Equation 19. This relationship is the basis of the volumetric flow analysis used in the test of exclusion for the second hypothesis. This relationship indicates that by measuring the temperature of the flowing gas, the pressure drop through the restrictive exit, and the absolute pressure of the system, a relationship exists between the mass flow rate, m, and the molecular weight, M, of the gas provided the constant k is known:

$$M = m^2 \left(\frac{k R_u T}{p \Delta p} \right) \tag{19}$$

If the flow gas is comprised of a mixture of ideal gases, the governing equation may be rewritten as Equation 20. This form incorporates the apparent molecular weight of the mixture and the mass flow of the gaseous mixture:

$$M_{mix} = m_{mix}^2 \left(\frac{k R_u T}{p \Delta p} \right) \tag{20}$$

The specific application of Equation 20 to the pyrolysis system suggests that the mass flow of the mixture is the sum of the mass flow of nitrogen, the noncondensable gases created by fast pyrolysis, the water vapor contained in the

collected bio-oil, and the fraction of dry oil in the vapor state. With the appropriate subscripts, the mass flow of the mixture is defined by Equation 21. The amount of nitrogen and noncondensable gases are directly measured.

$$m_{mix} = m_{N2} + m_{NC} + m_{H2O} + m_V \quad (21)$$

The amount of water is determined by Karl-Fischer titration of the bio-oil and determined the mass fraction, y, of water in the bio-oil. The equation for water mass flow is represented by Equation 22.

$$m_{H2O} = y\ m_{oil} \quad (22)$$

Also, the dry oil fraction collected is defined as the amount of bio-oil collected minus the water fraction as shown in Equation 23. The dry oil fraction in the vapor state is the fraction, f, of dry bio-oil that actually exists as a vapor at the exit of the reactor.

$$m_V = f\ (1-y) m_{oil} \quad (23)$$

Applying the Equations 22 and 23 to Equation 21 yields Equation 24, which illustrates the mass flow of the gaseous mixture.

$$m_{mix} = m_{N2} + m_{NC} + y\ m_{oil} + f\ (1-y)\ m_{oil} \quad (24)$$

An expression for the apparent molecular weight, M_{mix}, can be written in terms of the mole fraction, x, of each gaseous component as shown in Equation 25.

$$M_{mix} = x_{N2}\, M_{N2} + x_{NC}\, M_{NC} + x_{H2O}\, M_{H2O} + x_V\, M_V \qquad (25)$$

The mole fraction of the nitrogen, noncondensable gases, and water may be described by Equation 26.

$$x_i = \frac{V_i}{Q_{mix}} \qquad \text{with indice i for N2, NC, and H2O} \qquad (26)$$

In addition, the vapor fraction of the dry oil is defined by Equation 27 by the fact all of the mole fractions sum to unity.

$$x_V = 1 - x_{N2} - x_{NC} - x_{H2O} \qquad (27)$$

The molecular weight of the mixture, M_{mix}, can be described by Equation 28, which is a substitution of Equations 26 and 27 into Equation 25.

$$M_{mix} = \frac{\sum_i V_i\, M_i}{Q_{mix}} + \left(1 - \frac{\sum_i V_i}{Q_{mix}}\right) M_V \qquad (28)$$

The volumetric flow rate of the individual gases, V_i, may be defined by Equation 29 and the overall flow rate, Q_{mix}, is defined by taking Equation 16 and re-writing it in terms of a mixture as shown in Equation 30.

$$V_i = \frac{m_i R_u T}{p M_i} \tag{29}$$

$$Q_{mix} = \frac{\Delta p}{k m_{mix}} \tag{30}$$

Applying these definitions to Equation 28 yields the definition of the molecular weight of the gaseous mixture described by Equation 31.

$$M_{mix} = k m_{mix} \frac{R_u T}{\Delta p p} \left(m_{N2} + m_{NC} + m_{H2O}\right) + \left[1 - k m_{mix} \frac{R_u T}{\Delta p p} \left(\frac{m_{N2}}{M_{N2}} + \frac{m_{NC}}{M_{NC}} + \frac{m_{H2O}}{M_{H2O}}\right)\right] M_V \tag{31}$$

By substituting this definition of molecular weight of the mixture into the general formula represented by Equation 20, Equation 32 is generated:

$$k m_{mix} \frac{R_u T}{\Delta p p} \left(m_{N2} + m_{NC} + m_{H2O}\right) + \left[1 - k m_{mix} \frac{R_u T}{\Delta p p} \left(\frac{m_{N2}}{M_{N2}} + \frac{m_{NC}}{M_{NC}} + \frac{m_{H2O}}{M_{H2O}}\right)\right] M_V = m_{mix}^2 \left(\frac{k R_u T}{p \Delta p}\right) \tag{32}$$

Solving this equation for the molecular weight of the dry oil in the vapor state, M_V, yields Equation 33.

$$M_V = \frac{m_{mix} - m_{N2} - m_{NC} - m_{H2O}}{\frac{\Delta p p}{k m_{mix} R_u T} - \frac{m_{N2}}{M_{N2}} - \frac{m_{NC}}{M_{NC}} - \frac{m_{H2O}}{M_{H2O}}} \tag{33}$$

Recall that the mass flow rate of the mixture, m_{mix}, is represented by Equation 2 and m_{H2O} is represented by Equation 22. The substitution of m_{mix} and m_{H2O} yields Equation 34.

$$M_V = \frac{f\,(1-y)\,m_{oil}}{\dfrac{\Delta p\; p}{k\left[m_{N2}+m_{NC}+y\,m_{oil}+f\,(1-y)\,m_{oil}\right]R_u\,T} - \dfrac{m_{N2}}{M_{N2}} - \dfrac{m_{NC}}{M_{NC}} - \dfrac{y\,m_{oil}}{M_{H2O}}} \qquad (34)$$

By measuring Δp, p, T, m_{oil}, y, and m_{NC} for a test, the characteristic curve can be established for the molecular weight of the dry bio-oil in the vapor state and the fraction of dry bio-oil in the vapor state.

If the characteristic curve indicates the presence of aerosols, this excludes the hypothesis that the dry bio-oil exits the reactor as all condensable vapors. The constant k in the above equations must be found for the pressure drop associated with the flow exiting the reactor for the system depicted in Figure 20.

In the above derivation, the influence of liquid or solid particles on the pressure drop was assumed to be negligible. To establish what influence particles have on the pressure drop, corn starch, with its nominal diameter of 20 μm, was injected into the reactor system operating at atmospheric temperature. The rate of injection of corn starch, m_s, was varied to illustrate the influence of particle concentration on pressure drop. The flow rate of nitrogen remained steady for the duration of the test.

The influence of particles on the pressure drop is illustrated in Figure 21 and summarized in Table 9. As illustrated, the particle influence on pressure drop is negligible and no adjustment of the pressure drop is required for determining the characteristic curve as described by Equation 34.

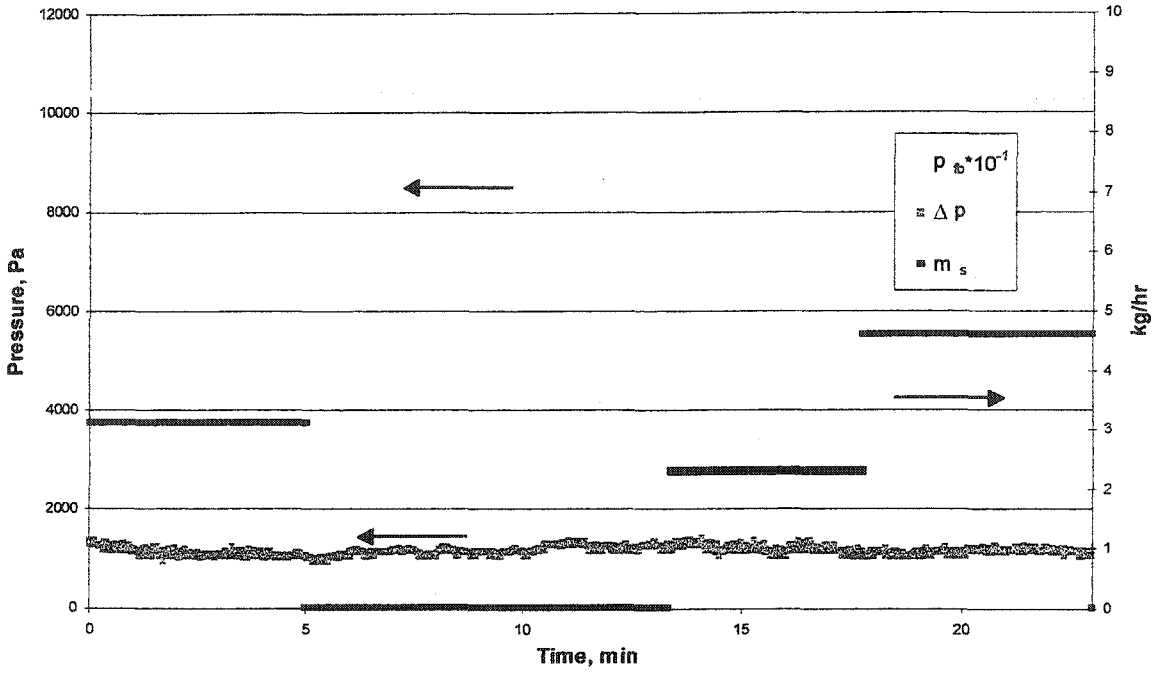

Figure 21. Influence of particle flow rate on pressure drop

Table 9. Summary of particle influence on pressure drop

m_s	C	ΔP	P_{fb}	T_{fb}	Time
kg/hr	kg/m^3	Pa	kPa	°C	min
0.0	0.00	1134	103.40	24.1	2-5
2.3	95.38	1085	103.50	22.9	15-18
3.1	127.17	1162	103.43	24.2	7-10
4.6	190.75	1151	103.42	22.9	20-23

The next step is to determine the value of constant k for Equations 12, 20, and 34. The system is brought up to operating temperature as described in the standard procedure in Chapter 3. To determine k, known amounts of pure nitrogen and pure argon flowed through the reactor at operating temperatures near 500 °C. By recording the exiting temperature, pressure, and pressure drop at locations as illustrated in Figure 20, and regulating the gas flow rate with a mass flow controller, the value of k could be determined. Once k is determined, a verification of the

theory can be performed by injecting known amounts of a pure substance at typical fast pyrolysis conditions. By injecting water and methanol in separate tests, a characteristic curve can be constructed with the theoretical molecular weight acting as a function of the percent of the substance in the vapor state. Of course, both water and methanol will completely evaporate leading to the measurement of the molecular weight of the substance evaluated at 100 wt-% vapor case. If the molecular weights agree well with the accepted values, sufficient confidence in the method is gained.

A calibration curve was developed by curve fitting the known flow rates of nitrogen and argon with the measured pressure drop in each case. This data was fitted as shown in Figure 22 and the raw analysis is illustrated in Appendix F with the corresponding k value determined as Log k = 7.3508. The gray curves represent the proposed uncertainty, σk, of a measurement using this k value.

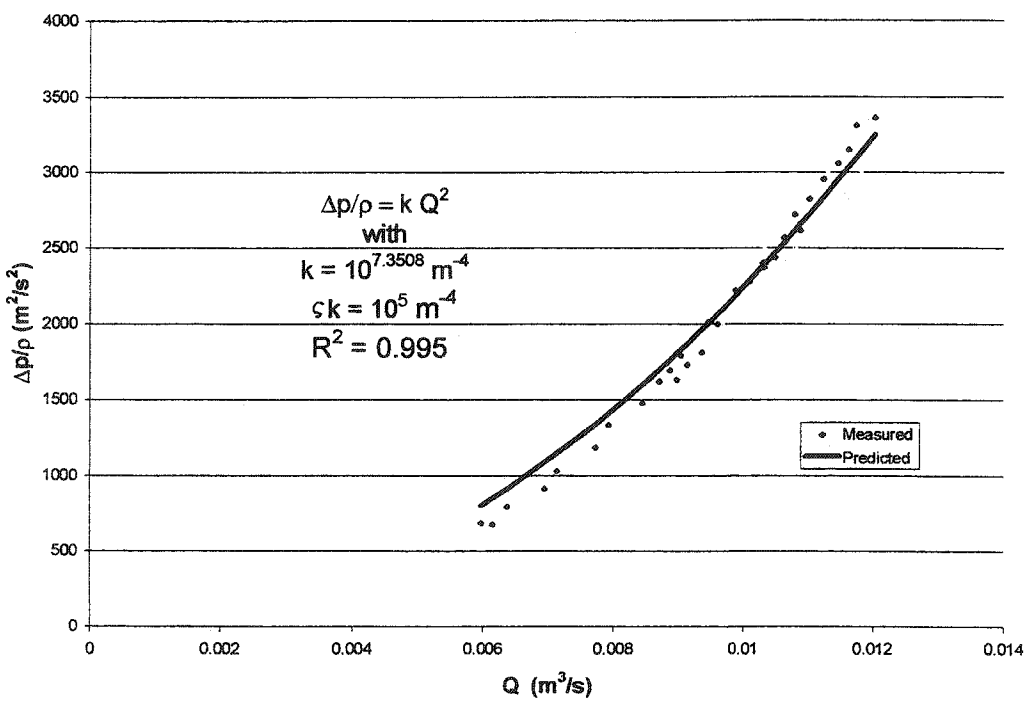

Figure 22. Curve fit of constant k

With the constant k established, it was possible to proceed with a test of the hypothesis. A verification of the procedure was conducted by simulating fast pyrolysis conditions and injecting a known mass rate of water and then methanol to measure the molecular weight of each substance. This is verified by the molecular weights indicated by the corresponding 100 wt-% vapor readings for water and methanol. The calculations are presented in Appendix G and the characteristic plots of each are illustrated assuming that the transport phase of the substances is unknown. As demonstrated, the procedure appears adequate for the hypothesis test based on the close approximation of the respective molecular weights of water and methanol.

Table 10. Verification of method with water and methanol

Substance	Measured M kg/kmol	Accepted M kg/kmol	error %
H_2O	18.87	18.02	4.72
CH_3OH	31.79	32.04	0.78

The next step is to measure the parameters of a test involving the fast pyrolysis of a biomass, namely Northern Red Oak (*Quercus rubra*). The system is brought up to temperature following the typical startup procedure. Under inert nitrogen conditions slightly greater than 500 °C, biomass is injected into the bed with all pertinent data recorded by the data acquisition system. The data is analyzed by utilizing Equation 34 in order to develop the corresponding characteristic curve.

This curve relates the molecular weight of the dry bio-oil to the fraction of dry bio-oil in the vapor state at the exit of the reactor. If at 100 wt-% vapor, the dry bio-oil has a low molecular weight near that of levoglucosan (162 kg/kmol), it is likely bio-oil exists as a vapor in the reactor. However, if at 100 wt-% vapor, the dry bio-oil has a much higher molecular weight; it is likely that aerosols are present in some fraction.

4.3. Freeboard Screen Test

An interception device in the freeboard should capture the aerosols in the product stream. If the captured aerosols evaporate, they will then contribute to the volumetric gas flow. The corresponding increased volumetric flow will be reflected in the characteristic curve discussed in the second hypothesis.

Statement of the Third Hypothesis. Aerosols exiting will evaporate if given sufficient time to do so.

Test of Exclusion. This method utilizes the equation presented in the second hypothesis, namely Equation 34. A metal mesh screen is placed into the reactor in order to intercept the liquid aerosol. If the characteristic curve does not indicate an increase in vapors from bio-oil at the exit of the reactor, this excludes the possibility of aerosol evaporating if given sufficient time.

Two screens with 38 μm openings are layered together and inserted in the freeboard as shown in Figure 23. The circumference of the screen housing is sealed to the wall of the reactor. A thermocouple passes through the center of the assembly to monitor the fluid bed temperature. Pressure transducers and the freeboard thermocouple are positioned as indicated in Figure 20. Red oak will be fast pyrolyzed at near 500 °C with the appropriate temperatures and pressures recorded. The resulting characteristic curve can then be compared to the pyrolysis tests of the second hypothesis.

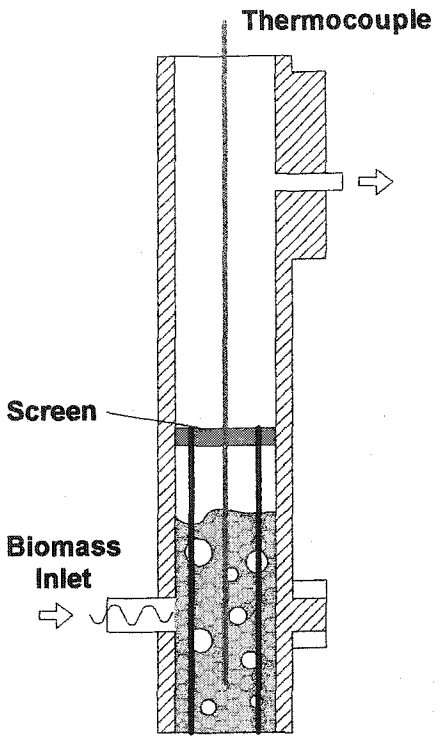

Figure 23. Freeboard screen in the fast pyrolysis reactor

4.4. Evaporation of Aerosols Evaluation

The focus of this test is to determine whether liquid aerosols have sufficient time to evaporate before entering the condenser. The statement of this hypothesis is nearly identical to the previous hypothesis. The difference lies in the test of exclusion. A mathematical approach is employed to determine the time required by a liquid aerosol to completely evaporate when captured by a fiber filter.

Statement of the Fourth Hypothesis. Although bio-oil leaves the bed of the pyrolyzer as aerosol, these droplets will evaporate if allowed sufficient time.

Test of Exclusion. A mathematical approach is employed to investigate this hypothesis. It is assumed that a liquid droplet exists in the reactor at the exit of the

freeboard. A filter downstream of the freeboard captures and evaporates the aerosol droplet with no significant chemical change due to cracking or coking. If the time required for evaporation is small, liquids would not be expected to be captured in the filter.

Heat transfer and mass transfer considerations are investigated based on the model described by Heinsohn [56:211-216] and Kabel [57:329-366] for the evaporation of a liquid droplet. The primary equations are described below.

Mass conservation is described as:

$$\frac{\pi}{2}\rho_p \, d_p^{\,2} \frac{d}{dt} d_p = R \tag{35}$$

where R, the rate of evaporation, is given by:

$$R = \pi \, M_p \, d_p \, T_g \, Nu \, \frac{D_{12}}{R_u \, T_g} \left(\frac{Sc}{Pr}\right)^b \frac{p_g}{p_{am}} \left(\frac{p_v}{T_p} - \frac{p_{pg}}{T_g}\right) \tag{36}$$

The energy equation for the droplet is described as:

$$\frac{d}{dt} T_p = \frac{6 \, h \left(T_g - T_p\right)}{d_p \, \rho_p \, C_v} - \frac{6 \, m_p \, h_{fg}}{\pi \, d_p^{\,3} \, \rho_p \, C_v} \tag{37}$$

where:

m_p = mass flow leaving droplet

M_p = molecular weight of liquid

d_p = diameter of droplet

T_g = temperature of gas

Nu = Nusselt Number

D_{12} = diffusivity of liquid to gas

R_u = universal gas constant

Sc = Schmidt Number

Pr = Prandtl Number

b = exponential constant

p_g = absolute pressure of gas

p_{am} = log mean pressure

p_v = saturated vapor pressure of the liquid

T_p = temperature of droplet

p_{pg} = vapor pressure of liquid in free stream

ρ_p = density of the liquid

C_v = specific heat of the liquid

h_{fg} = enthalpy of vaporization

t = time

Equation 35 represents the mass flow exiting the droplet due to evaporation. The change in diameter of the liquid aerosol with respect to time is represented in the Equation 36. The temperature of the aerosol also changes with time and is represented by Equation 37. Further details can be found in one of several references [56,57,58]. The surrounding gas is assumed to be pure nitrogen and the time needed to completely evaporate the droplet is based on the droplet evaporation model previously described.

Note that some assumptions are made about the properties of the droplet since it is very difficult to know the chemical composition of the aerosols that may exist. When available, the properties are assumed to be that of levoglucosan, which can comprise more than 30 wt-% of the bio-oil [29]. Note that the vapor pressure for levoglucosan [38] is applied. Data quantifying the diffusivity of levoglucosan in nitrogen was not found in literature. The diffusivity was estimated by calculating the empirical formula of the bio-oil and estimating the diffusivity based on the empirical chemical's critical point. The reported composition of collected bio-oil from an oak and maple mixture states that it is 58.5 wt-% carbon, 6.01 wt-% hydrogen, and 35.4

wt-% oxygen on a dry mass basis [59:109]. An empirical chemical formula was calculated as $C_{4.9}H_6O_{2.2}$, which implies a molecular weight of 106 kg/kmol. However, the properties of carbohydrates near this empirical formula are not readily available. A related component that does appear in bio-oil was selected. Furfural ($C_5H_4O_2$) properties with respect to the critical point [60:6-52] were utilized to develop a diffusivity relationship of furfural in nitrogen.

The critical properties are applied to the proposed equation by Chen and Othmer as reported by Vargaftik [61:339] to establish the diffusivity relationship shown as Equation 38. The diffusivity D_{12} has units of cm^2/s, with the critical volume, v_c, in units of $cm^3/gmol$, and the critical temperature, T_c, in Kelvin. This equation is applied to furfural and nitrogen and is provided in Appendix J. The diffusivity will be adjusted by a factor of 10 to determine its influence is significant on the time evaporation.

$$D_{12} = \frac{0.43\left(\frac{T}{100}\right)^{1.81}\sqrt{\frac{1}{M_2}+\frac{1}{M_1}}}{P\left(\frac{T_{c1}\,T_{c2}}{10000}\right)^{0.1405}\left[\left(\frac{v_{c1}}{100}\right)^{0.4}+\left(\frac{v_{c2}}{100}\right)^{0.4}\right]^2} \qquad (38)$$

The heat of vaporization and the saturation pressure for levoglucosan are from work by Suuberg and Oja [38] and can be found in Appendix J.

The droplet is assumed to be captured in the fiber of the filter. The flowing gas now passes by the droplet instead of entraining it. Therefore, the droplet is exposed to the full mass and heat transfer effects of the flowing gas. The system of equations is solved and is presented in the next chapter.

4.5. Hydrocarbon Cracking Test

When the product stream is filtered through fiber media, it is likely that the liquid converts to a vapor. It is possible that the organic aerosols simply evaporate. Alternatively, they may crack to noncondensable gases such as carbon dioxide and hydrogen. If the organic aerosols crack, this will lower the collected bio-oil yield and is not desirable in most pyrolysis applications. This hypothesis will clarify how much influence filtering has on the yield of bio-oil.

Statement of Fifth Hypothesis. Liquid aerosols that leave the reactor crack under filtering conditions and lower the bio-oil yield.

Test of Exclusion. To test this hypothesis, the exit stream from the reactor was first passed through the cyclone separators and then through a packed fibrous filter before the condenser train. The cyclones are designed with a 50% cut diameter of 3 μm, which is above the accepted sub-micron sized liquid aerosols that typically represent smoke [58:6]. The cyclones remove the solid char and ash allowing smaller particles that represent liquid aerosols to pass. Figure 24 illustrates the inline filter after the cyclones. The housing construction consists of a standard plumbing tee of a nominal diameter of 5 cm (2 in). During testing, heat tape was wrapped around the filter to help maintain the wall temperature. A thermocouple is located directly after the fiber to ensure the gas temperature is 425 °C or higher. The filter fiber has a diameter of 8 μm and it is established as a suitable liquid aerosol interceptor as indicated by the packed bed filter located at the exit of the system. Appendix E also indicated the theoretical capture efficiency is high even though the geometry is not identical to the modeled filter.

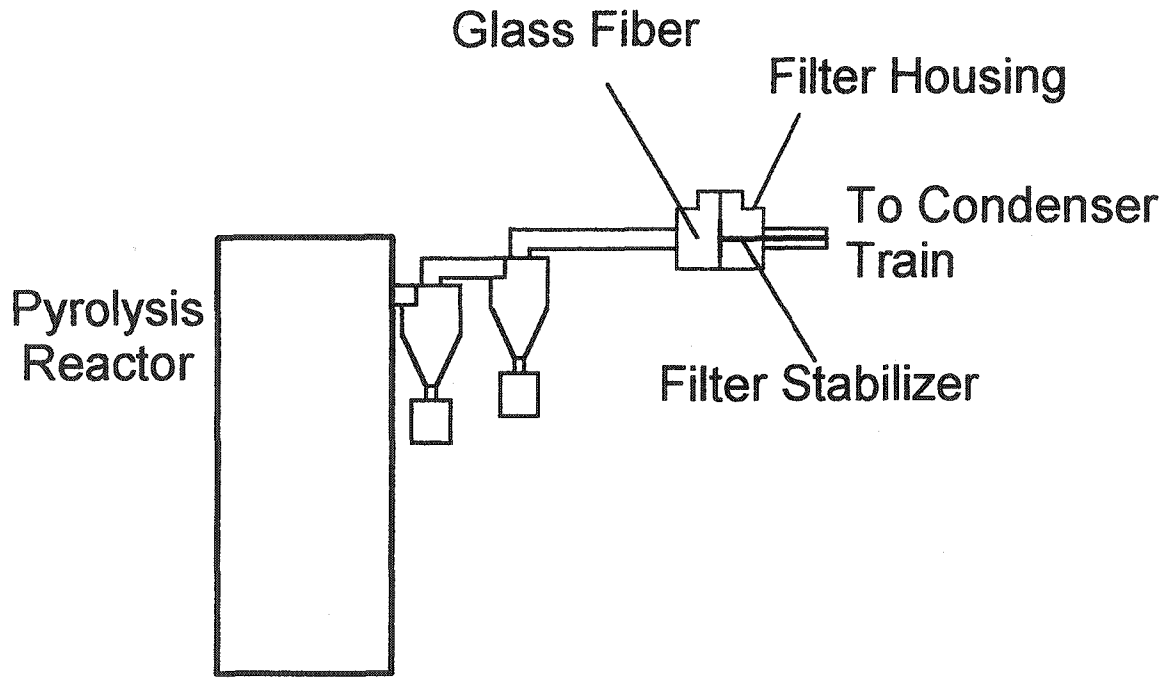

Figure 24. Inline glass fiber filter

To begin, the system follows the warm-up procedure as described in Chapter 3. Once the bed is at a suitable and steady temperature, the temperature in the hot gas filter is monitored by noting the gas temperature entering the first condenser. In addition, the thermocouple in the filter is also monitored manually throughout the test. This ensures that the hot gas filter is at a suitable high temperature to prevent condensation of any vapors that may exist.

If the bio-oil yield is not significantly decreased compared to the bio-oil catch from the second test, then the cracking of bio-oil aerosol in the filter is excluded.

4.6. Influence of Char on Aerosol Formation

The purpose of this test is to determine whether the presence of char generated during pyrolysis is an important determinant as to whether bio-oil exists as vapor or aerosol.

Statement of Sixth Hypothesis. Fast pyrolysis char influences the formation of bio-oil liquid aerosol.

Test of Exclusion. To test this hypothesis, corn starch, a biomass that is known to produce essentially no pyrolytic char or ash, is pyrolyzed. A characteristic curve relating the dry bio-oil's molecular weight to its mass fraction in the vapor state will be determined based on pressure drop data. From previous tests, corn starch yields less than 1 wt-% char. The characteristic curve determination is identical in method to the red oak tests presented in the second hypothesis. To determine the effect of char on aerosol formation, a second test is performed in which a corn starch and char mixture is pyrolyzed. If char acts as a nucleation site for bio-oil aerosols, the characteristic curve from corn starch will shift to indicate the presence of aerosols. The injected material contains 89 wt-% corn starch and 11 wt-% red oak char. This mixture is similar to the amount of char produced when red oak is fast pyrolyzed.

5. RESULTS AND DISCUSSION

In the previous chapter, several hypotheses concerning the formation and fate of bio-oil were proposed and corresponding tests of exclusion formulated. In this section, the results of the tests of exclusion are described.

5.1. High Temperature Filtration Test

This hypothesis states that the high molecular weight organic hydrocarbons that are eventually collected as bio-oil are produced as liquid aerosols in the fast pyrolysis reactor.

Results. The total duration of this red oak fast pyrolysis test was 26 minutes. The slip stream flow passed through the filter during the last 6 minutes. The steady-state operating parameters of the entire test are specified in Table 11. Note that Q_{ss} represents the flow rate of the slip stream.

Table 11. First hypothesis testing parameters

T_{bed}	m_{N2}	m_b	d_s	d_b	Q_{ss}	p_{fb}	h_{bed}
°C	kg/hr	kg/hr	μm	μm	LPM	kPa	cm
494.1	15.11	~8	735	339	34	109.4	32

After cooling of the filter housing, the glass fiber filter was qualitatively and quantitatively studied. The first observation was the fibers of the filter were blackened from their initial white state. There was also loose, dry char that was trapped in the front of the filter. This char had a length to diameter ratio that was greater than 10 and resembles char captured in the cyclones. The sieve diameter of the char in the filter was 53 μm. The amount of char that was collected in the filter

was 2.9 grams. The weight of the fiber material increased 0.18 grams from an initial weight of 10.13 grams to a final weight of 10.31 grams. If the bio-oil existed as an aerosol, most of it should have been trapped in the filter. The filter showed no evidence of liquid. The expected weight increase would be closer to 19 grams due to collected liquid. This assumes typical red oak fast pyrolysis yields of 65 wt-% bio-oil of which 27 wt-% is water, 10 wt-% char, and 25 wt-% noncondensable gas for this system. Since the filter was operated at higher temperatures, trapped liquids might have cracked. However, for this case, considerable fine coke, instead of pyrolytic char, would have been present. The expected amount of pyrolytic char collected should been near 4.1 grams. The collected amount is approximately this value and the 1.2 gram difference may be explained by large char particles not staying entrained in the flow and reaching the filter.

Discussion. The results appear to refute the hypothesis that the bio-oil exits the freeboard of the reactor as an aerosol. The results also suggest that the observation of a smoky stream at the top of the bed was due to rapid cooling of the stream at the exit of the reactor to condense the vapors to aerosols. The slight weight increase of the fiber filter may be attributed to very fine biomass char particles captured by the fibers. Bio-oil yield for the fast pyrolysis of red oak have typically been between 58 wt-% and 68 wt-% under similar operating conditions on this system. Because of the short duration of this test, the yield of bio-oil and char was not measured.

In short, the results suggest that none of the bio-oil collected in the condensers leaves as liquid aerosols from the reactor. This implies that all of the bio-oil is a condensable vapor at the outlet of the reactor. This refutes the statement of the first hypothesis as no evidence of liquid aerosols was found on the fiber filter.

5.2. Volumetric Flow Rate Test

The first hypothesis indicated that the bio-oil exists as vapor at the exit of the reactor. A characteristic curve describing the molecular weight of dry oil versus the mass fraction of the dry oil in the vapor state can be generated for a specific fast pyrolysis test. This curve will quantify the amount of dry bio-oil vapor exiting the reactor.

By measuring specified pressures and temperatures described in Chapter 4, it is theoretically possible to determine a characteristic curve relating the molecular weight of dry oil in the vapor state to the fraction of dry oil in the vapor state. The second hypothesis states that the organic hydrocarbons that are eventually collected as bio-oil are produced as condensable vapors in the fast pyrolysis reactor.

Results. In Table 12, a summary of the fast pyrolysis test data is given for this hypothesis.

Table 12. Summary of volumetric flow rate test

Test Description	T_{fb} °C	p_{fb} Pa	Δp Pa	m_b kg/hr	m_{N2} kg/hr
Red Oak Test 1	554.01	113358.9	1438.3	8.551	15.11
Red Oak Test 2	545.27	113030.4	1381.1	8.141	15.11

Test Description	m_c kg/hr	m_{oil} kg/hr	m_{nc}[a] kg/hr	y	m_{H2O} kg/hr
Red Oak Test 1	0.7813	5.157	2.538	0.274	1.415
Red Oak Test 2	0.7150	4.825	2.404	0.278	1.340

[a]The noncondensible gas is assumed to have a molecular weight of 30 kg/kmol

With the procedure verified, the testing of red oak yielded characteristic curves, as illustrated in Figure 25, which indicated the fraction of aerosols in product stream exceed 90 wt-%. The vapor fraction is illustrated and the liquid aerosol fraction is one minus the vapor fraction.

Appendix H provides detail on the calculation procedure for red oak tests. Pyrolysis modelers have assigned the molecular weight of the bio-oil ranging from 100 kg/kmol [62] to145 kg/kmol [35] in the vapor state. For analysis purposes, the molecular weight is assigned the value of 100 kg/kmol and the corresponding vapor fraction is calculated and is shown in Table 13. The uncertainty indicated is calculated in Appendix H based on propagation of uncertainty principles [63].

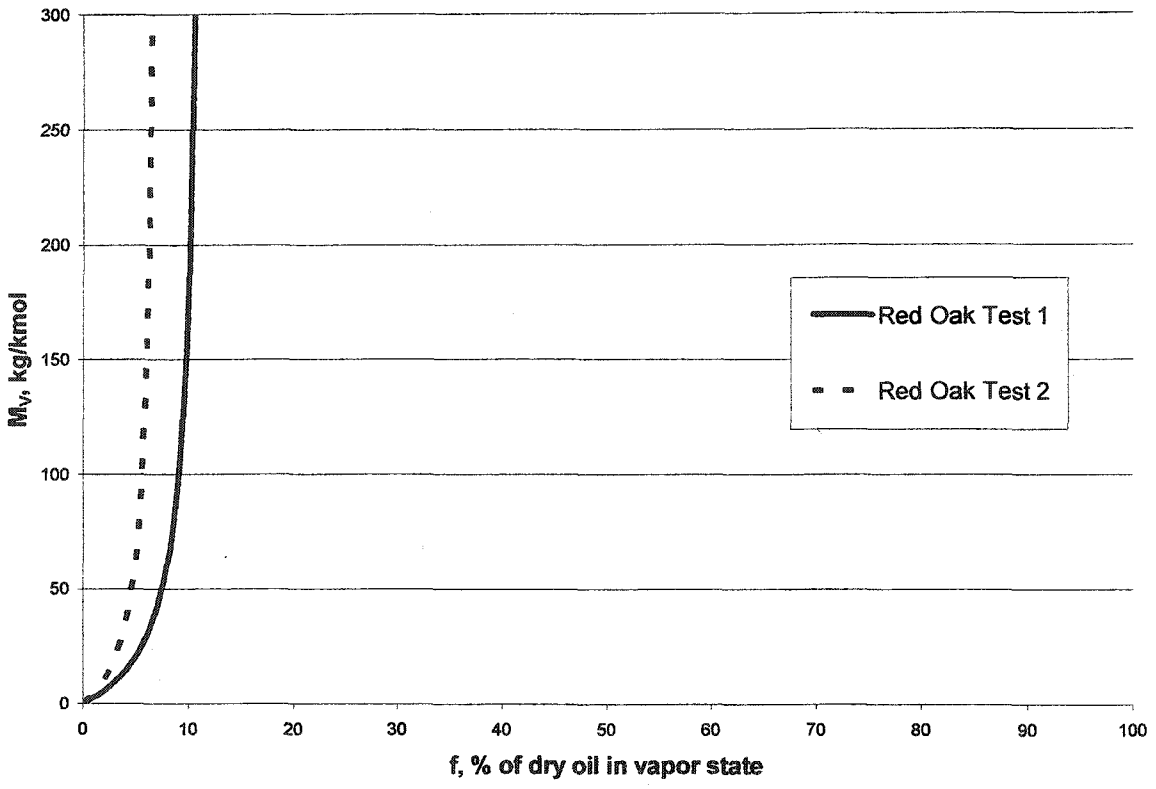

Figure 25. Characteristic test curves for red oak

Table 13. Vapor fraction analysis for red oak

	Red Oak Test 1	Red Oak Test 2
Vapor Fraction %	9.1 ± 22.6	5.5 ± 24.0

with M_V = 100 kg/kmol

Discussion. The results indicate that when red oak is fast pyrolyzed at approximately 500 °C, the product stream at the exit of the reactor contains bio-oil as aerosol. The fraction of the liquid aerosol is near 90 wt-%. Although the results of the two tests are not identical, the evidence of a high percentage of aerosols is repeatable. If the dry bio-oil was assumed to have a molecular weight of 100 kg/kmol, then the vapor fraction averages 7.3 wt-% for the two tests. The calculated uncertainty is approximately ±23 wt-%, but the actual error would be limited by zero on the lower end of the range. Although the uncertainty is large, it is acceptable for drawing conclusions for this test. The maximum vapor fraction of the dry oil is approximately 30 wt-% suggesting that the flow contains bio-oil predominantly in the liquid aerosol state for red oak. This refutes the hypothesis that the dry bio-oil exists as vapor.

5.3. Freeboard Screen Test

Contradictory results were obtained in the previous two hypothesis tests. The first hypothesis test indicated that liquid aerosols were not present while the second indicated that bio-oil exits mostly as liquid aerosols. In the first hypothesis test, if liquid droplets were captured by the filter and subsequently evaporated, this would give the appearance of dry bio-oil being in the vapor state at the entrance of the filter. The third hypothesis will determine if the liquid aerosols present, as determined by the second hypothesis test, will evaporate when captured. If the aerosols do evaporate, then it may be possible to filter char without filter clogging issues.

The third hypothesis states that aerosols exiting will evaporate if given sufficient time to do so. The characteristic curve of the molecular weight of the dry bio-oil versus the fraction of dry bio-oil in the vapor state will show an increase in vapor flow if the aerosols evaporate. If the aerosols do not evaporate, the curve should be similar to the curves found in the second hypothesis test.

Results. In Table 14, a summary of the fast pyrolysis test data is given for this hypothesis.

Table 14. Summary of red oak freeboard filter test

Test Description	T_{fb} °C	p_{fb} Pa	Δp Pa	m_b kg/hr	m_{N2} kg/hr
Red Oak with Filter	494	108855	1366	8.31	15.11

Test Description	m_c kg/hr	m_{oil} kg/hr	m_{nc}[a] kg/hr	y	m_{H2O} kg/hr
Red Oak with Filter	0.66	5.74	1.81	0.224	1.29

[a]The noncondensible gas is assumed to have a molecular weight of 30 kg/kmol

The resulting test conditions are given in Appendix I with the calculations based on the analysis detailed in the second hypothesis. In Figure 26, the characteristic curve is compared to the previous hypothesis test for red oak.

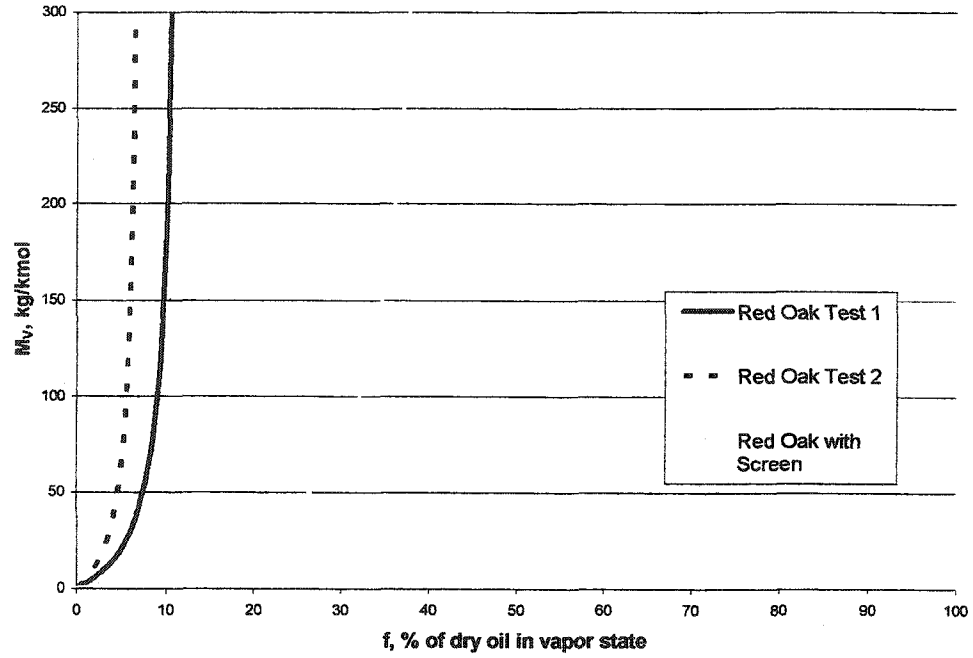

Figure 26. Red oak with a freeboard screen

The resulting vapor fraction increased from near 10 wt-% to approximately 40 wt-%. This suggests that the fraction of liquid aerosol decreased from 90 wt-% or greater to around 60 wt-%. The test was stopped at 27.5 minutes due to the onset of defluidization of the bed caused by retained char in the bed as well as increased pressure beneath the screen.

Discussion. The effect of adding the screen to the freeboard shifted the characteristic curve supporting the hypothesis that aerosols, given sufficient residence time, can evaporate. It appears that some liquid aerosols converted to vapors, which caused the shift. Most of the liquid droplets likely did not get captured in the mesh as a result of the relatively larger openings compared to the diameter of the aerosol droplets.

5.4. Evaporation of Aerosols Evaluation

The test of exclusion for the second and third hypotheses provided evidence that the bio-oil is an aerosol at the exit of the reactor. Using a theoretical approach, the purpose of this hypothesis is to clarify whether a bio-oil liquid aerosol evaporates in a relatively short time frame. The difference between this test and the third test is that a different test of exclusion will be utilized. The third test experimentally determined if sufficient time was available to evaporate the aerosols, and this test theoretically estimates the time needed for evaporation.

The first hypothesis suggests bio-oil forms as vapor. However, the first hypothesis did not consider the possibility that produced aerosols may evaporate. The fourth hypothesis investigates whether liquid aerosols that depart the reactor are likely to evaporate quickly if deposited on a filter.

Results. In Appendix J, the system of equations presented in Section 4.4 is solved utilizing the fourth order Runge-Kutta method to solve differential equations. To verify that the calculations are correct, the properties of water were applied at 293 °C ambient air and 0% humidity for various sized particles. The resulting values are compared to the values calculated by Hinds [58:301]. At 1 μm and larger, the results with water agree well with published values.

Table 15. Comparison of calculated water droplet life to published results

Initial Diameter μm	Hinds [38] Droplet Life s	Predicted Droplet Life s	Ratio
0.01	2.E-06	7.8E-08	25.64
0.1	3.E-05	7.8E-06	3.85
1	1.E-03	7.8E-04	1.28
10	0.08	0.078	1.03
40	1.3	1.24	1.05

in air at 293 °C and 0% humidity

With this confidence, the conditions of fast pyrolysis are applied to the system including temperature and flow velocity. The calculated lifetime of a 10 μm liquid droplet is 8.8 ms. If the diffusivity, D_{12}, is decreased by a factor of 10, the droplet lifetime increases 11.4 ms. A large change in the diffusivity will only increase the lifetime 2.6 ms. This indicates that using the diffusivity of furfural to approximate the overall bio-oil diffusivity is not critical in the calculation.

Discussion. The short lifetime indicates that there is sufficient time to evaporate and therefore supports the fourth hypothesis statement. The short lifetime of the droplet is due to the elevated temperature as well the heat and mass transfer associated with being in a forced flow. It should be noted that the particle size chosen of 10 μm is likely the maximum size of droplet to be expected unless significant coagulation occurs. Smaller particles will have shorter droplet lifetimes.

5.5. Hydrocarbon Cracking Test

This hypothesis states that liquid aerosols that leave the reactor crack under filtering conditions and lower the bio-oil yield. If the aerosols do crack when captured, the bio-oil yield will decrease and noncondensable gas will increase. Also, fine char from cracking should be present in the filter. This test differs from the first test in that the impact that cracking may have on bio-oil yield is determined.

Results. In Table 16 , this hypothesis test is compared to the two red oak tests performed as part of the second hypothesis. The bio-oil yield, 58.5 wt-%, was very near the same compared to the previous tests indicated. The fraction of bio-oil collected in each stage of the condenser did not significantly change in the three tests.

Table 16. Summary of inline filter test of red oak

Test Description	T_{bed} °C	Duration min	m_b kg/hr	m_{N2} kg/hr	m_{oil} kg/hr	Oil Yield %
Red Oak Test 1 (no filter)	502.9	60	8.55	15.11	5.16	60.3 ± 0.24
Red Oak Test 2 (no filter)	499.6	60	8.14	15.11	4.83	59.3 ± 0.26
Red Oak (filtered)	500.8	35	7.42	15.11	4.34	58.5 ± 0.28

The filter was weighed before and after the test and was found to have an increase in mass of 3.26 grams excluding loose char that was trapped at the front of the filter. This loose char likely escaped capture by the cyclone as its lengthy shape is similar to particles captured in the cyclones.

Discussion. The change in the bio-oil yield was negligible and therefore, the fourth hypothesis statement is refuted. Although the oil yield is slightly less than the two previous tests, the values are nominally the same. This suggests that the filter does not cause bio-oil aerosols to crack to noncondensable gases. The uncertainty

reported reflects only the bio-oil collected and does not account for any losses which can range from 0 to 3 wt-%. The results of this hypothesis imply that using a direct contact method to remove char does not affect the overall bio-oil yield.

5.6. Influence of Char on Aerosol Formation

This hypothesis states that during fast pyrolysis, char influences the formation of bio-oil liquid aerosol. A baseline test is established by fast pyrolyzing corn starch, a biomass which produces essentially no char. A second fast pyrolysis test is performed with a corn starch and char mixture. The characteristic curves from each test are compared and evaluated.

Results. In Table 17, a summary of the fast pyrolysis test data is given for this hypothesis.

Table 17. Summary of corn starch tests

Test Description	T_{fb} °C	p_{fb} Pa	Δp Pa	m_b kg/hr	m_{N2} kg/hr
Corn Starch	465	108932.0	1401.0	6.59	15.11
Corn Starch & Char	516	108431.9	1219.3	5.44	15.11

Test Description	m_c kg/hr	m_{oil} kg/hr	m_{nc}[a] kg/hr	y	m_{H2O} kg/hr
Corn Starch	0.05	4.82	1.51	0.200	0.96
Corn Starch & Char	0.62	2.93	1.87	0.198	0.58

[a]The noncondensible gas is assumed to have a molecular weight of 30 kg/kmol

Figure 27 illustrates the characteristic curve for pure corn starch and the mixture of corn starch and char. In addition, Table 18 summarizes what the percent vapor would be present if the molecular weight of the bio-oil was 100 kg/kmol.

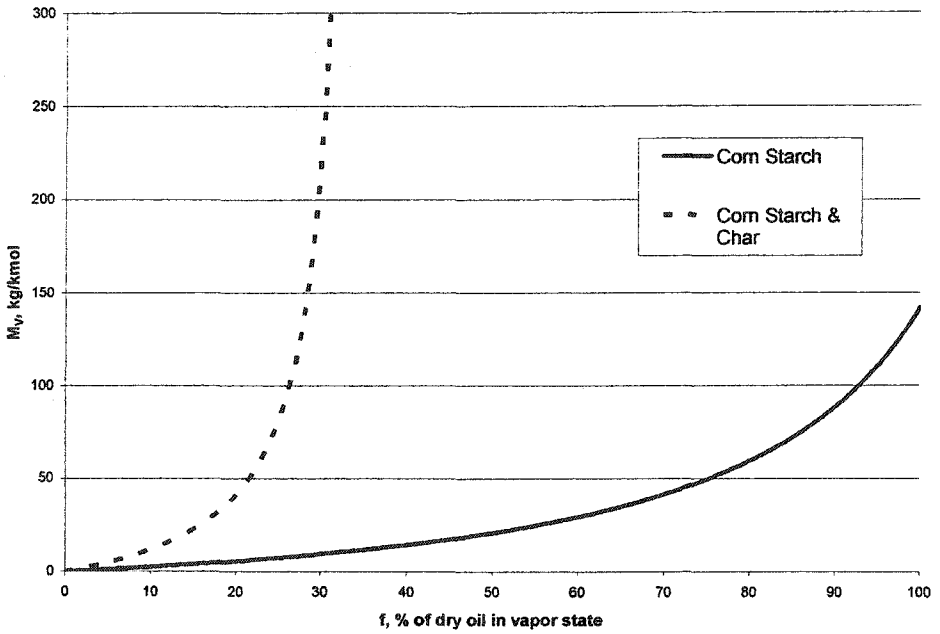

Figure 27. Characteristic curves of corn starch and corn starch-char mixture

Table 18. Vapor fraction analysis for corn starch

	Corn Starch Test	Corn Starch & Char Test
Vapor Fraction %	92.9 ± 23.2	26.4 ± 35.0
	with M_V = 100 kg/kmol	

The detailed calculations can be found in Appendix K. The difference in the amount of dry bio-oil in the vapor state is significant with a nominal decrease of 66.5 wt-%.

Discussion. The characteristic curve for corn starch suggests that the dry bio-oil is mostly vapor in the reactor. In fact, at 100 wt-% vapor, the molecular weight approaches 150 kg/kmol. This value is very near the molecular weight of a primary chemical in bio-oil, namely levoglucosan at 162 kg/kmol. At 100 kg/kmol, the molecular weight used by many pyrolysis modelers, the vapor fraction is upward of 90%. The char yield from the fast pyrolysis of corn starch is almost zero as illustrated in Table 17.

When red oak char is added to starch, the resulting characteristic curve is shifted in Figure 27 indicating a sharp increase in aerosol production. This observation indicates that char likely acts a nucleation site, supporting this hypothesis.

6. CONCLUSIONS

6.1. Experimental Conclusions

Examination of the filter catch from a fast pyrolysis stream suggested that aerosols are substantially absent. However, this test was based on a hypothesis that did not consider the potential evaporation of liquid aerosols once captured on the filter. Pressure drop measurements on the hot pyrolysis stream provided compelling evidence that aerosol represented a high percentage of the produced bio-oil. Further evidence in support of aerosols was obtained in tests designed to intercept aerosols on a screen assembly in the freeboard and convert them to vapor.

Theoretical calculations supported the hypothesis that liquid droplets captured in a filter will rapidly evaporate, explaining why no liquids were found in the first test. A subsequent test with an inline filter found no loss of bio-oil yield in the condensers, which gives further evidence that bio-oil intercepted in the filter evaporates rather than cracks to gas.

A fast pyrolysis test with corn starch suggested that essentially all the bio-oil is generated as vapor, in direct contradiction to the test with lignocellulosic biomass. Injection of char into the reactor during pyrolysis of corn starch dramatically increased the amount of aerosol, demonstrating the role of nucleation sites on formation of the liquid droplets during fast pyrolysis.

The majority of evidence supports that fast pyrolysis of red oak generates liquid aerosols in the reactor. However, the exit stream can undergo direct contact filtration with insignificant impact on the bio-oil yield.

6.2. Future Opportunities

Additional types of biomass should be studied to determine if general lignocellulosic material behaves similar to red oak with respect to aerosol generation during fast pyrolysis. In addition, other reactor types and configurations could also

be studied under fast pyrolysis conditions to determine if liquid aerosols are generated. This study also indicates that it is possible to used direct contact methods to filter the gas stream with minimal effect on bio-oil yield. Catalytic reforming may also be possible if direct contact methods are used.

REFERENCES

1. Bridgwater, A. V. and Peacocke, G.V.C. 2000. Fast pyrolysis processes for biomass. Renewable & Sustainable Energy Reviews. 4:1-73.

2. Brown, R. C. 2003. Biorenewable Resources: Engineering New Products from Agriculture. Ames, Iowa: Iowa State Press.

3. Borman, G. L. and Ragland, K. W. 1998. Combustion Engineering. Boston: McGraw-Hill.

4. Reed, T. B. ed. 1981. Biomass Gasification: Principles and Technology. Park Ridge, NJ: Noyes Data Corporation.

5. Reed, T. B. and Gaur, S. 1999. A Survey of Biomass Gasification 2000: Gasifier Projects and Manufacturers Around the World. Golden, CO: Biomass Energy Foundation Press.

6. Bridgewater, A. V. and Bridge, S. A. 1991. A review of biomass pyrolysis and pyrolysis technologies. In Biomass Pyrolysis Liquids Upgrading and Utilization. ed. Bridgwater, A. V. and Grassi, G. 11-92. Elsevier Science.

7. Demirbas, A. 2000. Mechanisms of liquefaction and pyrolysis reactions of biomass. Energy Conversion & Management. 41:633-646.

8. Minowa, T., Kondo, T., and Sudirjo, S. T. 1998. Thermochemical liquefaction of Indonesian biomass residues. Biomass & Bioenergy. 5/6:517-524.

9. Chornet, W. and Overend, R. P. 1985. Fundamentals of Thermochemical Biomass Conversion. Amsterdam: Elsevier.

10. Riegel, E. R. 1933. Industrial Chemistry. New York: The Chemical Catalog Company.

11. Diebold, J. P. and Bridgwater, A. V. 1999. Overview of fast pyrolysis of biomass for the production of liquid fuels. In Fast Pyrolysis of Biomass: A Handbook. 14-32. Newbury, UK: CPL Press.

12. Bridgwater, A.V., Meier, D., Radlein, D. 1999. An overview of fast pyrolysis of biomass. Organic Geochemistry. 30:1479-1493.

13. Daugaard, D. E. and Brown, R. C. 2003. In revision: Enthalpy for pyrolysis for several types of biomass. Energy and Fuels.

14. Scott, D. S., Majerski, P., Piskorz, J., and Radlein, D. 1999. A second look at fast pyrolysis of biomass – the RTI process. Journal of Analytical and Applied Pyrolysis. 51:23-27.

15. Kosstrin, H. M. 1980. Direct formation fo pyrolysis oil from biomass. In Proceedings of the Specialists Workshop on Fast Pyrolysis of Biomass. 105-21. Copper Mountain, CO.

16. Antal, M. J. 1982. Vapor phase pyrolysis of biomass derived volatile matter. In Fundamentals of Thermochemical Biomass Conversion. 511-37. London: Elsevier.

17. Diebold, J. P. 1985. The cracking kinetics of depolymerized biomass vapors in continuous, tubular reactor. M.S. thesis, Colorado Schools of Mines.

18. Liden, A. G., Berruti, F., and Scott, D. S. 1988. A kinetic model for the production of liquids from the flash pyrolysis of biomass. Chemical Engineering Communications. 65:207-21.

19. Boroson, M. L., Howard, J. B., Longwell, J. P., and Peters, A. W. 1989. Product yields and kinetics from the vapor phase cracking of wood pyrolysis tars. AIChE Journal. 35:120-8.

20. Chan, W. R., Kelbon, M., and Krieger, B. B. 1985. Modeling and experimental verification of physical and chemical processes during pyrolysis of a large biomass particle. Fuel. 64:1505-13.

21. Koufopanos, C. A., Papayannakos, N., Mashio, G., and Lucchesi, A. 1991. Modeling the pyrolysis of biomass particles: studies on kinetics, thermal and heat transfer effects. The Canadian Journal of Chemical Engineering. 69:907-15.

22. Di Blasi, C. 1993. Analysis of convection and secondary reaction effects within porous solid fuels undergoing pyrolysis. Combustion Science Technology. 90:315

23. Bryden, K. M., Ragland, K. W., and Rutland, C. J. 2002. Modeling thermally thick pyrolysis wood. Biomass and Bioenergy. 22:41-53.

24. Hagge, M. J. and Bryden, K. M. 2002. Modeling the impact of shrinkage on the pyrolysis of dry biomass. Chemical Engineering Science. 57: 2811-23.

25. Bryden, K. M. and Hagge, M. J. 2003. Modeling the combined impact of moisture and char shrinkage on the pyrolysis of a biomass particle. Fuel. 82:1633-44.

26. Melaaen, M. C. and Gronli, M. G. 1997. Modeling and simulation of moist wood drying and pyrolysis. In Developments in Thermochemical Biomass Conversion. 132-46. London: Blackie Academic and Professional.

27. Diebold, J.P., Milne, T. A., Czernik, S., Oasmaa, A., Bridgwater, A. V., Cuevas, A., Gust, S., Huffman, D., and Piskorz, J. 1999. Proposed specifications for various grades of pyrolysis oils. In Fast Pyrolysis of Biomass: A Handbook. 102-114. Newbury, UK: CPL Press.

28. Oasmaa, A. 1999. Testing standard methods. In Fast Pyrolysis of Biomass: A Handbook. 69-74. Newbury, UK: CPL Press.

29. Radlein, D. 1999. The production of chemicals from fast pyrolysis bio-oils. In Fast Pyrolysis of Biomass: A Handbook. 164-188. Newbury, UK: CPL Press.

30. Radlein, D. 2000. Study of Levoglucosan: A Review. PWGSC Contract No. 23348-8-3247/001/SQ. Waterloo, Canada: Resource Transforms International Ltd.

31. Radlein, D. 1999. The production of chemicals from fast pyrolysis bio-oils. In Fast Pyrolysis of Biomass: A Handbook. 164-188. Newbury, UK: CPL Press.

32. Wang, D., Czernik, S., and Chornet, E. 1998. Production of hydrogen from biomass by catalytic steam reforming of fast pyrolysis oils. Energy & Fuels. 12:19-24.

33. Sandvig, E., Walling, G., Daugaard, D. E., Pletka, R., Radlein, D., Johnson, W., and Brown, R. C. 2003. The prospects for integrating fast pyrolysis into biomass power systems. International Journal of Power and Energy Systems. In publication.

34. Gronli, M. G. 2000. Mathematical model for wood pyrolysis – comparison of experimental measurements with model predictions. Energy & Fuels. 14:791-800.

35. Janse, A. M. C., Westerhout, R. W. J., Prins, W. 2000. Modeling of flash pyrolysis of single wood particle. Chemical Engineering and Processing. 39:239-252.

36. Lathouwers, D. and Bellan, J. 2001. Modeling of dense gas – solid reactive mixtures applied to biomass pyrolysis in a fluidized bed. International Journal of Multiphase Flow. 27:2155-2187.

37. Di Blasi, C. 2000. Modeling the fast pyrolysis of cellulosic particles in fluid-bed reactors. Chemical Engineering Science. 55:5999-6013.

38. Oja, V. and Suuberg, E. M. 1999. Vapor pressures and enthalpies of sublimation of D-Glucose, D-Xylose, Cellobiose, and Levoglucosan. J. Chem. Eng. Data. 44:26-29.

39. Suuberg, E. M., Milosavljevic, I., and Oja, V. 1996. Two-regime global kinetics of cellulose pyrolysis: The role of tar evaporation. In Twenty-Sixth Symposium (International) on Combustion. 1515-1521. Pittsburgh, PA: The Combustion Institute.

40. Colbeck, I. 1998. Introduction to aerosol science. In Physical and Chemical Properties of Aerosols. ed. Colbeck, I. 1-30. New York: Blackie Academic and Professional.

41. Reist, P. C. 1984. Introduction to Aerosol Science. New York: Macmillan Publishing.

42. Diebold, J. P. 1980. Ablative pyrolysis of macroparticles of biomass. In Proceedings of Specialists Workshop on Fast Pyrolysis of Biomass. Copper Mountain Colorado. 237-251.

43. Lédé, J., Panagopoulos, J., Li, H. Z., and Villermaus, J. 1985. Fast pyrolysis of wood: direct measurement and study of ablation rate. Fuel. 64:1514-1520.

44. Lédé, J., Diebold, J. P., Peacocke, G. V. C., and Piskorz, J. 1996. The nature and properties of intermediate and uvaporized biomass pyrolysis materials. In Fast Pyrolysis of Biomass: A Handbook. 51-65. Newbury, UK: CPL Press.

45. Lédé, J., Diebold, J. P., Peacocke, G. V. C., and Piskorz, J. 1999. The nature and properties of intermediate and unvaporized biomass pyrolysis materials. In Fast Pyrolysis of Biomass: A Handbook. 51-65. Newbury, UK: CPL Press.

46. Piskorz, J., Peacocke, G. V. C., and Bridgwater, A. V. 1999. IEA pyrolysis fundamentals review. In Fast Pyrolysis of Biomass: A Handbook. 33-50. Newbury, UK: CPL Press

47. Bridgwater, A.V. 1999. An introduction to fast pyrolysis of biomass for fuels and chemicals. In Fast Pyrolysis of Biomass: A Handbook. 1-13. Newbury, UK: CPL Press.

48. Meir, D. and Faix, O. 1999. State of the art of applied fast pyrolysis of lignocellulosic materials – a review. Bioresource Technology. 68:71-77.

49. Scott, D. S., Piskorz, J. and Radlein, D. 1985. Liquid products from the continuous flash pyrolysis of biomass. Ind. Eng. Chem. Process. Des. Dev. 24:581-586.

50. Diebold, J. P. and Scahill, J. W. 1997. Improvements in the vortex reactor design. In Developments in Thermochemical Biomass Conversion. 242-52. London: Blackie Academic and Professional.

51. Hoffman, A.C. and Stein, L.E. 2002. Gas Cyclones and Swirl Tubes: Principles, Design and Operation. New York: Springer.

52. Czernik, S., Maggi, R., and Peacoke, G. V. C. 1999. A review of physical and chemical methods of upgrading biomass-derived fast pyrolysis liquids. In Biomass: A Growth Opportunity in Green Energy and Value-added Products. Proceedings of the 4th Biomass Conference of the Americas. 1235-1240.

53. Colver, G., Brown, R. C., Shi, H., and Soo, S. Improving efficiency of a counter-current flow moving bed granular filter, Fifth International Symposium on Gas Cleaning at High Temperature, Morgantown, West Virginia, September 18-20, 2002.

54. Fan, M., Marshall, W., Daugaard, D., and Brown, R. C. 2003. Steam activation of chars produced from oat hulls and corn stover. Biomass & Bioenergy. In revision.

55. Munson, B. R., Young, D. F., and Okiishi, T. H. 1994. Fundamentals of Fluid Mechanics. 2nd ed. New York: John Wiley & Sons, Inc.

56. Heinsohn, R. J. 1991. Industrial Ventilation: Engineering Principles. New York: John Wiley and Sons.

57. Heinsohn, R. J. and Kabel, R. L. 1999. Sources and Control of Air Pollution. Upper Saddle River, NJ: Prentice Hall.

58. Hinds, W. C. 1999. Aerosol Technology. 2nd ed. New York: John Wiley and Sons.

59. Diebold, J. P., Oasmaa, A., Bridgwater, A. V., Cuevas, A., Gust, S., Huffman, D., Piskorz, J. 1999. Proposed specifications for various grades of pyrolysis oils. In Fast Pyrolysis of Biomass: A Handbook. 102-114. Newbury, UK: CPL Press.

60. Lide, D. R. 1998. CRC Handbook of Chemistry and Physics. 79th ed. New York: CRC Press.

61. Vargaftik, N. B. 1975. Tables of Thermophysical Properties of Liquids and Gases. 2nd ed. Washington, D. C.: Hemisphere.

62. Lathouwers, D. and Bellan, J. 2001. Yield optimization and scaling of fluidized beds for tar production from biomass. Energy & Fuels. 15:1247-1262.

63. Beckwith, T. G., Marangoni, R. D., and Lienhard V, J. H. 1993. Mechanical Measurements. 5th ed. New York: Addison-Wesley Publishing Co. 45-125.

APPENDIX A. OPERATING PROCEDURES

The following procedure is provided for reference to the normal operation of the fast pyrolysis reactor.

Fast Pyrolysis Fluidized Bed Reactor Operation
Biomass Energy Conversion (BECON) Facility – Ames, IA
Written by Daren Daugaard – 6/3/01
Last Updated: 4/1/03

A. General

Pyrolysis (fast) – The thermal decomposition of a material in the absence of oxygen. The reaction is considered endothermic and thus energy will be provided for the reaction in the form of heat from a natural gas burner. Pyrolysis produces a product stream in which a condensable liquid is yielded called pyrolysis oil or bio-oil. Bio-oil is the primary product.

Producer gas – The gas that is produced during pyrolysis. The gas may contain carbon monoxide (CO), methane (CH_4), hydrogen (H_2), carbon dioxide (CO_2), and nitrogen (N_2). There may be trace amounts of higher hydrocarbons (C_2H_2, C_2H_4, C_2H_6, etc.).

Fluidized bed – A bed is fluidized when the force of a gas flowing up through a bed of solid particles overcomes the inter-particle and gravitational forces acting on the particles. The bed has properties of a liquid in the fluidized state. A fluidized bed applied to the pyrolysis of biomass is a safe means of converting solid fuel to primarily a liquid bio-oil, and secondarily to solid char

and low heating value gas. However, in the unlikely event the bed is not properly maintained or operated, serious injury or death may result.

Biomass fuel – any material that is primarily organic (i.e., composed of carbon) in nature and comes from a plant or tree. Corn, seed corn, cobs, husks, and various woods are all types of biomass fuel.

The remainder of this document is to be used as a guide. It is not an exhaustive explanation of the system and how it is to be operated. Therefore, it is recommended that the operator use great caution and respect when operating the pyrolysis unit.

B. Potential Hazards

The following list is not exhaustive but gives a brief overview of some of the hazards.

- The reactor and auxiliary equipment are constructed of stainless steel and cold rolled steel and may injure someone if the equipment should fall. Steel toe shoes are required.
- Small and large particles and other debris may become airborne. Safety glasses are required.
- The reactor operates at high temperatures. Even though the reactor is well insulated, the surface temperatures are still may be very hot. Contact with the reactor should be avoided. If contact with the reactor is necessary, high temperature clothing (gloves, etc.) is recommended.
- The effluent from the reactor may be hazardous if inhaled. In particular, during pyrolysis, significant concentrations of carbon monoxide and liquid aerosols may be produced which could cause dizziness or even asphyxiation.

- Motor driven augers are used to transport biomass within the system. Stay clear of all moving parts including motor shafts during operation. Do not remove guard equipment unless the piece of equipment has been locked out by standard lockout/tagout procedures.

C. Pre-operation Checklist

Prior to operation, the following checks should be performed:

- The blower and/or compressed nitrogen supply is operational and the valves are in their proper orientation.
- All cyclone catches contain ample room to collect char.
- The packed bed is re-charged with glass wool.
- The system has bio-oil collection containers weighed and installed on the condenser train.
- The fluidized bed contains sufficient material for operation.
- All data acquisition equipment (thermocouples, pressure transducers, etc.) is operating properly.
- The control system is operating correctly.
- All other controls, equipment, motors, etc. are operating properly.

D. System Startup

1. Turn on the main power supply to all panels located on Panel #1 (both 460 V and 120 V). Plug in compressor drains (two) located in the Mechanical Room. Power up the data acquisition computer and the signal conditioner located in Panel #2.

2. Turn on blower or compressed air to initiate fluidization of the bed. Turn on compressed air to natural gas burner. On the Panel #3, turn the burner valve open to 34. Then turn the burner power switch to on. Watch until the ignition light turns on and then off to signal a successful ignition. Once the burner is ignited, set the annulus temperature to the desired set point. Then start the data acquisition program.
3. Start the purge nitrogen to the injection auger. This should be set at minimum of 20 SCFH.
4. Bring the bed to temperature by monitoring the data acquisition computer. Be sure to adjust down the fluidization velocity of the blower as the temperature of the bed increases. When the system comes to a steady state temperature, then pyrolysis may begin.

E. Pyrolysis Mode

1. To begin pyrolysis, turn off the blower or compressed air and fluidize with nitrogen at the desired gas flow rate as was air. Verify the steady state condition of the temperature with the nitrogen flowing. If the desired bed temperature is reached, then proceed to the next step. Adjustments to the temperature may be made by altering the set-point of the burner by adjusting the controls on Panel #3.
2. The biomass agitator for the hopper and injection auger may now be turned on. In addition, the metering auger may be turned on the specific mass flow desired. Typical mass flow rates are between 4 kg/hr and 10 kg/hr. All of the controls are located on and next to Panel #1.
3. The unit may be run for several hours until either the nitrogen or biomass is depleted. Attention should be paid to various temperatures and pressures. Typical temperatures in the bed are usually approximately 500 °C. Typical

bed pressures are near 20 inches of water (above atmospheric). If these conditions are greatly exceeded, the unit should be shut down.

4. During testing, bio-oil collection containers on the bottom of the condenser train should be closely monitored and changed out as required.

F. System Shut Down

1. Shut down begins by stopping the biomass fuel flow. Turning off the metering auger will accomplish this. The agitator may also be shut off at this time. The bed should continue to be fluidized by nitrogen and heated for typically 10 minutes after shutting off the biomass fuel flow.
2. After the required 10 minutes, the nitrogen may be shut off and the blower or compressed air may then fluidize the bed. Also, the burner should be shut off using the toggle switch on Panel #3. Note, the pyrolysis oil should continue to drain from the condensers.
3. The bed will likely heat up from the running temperature due to combustion of residual material and then fall back down. The bed temperature during shut down should be kept below 900 °C. If at any time this is exceeded, fluidize the bed with nitrogen until the temperature falls to 350 °C.
4. Once the bed is at 350 °C under air or nitrogen, then the fluidization should be stopped by shutting off the gas flow. The injection auger may be turned off at this time. In addition, the purge nitrogen can also be discontinued to the injection auger. The compressed air line to the burner may also be turned off. The data acquisition computer and signal conditioner may also be turned off. The water release valves for the air compressor located in the Mechanical Room may be unplugged at this time.

G. System Maintenance

The system must be maintained to ensure proper and safe operation of the equipment. Many components of the system will require regular maintenance while other parts should be inspected at least twice a year.

Maintenance:

- Empty the cyclone catch containers: When emptying the containers the contents can become airborne. Therefore protective eye-goggles and breathing mask should be worn.
- The bed should be inspected for both residual biomass and depth of sand after every run. Removing the cover of the bed allows access to the bed. If need, more sand may be added. Bed material may also be removed through the top of the bed.
- The bio-oil outlets at the bottom of the condensers should also be inspected for blockage once the unit cools. If unusually high pressures were noted, the condenser tubes should be inspected for blockage.
- The blower oil should be checked at least twice a year. The bearings on all motors should be greased at least twice a year.

APPENDIX B. NOMENCLATURE

The nomenclature is provided to clarify the use of symbols within this document.

Letter	Description
a	height of cyclone inlet
A	area
am	log mean difference
b	width of cyclone inlet, equation constant
Bi	Biot Number
C	specific heat, discharge coefficient for non-ideal flow
C_c	Cunningham's slip factor
c_o	inlet mass fraction of particles to gas
d	diameter
D	diffusivity, cyclone diameter
d_{p50}	50% cut particle size
E	Efficiency
f	mass fraction of dry bio-oil in vapor state, friction factor
F	function
G	gravitational settling parameter
h	height, convection heat transfer coefficient, enthalphy
H	height
J	Diffusion Flux
k	flow constant
Ku	Kuwabara Hydrodynamic factor
L	length
m	mass flow rate
M	molecular weight
Nu	Nusselt number
p	pressure in freeboard, general pressure
Pe	Peclet Number
Pr	Prandtl Number
Q	volumetric flow rate
R	radius, diameter ratio
Re	Reynolds Number
rh	relative humidity
R_u	Univerisal gas constant
S	length of cyclone vortex finder
Sc	Schmidt Number
Stk	Stokes Number
T	freeboard temperature, general temperature
t	time
U_o	superificial velocity
v	specific volume, velocity
V	volumetric flow rate
vg	Mathcad parameter
x	mole fraction
y	water mass fraction of bio-oil
z	mass fraction

Greek Letter	Description
α	constriction coefficient, volume fraction of fibers in filter
β	diameter ratio
Δ	difference
η	viscosity
μ	viscosity
ρ	density
σ	uncertainity

Subscript	Description
0	initial
1	species 1
2	species 2
b	biomass
bed	sand bed
c	char, critical, cone
CS	imagined cylinder surface
d	cyclone outlet
D	diffusion
DR	diffusion-interception interaction
f	fiber
fb	freeboard
fg	vaporization
g	gas
G	gravitational settling
H20	water
i	indice
I	impaction
in	inlet
mix	gas mixture
N2	nitrogen
NC	non-condensible
oil	wet bio-oil
p	particle
pg	partial of particle species
θ	tangential
r	radial
R	interception
res	residence
s	sand, corn starch, standard
ss	slip stream
v	saturated vapor, constant volume
V	vapor, dry bio-oil vapor
w	wall
x	cyclone exit

APPENDIX C. CYCLONES SOLID SEPARATOR DESIGN

The following analysis provides the mathematical details in the design of the cyclone separators.

Analysis of the cut diameter of the cyclones.
Based on methodology found in Hoffman and Steins [51]

Dimensions of Cyclones

$a := 0.0302m$

$b := 0.0127m$

$D := 0.0604m$

$D_x := 0.0318m$

$D_d := 0.0254m$

$S := 0.0508m$

$H := 0.2637m$

$H_c := 0.1715m$

Conditions and Properites of Gas and Char

$Q_s := 220 \frac{liter}{min}$

$T_s := 298.15K$

$P_s := 101325Pa$

$T_c := (273.15 + 450)K$

$P_c := P_s$

$Q := Q_s \left(\frac{T_c}{T_s}\right)\left(\frac{P_s}{P_c}\right)$

$c_o := \frac{0.85\frac{kg}{hr}}{15.11\frac{kg}{hr}}$ $c_o = 0.056$

$\rho_p := 400\frac{kg}{m^3}$

$\mu_{N2} := 3.51\ 10^{-5} N \frac{s}{m^2}$

$Q = 533.601 \frac{liter}{min}$

Calculations

$R := \frac{D}{2}$

$R_x := \frac{D_x}{2}$

$R_d := \frac{D_d}{2}$

$v_{in} := \frac{Q}{a\,b}$ $v_{in} = 23.188\frac{m}{s}$ Inlet velocity

$R_{in} := R - \frac{b}{2}$ $R_{in} = 0.024\,m$ Equivalent inlet radius

$H_{CS} := (H - S) - H_c \frac{(R_x - R_d)}{R - R_d}$ $H_{CS} = 0.182\,m$ Height of imaginary cylinder surface

$$v_{rCS} := \frac{Q}{\pi\ D_x\ H_{CS}} \qquad v_{rCS} = 0.49\frac{m}{s}$$ Radial Velocity

$$\alpha := 1.04\left(\frac{b}{R}\right)^{0.5} \qquad \alpha = 0.674$$ Constriction coefficient

Barth model [51:78]

$$v_{\theta w} := \frac{\left(v_{in}\ R_{in}\right)}{\alpha\ R} \qquad v_{\theta w} = 27.152\frac{m}{s}$$ Tangential wall velocity

$$f := 0.005\left[1 + 3\left(c_o\right)^{0.5}\right] \qquad f = 8.558 \times 10^{-3}$$ Friction factor

$$v_{\theta CS} := \frac{v_{\theta w}\left(\frac{R}{R_x}\right)}{1 + \frac{\left(H_{CS}\ R\ \pi\ f\ v_{\theta w}\right)}{Q}} \qquad v_{\theta CS} = 35.567\frac{m}{s}$$ Tangential cylinder surface velcoity

$$d_{p50} := \left[\frac{\left(v_{rCS}\ 9\ \mu_{N2}\ D_x\right)}{\rho_p\ v_{\theta CS}^{\ 2}}\right]^{0.5} \qquad d_{p50} = 3.12 \times 10^{-6}\,m$$ Cut Diameter - 50%

$$\eta\left(d_p\right) := \frac{1}{1 + \left(\frac{d_{p50}\ 1\ 10^6}{d_p}\right)^{6.4}}$$ Dirgo and Leith efficiency curve [51:79]

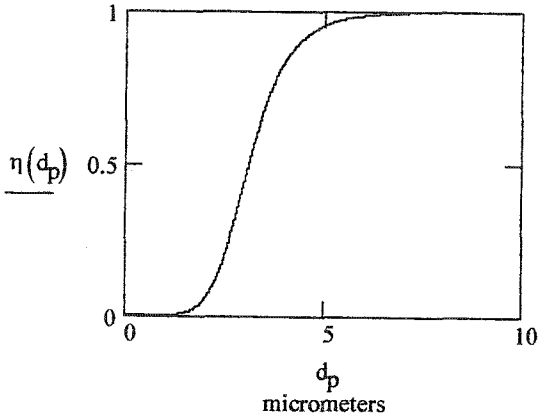

Diagram of cyclone showing dimensions

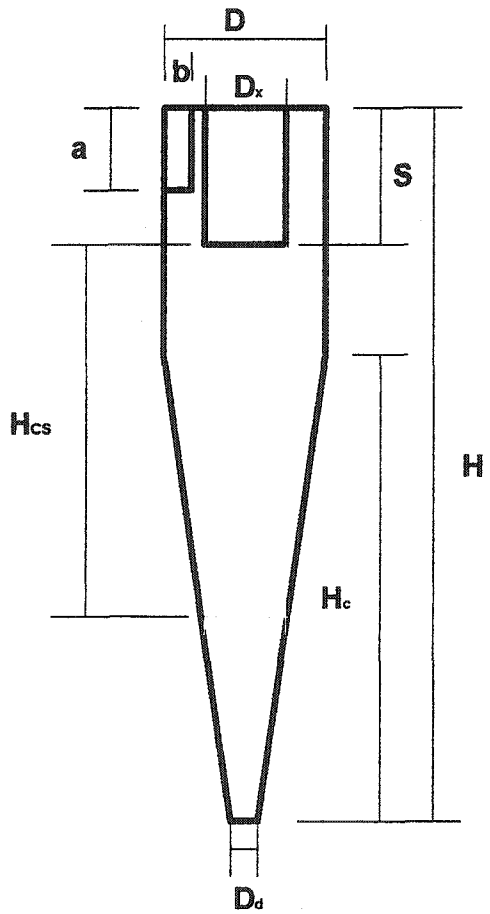

APPENDIX D. COMPONENT DESCRIPTIONS

The tables below provide details about the equipment incorporated in the fast pyrolysis system.

General Component	Make / Model	Serial Number	Rating
Blower	Roots Universal RAI 22URAI	3905863	460 V
Blower VFD	Toshiba VF-S7		400 V - 0.75 KW
Burner	Eclipse Thermjet TJ015	TJ015MATN-NF	44 kW (thermal)
Computer	Dell Dimension L500r	432746	
Data Acquisition Chasis	National Instruments SCXI-1000	B78442	
Data Acquisition Software	LabVIEW 5.1		
Hopper Agitator Motor	Dayton 1K058		1/4 HP / 460V / 1725 RPM
Injection Auger Motor	Dayton 4Z393A		1/2 HP / 460V / 133 RPM
Metering Auger Motor	Dayton 4Z385A		1/3 HP / 460V / 39.7RPM
Metering Auger VFD	Toshiba VF-S7		400 V - 0.75 KW
Sample Line Pump	Thomas Pumps 47436		1/12 HP / 120 V / 34 LPM
Sieve, Ro-Tap	CE Tyler B	4837	120V
Sonic Sifter	ATM Co. L3P	A-1941	120V

Data Collection Component	Make / Model	Serial Number	Uncertainty	Rating
Mass Flow Meter (gas)	Alicat Scientific MC-500SLPM-D(N2)	13694	2.5 SLPM	500 SLPM
Micro Gas Chromatagraph	Varian CP-2003	941469	1% Abs.	
Pressure Transducers	Omega 14PC		0.75% F. S.	
Scale	Setra 1000	01000-509-0619	0.02 g	1500 g
Scale	Sauter Multi Scale	703830	0.02 kg	1360 kg
Thermocouples	Omega Type K		4 °C at 500 °C	
Titrator, Karl-Fischer	KEM MKS-500	NDB12868	1% Abs.	
Volumetric Gas Meter	American Meter Co. AC-630		1% Abs.	300 LPM

APPENDIX E. GLASS FIBER FILTER CAPTURE EFFICIENCY

The following analysis details the collection efficiency of a packed fiber filter.

Glass Fiber Capture Efficiency [58]

$d_p := 1\ 10^{-6}\,m$ — Aerosol particle diameter

$d_f := 8\ 10^{-6}\,m$ — Fiber diameter

$R := \frac{d_p}{d_f}$ $R = 0.125$ — Diameter ratio

$d_{filter} := 4.4cm$ $L_{filter} := 8.9cm$ — Length of Filter

$m_f := 10.31gm$ $\rho_f := 2600\frac{kg}{m^3}$ — Density of fiber

$$\alpha := \frac{\frac{m_f}{\rho_f}}{L_{filter}\frac{\pi\, d_{filter}^2}{4}}$$ $\alpha = 0.029$ — Volume fraction of fibers in filter

$$Ku := \frac{-\ln(\alpha)}{2} - \frac{3}{4} + \alpha - \frac{\alpha^2}{4}$$ $Ku = 1.044$ — Kuwabara hydrodynamic factor

$$E_R := \frac{(1-\alpha)\,R^2}{Ku\,(1+R)}$$ $E_R = 0.013$ — Single fiber efficiency for interception

$\rho_p := 1200\frac{kg}{m^3}$ — Density of bio-oil particle

$C_c := 1.155$ — Cunningham Slip Factor for 1 micron water droplet

$Q := 42\frac{liter}{min}$ — Based on flow rate of vein pump

$$A := \pi\left(\frac{d_{filter}}{2}\right)^2$$ — Area of filtter

$U_o := \frac{Q}{A}$ $U_o = 0.46\frac{m}{s}$ — Superficial Velocity

$\eta := 3.5\ 10^{-5}\,Pa\,s$ — Viscosity of nitrogen at temperature

$$Stk := \frac{\rho_p \, d_p^{\,2} \, C_c \, U_o}{18 \, \eta \, d_f}$$ $Stk = 0.127$ Stokes number

$$J := \left(29.6 - 28 \, \alpha^{0.62}\right) R^2 - 27.5 R^{2.8}$$ $J = 0.332$ Diffusion flux

$$E_I := \frac{(Stk \, J)}{2Ku^2}$$ $E_I = 0.019$ Single fiber impaction efficiency

$$D := 2.74 \, 10^{-11} \frac{m^2}{s}$$ Particle diffusion coefficient

$$Pe := \frac{\left(d_f \, U_o\right)}{D}$$ $Pe = 1.344 \times 10^5$ Peclet number

$$E_D := 2 \, Pe^{\frac{-2}{3}}$$ $E_D = 7.622 \times 10^{-4}$ Single fiber efficiency for diffusion

$$E_{DR} := \frac{1.24 \, R^{\frac{2}{3}}}{(Ku \, Pe)^{0.5}}$$ $E_{DR} = 8.275 \times 10^{-4}$ Single fiber efficiency for diffusion-interception interaction

$$\rho_g := 0.44 \frac{kg}{m^3}$$ Density of gas

$$G := \frac{\left(\rho_g \, d_p^{\,2} \, C_c \, g\right)}{18 \, \eta \, U_o}$$ Gravitational settling parameter

$$E_G := G \, (1 + R)$$ $E_G = 1.933 \times 10^{-8}$ Single fiber efficieny for settling

$$E_{sum} := E_R + E_I + E_D + E_{DR} + E_G$$ $E_{sum} = 0.034$ Total Single fiber efficiency

$$t := L_{filter}$$

$$E := 1 - \exp\left(\frac{-4 \, \alpha \, E_{sum} \, t}{\pi \, d_f}\right)$$ $E = 0.9999992$ Efficiency of collecting specified paticle

APPENDIX F. CONSTANT k FIT

The following data and analysis illustrates how the constant k value was determined.

Calibration Raw Data

Gas	Q_s	T_{fb}	p_{fb}	Δp	Q	mw	$\Delta p/\rho$
	SLPM	°C	kPa	Pa	LPM	kg/kmol	kg/m^3
N_2	220	478.8	103.8	832	541.8	28.01	1790.5
N_2	230	481.2	104.0	933	566.7	28.01	2008.7
N_2	240	484.3	104.3	1030	592.4	28.01	2219.8
N_2	250	487.2	104.5	1111	618.0	28.01	2399.4
N_2	260	482.8	104.8	1197	637.6	28.01	2564.8
N_2	260	471.6	104.6	1153	629.0	28.01	2435.1
N_2	270	473.6	104.9	1236	653.2	28.01	2611.6
N_2	280	473.6	105.3	1403	674.6	28.01	2951.1
N_2	290	474.8	105.6	1499	697.9	28.01	3149.6
N_2	300	477.3	106.0	1598	722.0	28.01	3359.7
N_2	220	483.7	105.2	764	537.9	28.01	1632.2
N_2	230	485.2	105.6	849	561.4	28.01	1810.7
N_2	250	486.0	106.5	1077	605.9	28.01	2279.5
N_2	270	484.7	107.4	1297	647.5	28.01	2717.4
N_2	290	482.6	108.3	1476	687.7	28.01	3057.3
N_2	300	479.7	108.9	1612	704.8	28.01	3308.7
N_2	280	477.6	108.0	1366	661.4	28.01	2819.1
N_2	260	477.1	107.1	1139	619.1	28.01	2369.3
N_2	240	477.1	106.3	955	575.5	28.01	1999.6
N_2	220	478.1	105.7	801	531.5	28.01	1690.7
Ar	150	481.5	104.1	448	369.4	39.95	675.4
Ar	170	486.4	104.9	606	418.4	39.95	913.7
Ar	190	486.8	105.7	793	464.1	39.95	1186.0
Ar	210	484.2	106.8	1000	506.3	39.95	1477.0
Ar	230	481.0	107.7	1185	547.6	39.95	1727.6
Ar	220	476.2	107.3	1114	522.1	39.95	1618.3
Ar	200	471.6	106.4	914	475.6	39.95	1330.9
Ar	180	467.9	105.6	704	429.4	39.95	1028.3
Ar	160	464.6	104.8	541	382.8	39.95	793.0
Ar	150	461.4	104.4	468	358.7	39.95	684.6

Fitting calibration data:

$H = \frac{\Delta p}{\rho}$ H is a dummy variable representing the pressure drop divided by density.

$F(Q) := Q^2$

Fits the equation of: $\frac{\Delta p}{\rho} = k\,Q^2$

$vg := 1$

$k := \text{linfit}(Q, H, F)$

$\log(k) = 7.35079$

$k = 2.243 \times 10^7$ Constant k with units m^4

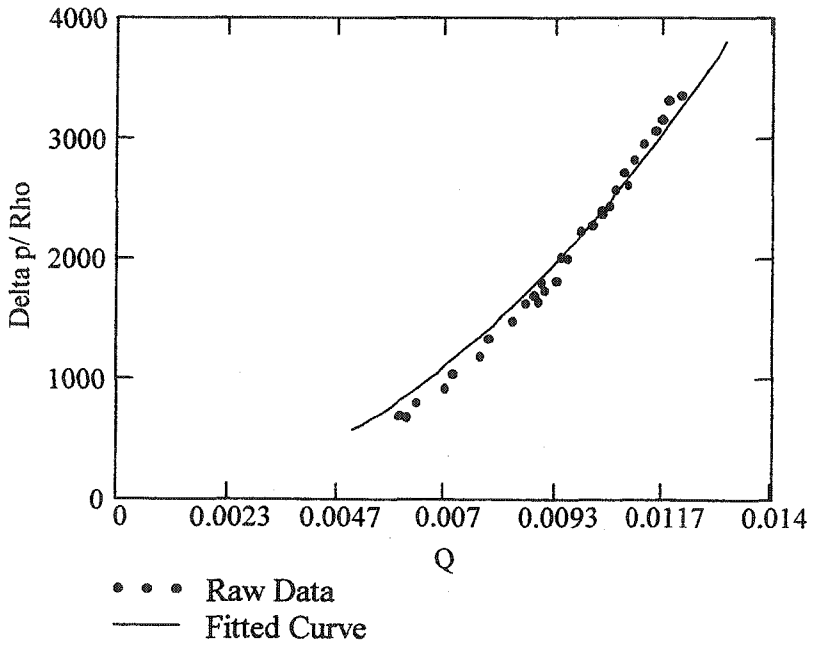

APPENDIX G. WATER AND METHANOL VERIFICATION

The following analysis verifies the developed theory by testing water and methanol.

Verification tests of second hypothesis:

Water (assumed unknown liquid)

$\Delta p := 1689.78\,Pa$ $\quad m_{liquid} := 4.98\frac{kg}{hr}$ $\quad \sigma k := 10\,10^{5-4}\,m$ $\quad \sigma p := 259\,Pa$

$p := 112652.2\,Pa$ $\quad R_u := 8314.47\frac{J}{mol\,K}$ $\quad \sigma m_{N2} := 0.17\frac{kg}{hr}$ $\quad \sigma\Delta p := 37\,Pa$

$T := (546.49 + 273.15)K$ $\quad \sigma y := 0.01$ $\quad \sigma T := 4K$

$m_{N2} := 15.111\frac{kg}{hr}$ $\quad M_{N2} := 28.01\frac{kg}{mol}$ $\quad \sigma m_{liquid} := 0.01\frac{kg}{hr}$ $\quad \sigma M_V := 0\frac{kg}{mol}$

$k := 10^{7.3508\,m-4}$

$f := 0.0, 0.002 .. 1$

$m_{mix}(f) := m_{N2} + f\,m_{liquid}$ Mass flow of mixture in vapor state

$M_V(f) := \frac{k\,m_{mix}(f)\,R_u\,T\,(m_{mix}(f) - m_{N2})\,M_{N2}}{\Delta p\,p\,M_{N2} - k\,m_{mix}(f)\,R_u\,T\,m_{N2}}$ Molecular weight of portion of liquid in vapor state

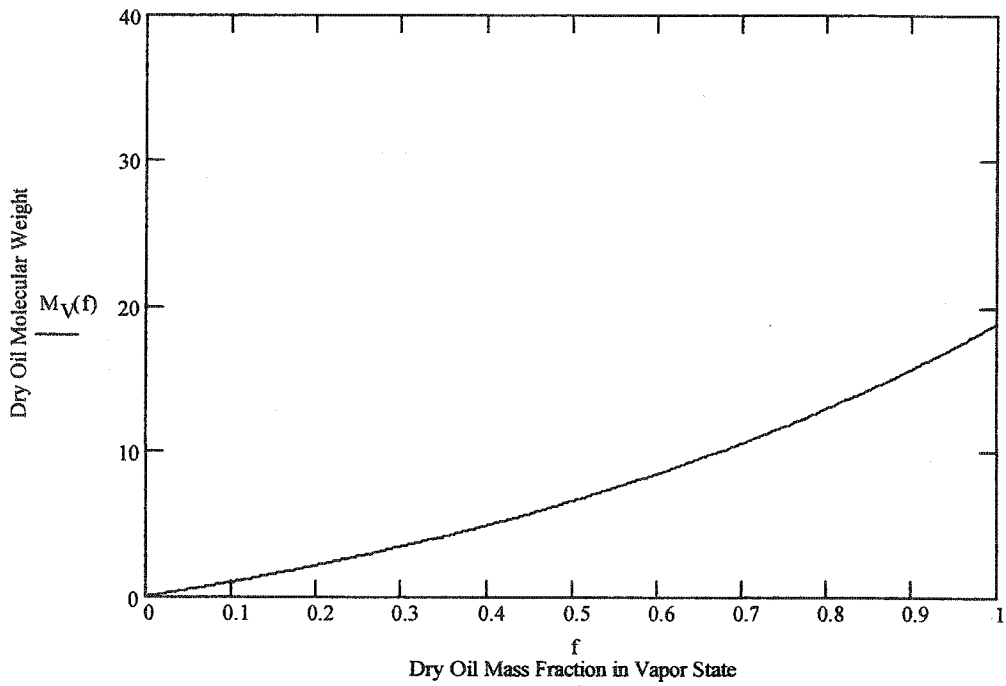

Molecular weigh of liquid assuming 100% vapor

$f := 1 \qquad M_V(f) = 18.872 \frac{kg}{mol}$

Uncertainty analysis:

$M_V := 18.02 \frac{kg}{mol}$ Molecular Weight Value to be Analyzed

Solving governing equation for vapor fraction f:

$$f(m_{liquid}, m_{N2}, M_V, p, \Delta p, k, T) := \frac{\left[\left(\frac{-1}{2} M_V \frac{m_{N2}}{M_{N2}} - \frac{1}{2} m_{N2}\right) \ldots + \frac{1}{2}\left[m_{N2}^{\,2} \frac{\left(M_V^{\,2} - 2 M_V M_{N2} + M_{N2}^{\,2}\right)}{M_{N2}^{\,2}} + 4 M_V \frac{p \Delta p}{k R_u T}\right]^{\frac{1}{2}}\right]}{m_{liquid}}$$

Uncertainty analysis for vapor fraction f:

$$\sigma f := \left[\begin{array}{l} \left(\frac{d}{dm_{liquid}} f(m_{liquid}, m_{N2}, M_V, p, \Delta p, k, T)\, \sigma m_{liquid}\right)^2 \ldots \\ + \left(\frac{d}{dm_{N2}} f(m_{liquid}, m_{N2}, M_V, p, \Delta p, k, T)\, \sigma m_{N2}\right)^2 \ldots \\ + \left(\frac{d}{dM_V} f(m_{liquid}, m_{N2}, M_V, p, \Delta p, k, T)\, \sigma M_V\right)^2 \ldots \\ + \left(\frac{d}{dp} f(m_{liquid}, m_{N2}, M_V, p, \Delta p, k, T)\, \sigma p\right)^2 \ldots \\ + \left(\frac{d}{d\Delta p} f(m_{liquid}, m_{N2}, M_V, p, \Delta p, k, T)\, \sigma \Delta p\right)^2 \ldots \\ + \left(\frac{d}{dk} f(m_{liquid}, m_{N2}, M_V, p, \Delta p, k, T)\, \sigma k\right)^2 \ldots \\ + \left(\frac{d}{dT} f(m_{liquid}, m_{N2}, M_V, p, \Delta p, k, T)\, \sigma T\right)^2 \end{array}\right]^{\frac{1}{2}}$$

$f(m_{liquid}, m_{N2}, M_V, p, \Delta p, k, T) = 0.974$

$\sigma f = 0.089$

Verification tests of second hypothesis:

Methanol (assumed unknown liquid)

$\Delta p := 1253.7\text{Pa}$ $\quad m_{liquid} := 3.84\frac{kg}{hr}$ $\quad \sigma k := 4.5\,10^{-4}\,m^{5}$ $\quad \sigma p := 50\text{Pa}$

$p := 111552.3\text{Pa}$ $\quad R_u := 8314.47\frac{J}{mol\,K}$ $\quad \sigma m_{N2} := 0.17\frac{kg}{hr}$ $\quad \sigma\Delta p := 35\text{Pa}$

$T := (503.62 + 273.15)\text{K}$ $\quad \sigma y := 0.01$ $\quad \sigma T := 4\text{K}$

$m_{N2} := 15.111\frac{kg}{hr}$ $\quad M_{N2} := 28.01\frac{kg}{mol}$ $\quad \sigma m_{liquid} := 0.01\frac{kg}{hr}$ $\quad \sigma M_V := 0\frac{kg}{mol}$

$k := 10^{7.3508}\,m^{-4}$

$f := 0.0, 0.002 .. 1$

$m_{mix}(f) := m_{N2} + f\,m_{liquid}$ Mass flow of mixture in vapor state

$$M_V(f) := \frac{k\,m_{mix}(f)\,R_u\,T\,(m_{mix}(f) - m_{N2})\,M_{N2}}{\Delta p\,p\,M_{N2} - k\,m_{mix}(f)\,R_u\,T\,m_{N2}}$$

Molecular weight of portion of liquid in vapor state

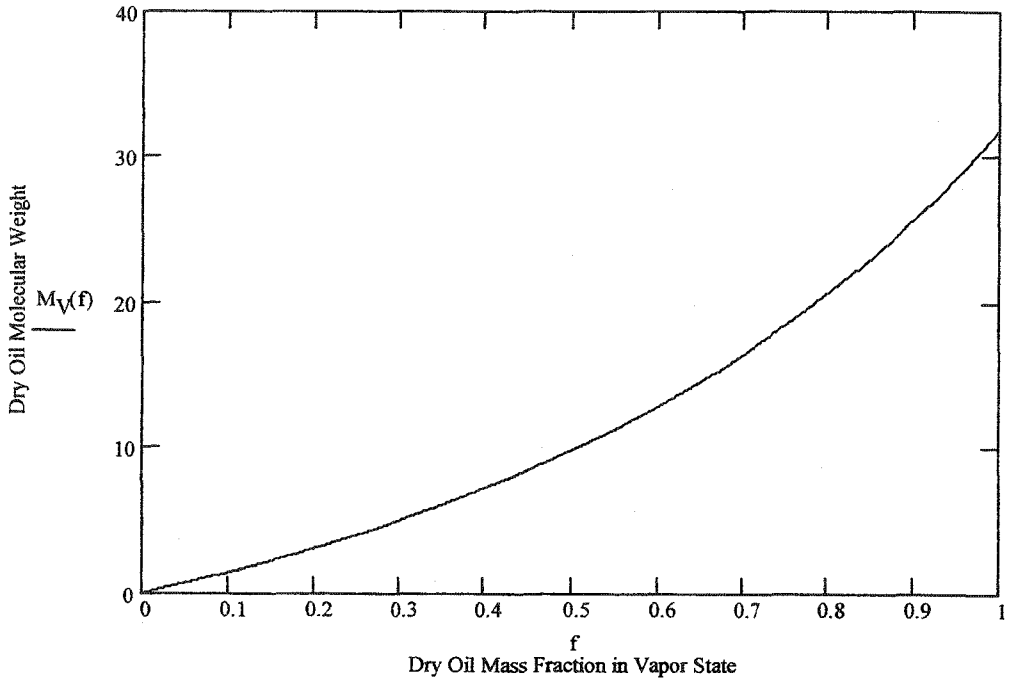

Molecular weigh of liquid assuming 100% vapor

$f := 1$ $\quad M_V(f) = 31.794 \frac{kg}{mol}$

Uncertainty analysis:

$M_V := 32.04 \frac{kg}{mol}$ Molecular Weight Value to be Analyzed

$f\left(m_{liquid}, m_{N2}, M_V, p, \Delta p, k, T\right) = 1.004$

$\sigma f = 0.102$

APPENDIX H. PRESSURE DROP RELATIONSHIP CALCULATIONS

The following analysis illustrates the calculation of the characteristic curve for red oak.

Red oak test #1 for second hypothesis

Test Values

$\Delta p = 1438.3\,Pa$

$p = 113358.9\,Pa$

$T = (554.01 + 273.15)\,K$

$m_{N2} = 15.111\,\frac{kg}{hr}$

$m_{NC} = 2.538\,\frac{kg}{hr}$

$k = 10^{7.3508}\,m^{-4}$

$m_{H2O} = 1.415\,\frac{kg}{hr}$

$M_{NC} = 30\,\frac{kg}{mol}$

$m_{biomass} = 8.551\,\frac{kg}{hr}$

$f = 0.0, 0.002 .. 1$

$m_{oil} = 5.157\,\frac{kg}{hr}$

$y = 0.2744$

$M_{H2O} = 18.02\,\frac{kg}{mol}$

$M_{N2} = 28.01\,\frac{kg}{mol}$

$R_u = 8314.47\,\frac{J}{mol\ K}$

$$m_{mix}(f) = m_{N2} + m_{NC} + y\ m_{oil} + f\ (1 - y)\ m_{oil}$$

$$M_V(f) = \frac{f\ (1 - y)\ m_{oil}}{\frac{\Delta p\ p}{k\left[m_{N2} + m_{NC} + y\ m_{oil} + f\ (1 - y)\ m_{oil}\right] R_u\ T} - \frac{m_{N2}}{M_{N2}} - \frac{m_{NC}}{M_{NC}} - \frac{y\ m_{oil}}{M_{H2O}}}$$

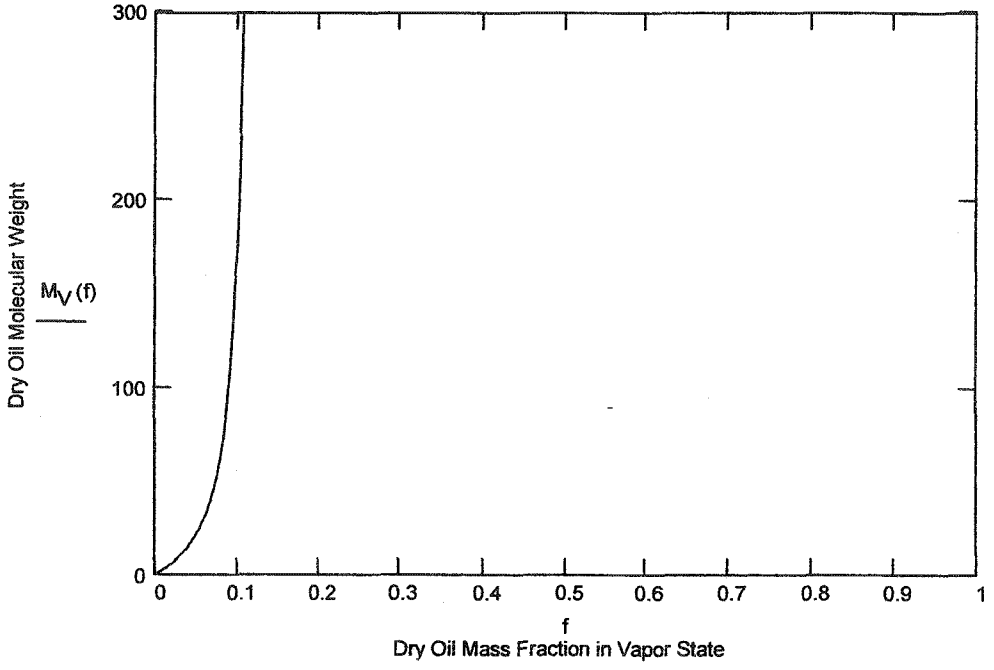

Error Analysis Derivation for Vapor Fraction:

Uncertainty for specified variables:

$\sigma k = 10\ 10^{5} m^{-4}$

$\sigma p = 259 Pa$

$\sigma m_{N2} = 0.17 \frac{kg}{hr}$

$\sigma \Delta p = 37 Pa$

$\sigma m_{NC} = 0.03 \frac{kg}{hr}$

$\sigma T = 4K$

$\sigma M_{NC} = 2 \frac{kg}{mol}$

$\sigma y = 0.01$

$\sigma m_{oil} = 0.01 \frac{kg}{hr}$

$\sigma M_V = 0 \frac{kg}{mol}$

$\sigma m_{H2O} = \left[\left(m_{oil}\ \sigma y \right)^2 + \left(y\ \sigma m_{oil} \right)^2 \right]^{\frac{1}{2}}$

$\sigma m_{H2O} = 0.052 \frac{kg}{hr}$

$M_V = 100 \frac{kg}{mol}$ Molecular Weight Value to be Analyzed

Derivation of Uncertainty Analysis

Taking the following:

$$M_V = \frac{m_V}{n_{mix} - n_{H2O} - n_{N2} - n_{NC}} = \frac{m_V}{\frac{m_{mix}}{M_{mix}} - \frac{m_{H2O}}{M_{H2O}} - \frac{m_{N2}}{M_{N2}} - \frac{m_{NC}}{M_{NC}}}$$

Subsituting:

$m_V = f\ (1 - y) m_{oil}$

$m_{mix} = m_{N2} + m_{NC} + y\ m_{oil} + f\ (1 - y)\ m_{oil}$

$M_{mix} = m_{mix} 2 \left(\frac{k\ R_u\ T}{p\ \Delta p} \right)$

Soving for function f :

$$f\left(M_{NC}, m_{NC}, y, m_{oil}, m_{H2O}, m_{N2}, M_V, p, \Delta p, k, T\right) = \frac{\left[\begin{array}{l} \frac{-1}{2} M_V \frac{m_{H2O}}{M_{H2O}} - \frac{1}{2} M_V \frac{m_{N2}}{M_{N2}} \ldots \\ + \frac{-1}{2} M_V \frac{m_{NC}}{M_{NC}} - \frac{1}{2} \left(m_{N2} + m_{NC} + y\ m_{oil}\right) \ldots \\ \\ + \frac{1}{2} \left[\begin{array}{l} {M_V}^2 \left(\frac{m_{H2O}}{M_{H2O}}\right)^2 \ldots \\ + 2\ {M_V}^2 \frac{m_{H2O}}{M_{H2O}} \frac{m_{N2}}{M_{N2}} \ldots \\ + 2\ {M_V}^2 \frac{m_{H2O}}{M_{H2O}} \frac{m_{NC}}{M_{NC}} \ldots \\ + -2\ M_V \frac{m_{H2O}}{M_{H2O}} \left(m_{N2} + m_{NC} + y\ m_{oil}\right) \ldots \\ + {M_V}^2 \left(\frac{m_{N2}}{M_{N2}}\right)^2 \ldots \\ + 2\ {M_V}^2 \frac{m_{N2}}{M_{N2}} \frac{m_{NC}}{M_{NC}} \ldots \\ + -2\ M_V \frac{m_{N2}}{M_{N2}} \left(m_{N2} + m_{NC} + y\ m_{oil}\right) \ldots \\ + {M_V}^2 \left(\frac{m_{NC}}{M_{NC}}\right)^2 \ldots \\ + -2\ M_V \frac{m_{NC}}{M_{NC}} \left(m_{N2} + m_{NC} + y\ m_{oil}\right) \ldots \\ + \left(m_{N2} + m_{NC} + y\ m_{oil}\right)^2 + 4\ M_V \frac{p\ \Delta p}{k\ R_u\ T} \end{array}\right]^{\frac{1}{2}} \end{array}\right]}{(1 - y)\ m_{oil}}$$

Uncertainty associated with fractioin of dry oil in vapor state
at a specified dry oil molecular weight:

$$\sigma f = \left[\left(\frac{d}{dM_{NC}} f(M_{NC}, m_{NC}, y, m_{oil}, m_{H2O}, m_{N2}, M_V, p, \Delta p, k, T)\, \sigma M_{NC} \right)^2 \dots \right.$$
$$+ \left(\frac{d}{dm_{NC}} f(M_{NC}, m_{NC}, y, m_{oil}, m_{H2O}, m_{N2}, M_V, p, \Delta p, k, T)\, \sigma m_{NC} \right)^2 \dots$$
$$+ \left(\frac{d}{dy} f(M_{NC}, m_{NC}, y, m_{oil}, m_{H2O}, m_{N2}, M_V, p, \Delta p, k, T)\, \sigma y \right)^2 \dots$$
$$+ \left(\frac{d}{dm_{oil}} f(M_{NC}, m_{NC}, y, m_{oil}, m_{H2O}, m_{N2}, M_V, p, \Delta p, k, T)\, \sigma m_{oil} \right)^2 \dots$$
$$+ \left(\frac{d}{dm_{H2O}} f(M_{NC}, m_{NC}, y, m_{oil}, m_{H2O}, m_{N2}, M_V, p, \Delta p, k, T)\, \sigma m_{H2O} \right)^2 \dots$$
$$+ \left(\frac{d}{dm_{N2}} f(M_{NC}, m_{NC}, y, m_{oil}, m_{H2O}, m_{N2}, M_V, p, \Delta p, k, T)\, \sigma m_{N2} \right)^2 \dots$$
$$+ \left(\frac{d}{dM_V} f(M_{NC}, m_{NC}, y, m_{oil}, m_{H2O}, m_{N2}, M_V, p, \Delta p, k, T)\, \sigma M_V \right)^2 \dots$$
$$+ \left(\frac{d}{dp} f(M_{NC}, m_{NC}, y, m_{oil}, m_{H2O}, m_{N2}, M_V, p, \Delta p, k, T)\, \sigma p \right)^2 \dots$$
$$+ \left(\frac{d}{d\Delta p} f(M_{NC}, m_{NC}, y, m_{oil}, m_{H2O}, m_{N2}, M_V, p, \Delta p, k, T)\, \sigma \Delta p \right)^2 \dots$$
$$+ \left(\frac{d}{dk} f(M_{NC}, m_{NC}, y, m_{oil}, m_{H2O}, m_{N2}, M_V, p, \Delta p, k, T)\, \sigma k \right)^2 \dots$$
$$\left. + \left(\frac{d}{dT} f(M_{NC}, m_{NC}, y, m_{oil}, m_{H2O}, m_{N2}, M_V, p, \Delta p, k, T)\, \sigma T \right)^2 \right]^{\frac{1}{2}}$$

$M_V = 100 \frac{kg}{mol}$ — Selected molecular weight for analysis

$f(M_{NC}, m_{NC}, y, m_{oil}, m_{H2O}, m_{N2}, M_V, p, \Delta p, k, T) = 0.091$ — Vapor fraction at specifed molecular weight

$\sigma f = 0.226$ — Uncertainty of vapor fraction at specified molecular weight

Red oak test #2 for second hypothesis

Test Values

$\Delta p = 1381.1\,Pa$

$p = 113030.4\,Pa$

$T = (545.27 + 273.15)\,K$

$m_{N2} = 15.111\,\frac{kg}{hr}$

$m_{NC} = 2.404\,\frac{kg}{hr}$

$k = 10^{7.3508}\,m^{-4}$

$m_{H2O} = 1.340\,\frac{kg}{hr}$

$M_{NC} = 30\,\frac{kg}{mol}$

$m_{biomass} = 8.141\,\frac{kg}{hr}$

$f = 0.0, 0.002 .. 1$

$m_{oil} = 4.825\,\frac{kg}{hr}$

$y = 0.2778$

$M_{H2O} = 18.02\,\frac{kg}{mol}$

$M_{N2} = 28.01\,\frac{kg}{mol}$

$R_u = 8314.47\,\frac{J}{mol\ K}$

$$m_{mix}(f) = m_{N2} + m_{NC} + y\ m_{oil} + f\ (1 - y)\ m_{oil}$$

$$M_V(f) = \frac{f\ (1 - y)\ m_{oil}}{\frac{\Delta p\ p}{k\left[m_{N2} + m_{NC} + y\ m_{oil} + f\ (1 - y)\ m_{oil}\right] R_u\ T} - \frac{m_{N2}}{M_{N2}} - \frac{m_{NC}}{M_{NC}} - \frac{y\ m_{oil}}{M_{H2O}}}$$

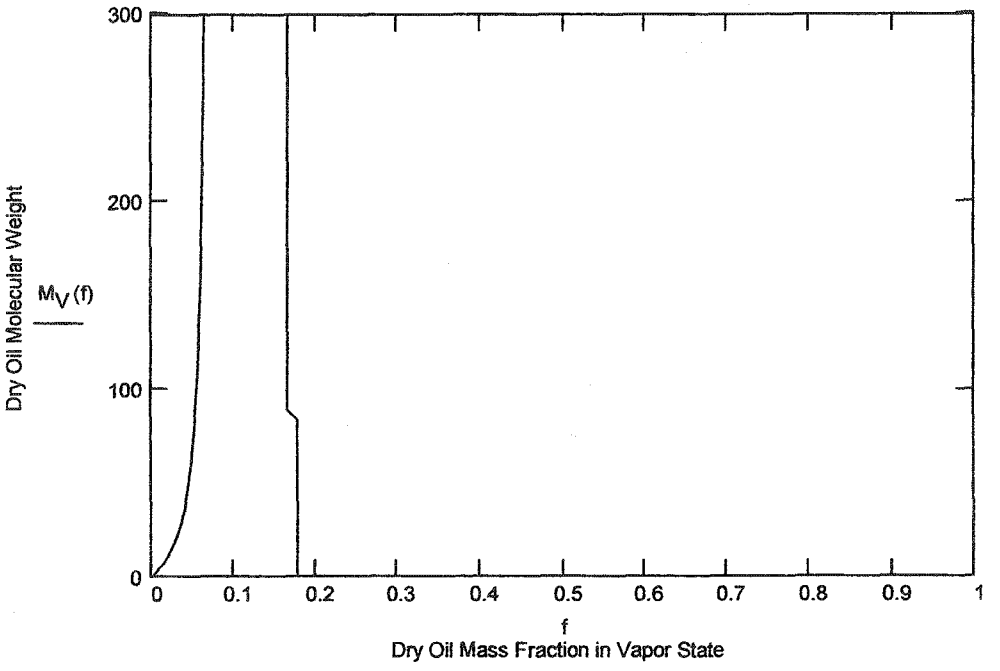

Uncertainty Analysis for Vapor Fraction:

$M_V = 100 \frac{kg}{mol}$ Selected molecular weight for analysis

$f(M_{NC}, m_{NC}, y, m_{oil}, m_{H2O}, m_{N2}, M_V, p, \Delta p, k, T) = 0.055$ Vapor fraction at specifed molecular weight

$\sigma f = 0.24$ Uncertainty of vapor fraction at specified molecular weight

APPENDIX I. FREEBOARD SCREEN CALCULATIONS

The following analysis illustrates the calculation of the characteristic curve for red oak with the screen capturing aerosols in the freeboard.

Red oak with screen in freeboard for the third hypothesis

Test Values

$\Delta p = 1366.1\,Pa$

$p = 108854.9\,Pa$

$T = (494.37 + 273.15)\,K$

$m_{N2} = 15.111\,\frac{kg}{hr}$

$m_{NC} = 1.810\,\frac{kg}{hr}$

$k = 10^{7.3508}\,m^{-4}$

$m_{H2O} = 1.286\,\frac{kg}{hr}$

$M_{NC} = 30\,\frac{kg}{mol}$

$m_{biomass} = 8.307\,\frac{kg}{hr}$

$f = 0.0, 0.002 .. 1$

$m_{oil} = 5.741\,\frac{kg}{hr}$

$y = 0.2240$

$M_{H2O} = 18.02\,\frac{kg}{mol}$

$M_{N2} = 28.01\,\frac{kg}{mol}$

$R_u = 8314.47\,\frac{J}{mol\ K}$

$$m_{mix}(f) = m_{N2} + m_{NC} + y\ m_{oil} + f\ (1 - y)\ m_{oil}$$

$$M_V(f) = \frac{f\ (1 - y)\ m_{oil}}{\frac{\Delta p\ p}{k\left[m_{N2} + m_{NC} + y\ m_{oil} + f\ (1 - y)\ m_{oil}\right] R_u\ T} - \frac{m_{N2}}{M_{N2}} - \frac{m_{NC}}{M_{NC}} - \frac{y\ m_{oil}}{M_{H2O}}}$$

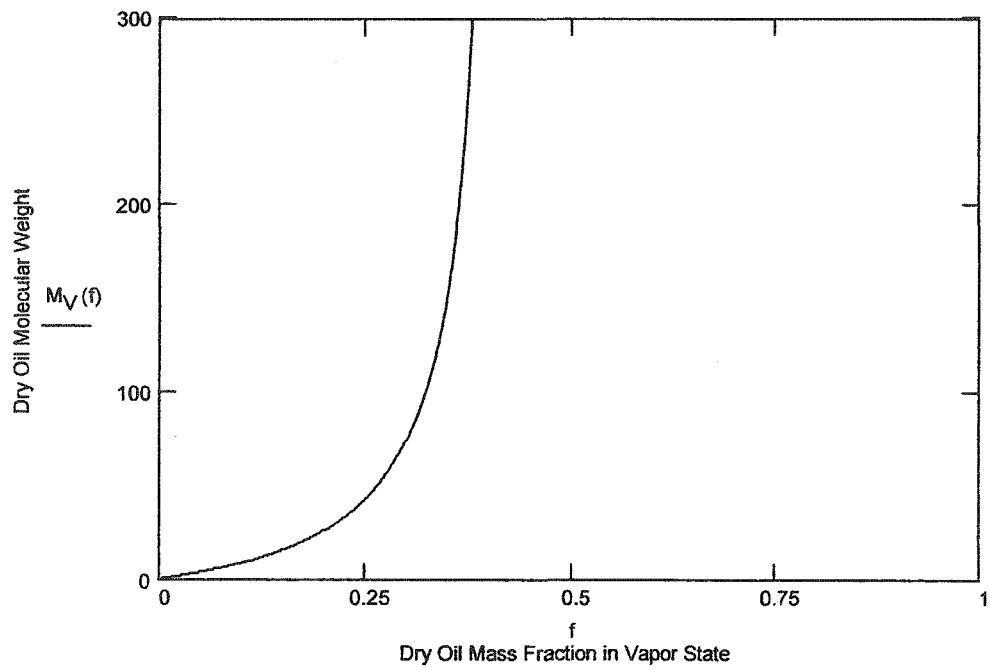

Uncertainty Analysis for Vapor Fraction:

$M_V = 100 \frac{kg}{mol}$ Selected molecular weight for analysis

$f(M_{NC}, m_{NC}, y, m_{oil}, m_{H2O}, m_{N2}, M_V, p, \Delta p, k, T) = 0.322$ Vapor fraction at specifed molecular weight

$\sigma f = 0.192$ Uncertainty of vapor fraction at specified molecular weight

APPENDIX J. DROPLET EVAPORATION FOR CAPTURED AEROSOL

The following analysis illustrates the calculation of the evaporation time of a bio-oil droplet captured in a fibrous filter.

Droplet evaporation of captured aerosol [56,57] for fifth hypothesis

Levoglucosan/Oil		Nitrogen
Particle Properties (p)		Gas properties (g)
$d_{p0} := 10\ 10^{-6}\text{m}$	Droplet diameter	$T_g := 773\text{K}$
$T_{p0} := 500\text{K}$	Droplet initial temperature	$p_g := 101325\text{Pa}$
$M_p := 162.14\frac{\text{kg}}{\text{mol}}$	Molecular weight of levoglucosan	$R_u := 8314.47\frac{\text{J}}{\text{mol K}}$
$D_{12} := 2.9135\ 10^{-15}\ p_g \frac{T_g^{1.81}}{\text{K}^{1.81}} \frac{\text{m}^3\text{s}}{\text{kg}}$	Furfural [60] and nitrogen [61]	$k_g := 0.0537\frac{\text{W}}{\text{m K}}$
$\rho_p := 1200\frac{\text{kg}}{\text{m}^3}$	Density of bio-oil	$\mu_g := 3.51\ 10^{-5}\text{Pa s}$
$k_p := 0.39\frac{\text{W}}{\text{m K}}$	Conductivity of bio-oil	$\mu_s := \mu_g$
$C_v := 3150\frac{\text{J}}{\text{kg K}}$	Specific heat of bio-oil	$C_p := 1115.5\frac{\text{J}}{\text{kg K}}$
$h_{fg} := 7.716\ 10^{5}\frac{\text{J}}{\text{kg}}$	Levoglucosan [38]	$M_g := 28.02\frac{\text{kg}}{\text{mol}}$
$p_v(T_p) := \exp\left(31.19 - \frac{12066\text{K}}{T_p}\right)\text{Pa}$	Levoglucosan [38]	$rh := 0.0$
		$b := 0.4$
$U_g(d_p) := 4.7\frac{\text{m}}{\text{s}}$	Gas velocity	

Calculations:

$p_v(T_{p0}) = 1.162 \times 10^3 \text{ Pa}$ Saturated vapor pressure

$p_{pg} := rh\, p_v(T_g) \qquad p_{pg} = 0 \text{ Pa}$ Vapor pressure in free stream

$Pr := C_p \frac{\mu_g}{k_g} \qquad Pr = 0.729$ Prandtl number

$Sc := \frac{\mu_g}{\rho_g D_{12}} \qquad Sc = 0.585$ Schmidt number

$\rho_g := \frac{p_g M_g}{(R_u T_g)} \qquad \rho_g = 0.442 \frac{kg}{m^3}$ Density of gas

$p_{am}(T_p) := \left[\frac{[(p_g - p_{pg}) - (p_g - p_v(T_p))]}{\ln\left(\frac{p_g - p_{pg}}{p_g - p_v(T_p)}\right)} \right]$ Log mean pressure

$p_{am}(T_{p0}) = 1.007 \times 10^5 \text{ Pa}$

$Re(d_p) := \frac{\rho_g U_g(d_p) d_p}{\mu_g} \qquad Re(d_{p0}) = 0.592$ Reynolds number

$Nu(d_p) := 2 + \left(0.4 Re(d_p)^{\frac{1}{2}} + 0.06 Re(d_p)^{\frac{2}{3}}\right) (Pr^{0.4}) \left(\frac{\mu_g}{\mu_s}\right)^{\frac{1}{4}}$ Nusselt number

$Nu(d_{p0}) = 2.308$

$m_p(d_p, T_p) := \pi\, M_p\, d_p\, T_g\, Nu(d_p) \left(\frac{D_{12}}{R_u T_g}\right) \left(\frac{Sc}{Pr}\right)^b \left(\frac{p_g}{p_{am}(T_p)}\right) \left(\frac{p_v(T_p)}{T_p} - \frac{p_{pg}}{T_g}\right)$ Mass leaving droplet

$h(d_p) := Nu(d_p) \frac{k_g}{d_p} \qquad h(d_{p0}) = 1.24 \times 10^4 \frac{W}{m^2 K}$ Convection coefficient

$Bi(d_p) := \frac{(h(d_p) d_p)}{2 k_p} \qquad Bi(d_{p0}) = 0.159$ Biot number

Runge-Kutta method to solve:

$$x := \begin{pmatrix} \frac{d_{p0}}{m} \\ \frac{T_{p0}}{K} \end{pmatrix} \qquad x = \begin{pmatrix} 1 \times 10^{-5} \\ 500 \end{pmatrix}$$

$$D(t,x) := \begin{bmatrix} \left[-\frac{2\, m_p(x_0, x_1)}{\pi\, \rho_p\, (x_0)^2} \right] \\ \frac{6\, h(x_0)\, (T_g - x_1)}{x_0\, \rho_p\, C_v} - \frac{6\, m_p(x_0, x_1)\, h_{fg}}{\pi\, (x_0)^3\, \rho_p\, C_v} \end{bmatrix}$$

$t_f := 0.00088$

$Z := \text{rkfixed}(x, 0, t_f, 10000, D)$

$n := 0 .. 200000$

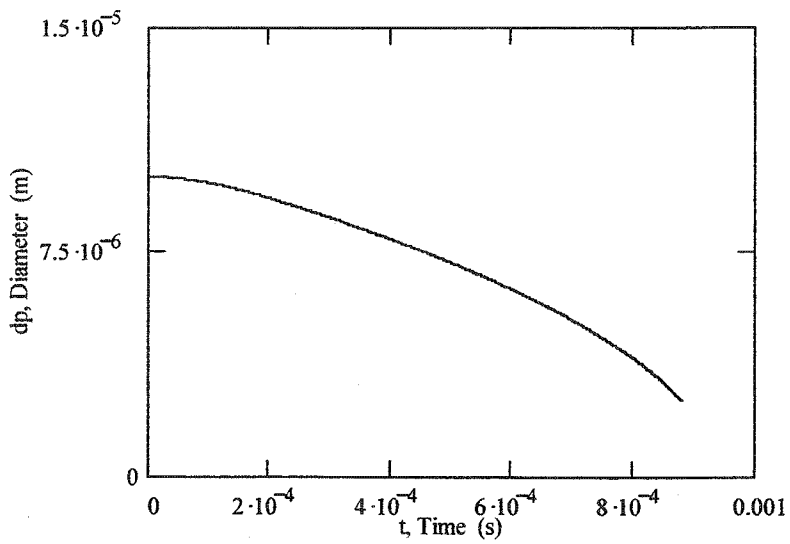

APPENDIX K. CHAR NUCLEATION CALCULATIONS

The following analysis illustrates the calculation of the characteristic curve for corn starch and a mixture of corn starch and char.

Corn starch test for sixth hypothesis

Test values

$\Delta p = 1401.0\,Pa$

$p = 108932.0\,Pa$

$T = (465.01 + 273.15)\,K$

$m_{N2} = 15.111\,\frac{kg}{hr}$

$m_{NC} = 1.506\,\frac{kg}{hr}$

$k = 10^{7.3508}\,m^{-4}$

$m_{H2O} = 0.965\,\frac{kg}{hr}$

$M_{NC} = 30\,\frac{kg}{mol}$

$m_{biomass} = 6.594\,\frac{kg}{hr}$

$f = 0.0, 0.002 .. 1$

$m_{oil} = 4.816\,\frac{kg}{hr}$

$y = 0.2003$

$M_{H2O} = 18.02\,\frac{kg}{mol}$

$M_{N2} = 28.01\,\frac{kg}{mol}$

$R_u = 8314.47\,\frac{J}{mol\ K}$

$$m_{mix}(f) = m_{N2} + m_{NC} + y\,m_{oil} + f\,(1-y)\,m_{oil}$$

$$M_V(f) = \frac{f\,(1-y)\,m_{oil}}{\frac{\Delta p\,p}{k\left[m_{N2} + m_{NC} + y\,m_{oil} + f\,(1-y)\,m_{oil}\right] R_u\,T} - \frac{m_{N2}}{M_{N2}} - \frac{m_{NC}}{M_{NC}} - \frac{y\,m_{oil}}{M_{H2O}}}$$

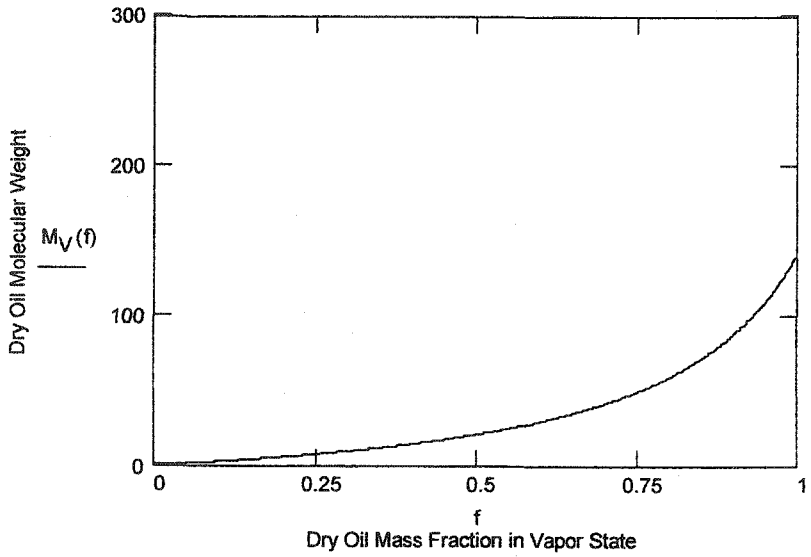

Uncertainty Analysis for Vapor Fraction:

$M_V = 100\frac{kg}{mol}$ Selected molecular weight for analysis

$f(M_{NC}, m_{NC}, y, m_{oil}, m_{H2O}, m_{N2}, M_V, p, \Delta p, k, T) = 0.929$ Vapor fraction at specifed molecular weight

$\sigma f = 0.232$ Uncertainty of vapor fraction at specified molecular weight

Corn starch and char test for sixth hypothesis

Test Values

$\Delta p = 1219.3\,Pa$

$p = 108431.9\,Pa$

$T = (515.84 + 273.15)\,K$

$m_{N2} = 15.111\,\frac{kg}{hr}$

$m_{NC} = 1.872\,\frac{kg}{hr}$

$k = 10^{7.3508}\,m^{-4}$

$m_{H2O} = 0.582\,\frac{kg}{hr}$

$M_{NC} = 30\,\frac{kg}{mol}$

$m_{biomass} = 5.435\,\frac{kg}{hr}$

$f = 0.0, 0.002 .. 1$

$m_{oil} = 2.934\,\frac{kg}{hr}$

$y = 0.1984$

$M_{H2O} = 18.02\,\frac{kg}{mol}$

$M_{N2} = 28.01\,\frac{kg}{mol}$

$R_u = 8314.47\,\frac{J}{mol\,K}$

$$m_{mix}(f) = m_{N2} + m_{NC} + y\,m_{oil} + f\,(1 - y)\,m_{oil}$$

$$M_V(f) = \frac{f\,(1 - y)\,m_{oil}}{\frac{\Delta p\,p}{k\left[m_{N2} + m_{NC} + y\,m_{oil} + f\,(1 - y)\,m_{oil}\right] R_u\,T} - \frac{m_{N2}}{M_{N2}} - \frac{m_{NC}}{M_{NC}} - \frac{y\,m_{oil}}{M_{H2O}}}$$

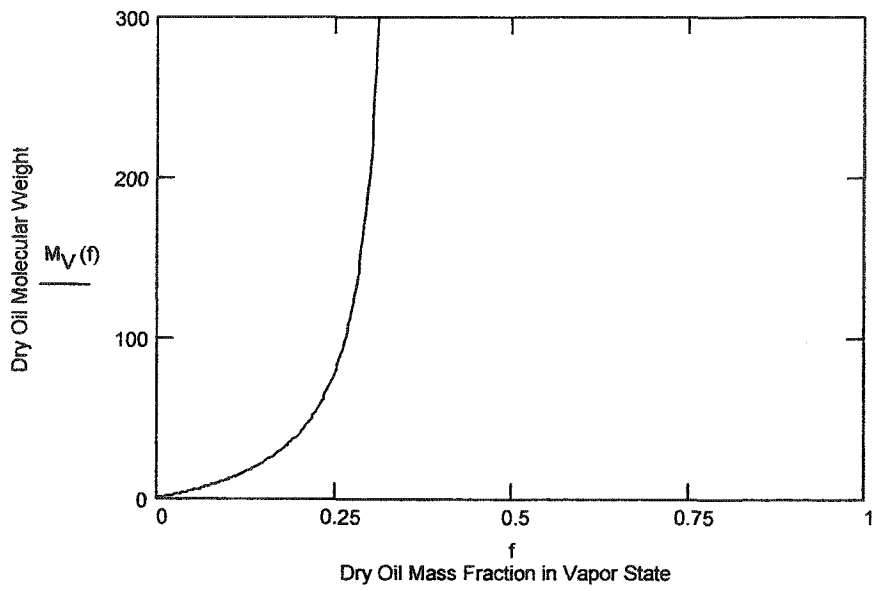

Uncertainty Analysis for Vapor Fraction:

$M_V = 100 \frac{kg}{mol}$ Selected molecular weight for analysis

$f(M_{NC}, m_{NC}, y, m_{oil}, m_{H2O}, m_{N2}, M_V, p, \Delta p, k, T) = 0.264$ Vapor fraction at specifed molecular weight

$\sigma f = 0.35$ Uncertainty of vapor fraction at specified molecular weight